Assessment of Thermal Behavior and Development of Thermal Design Guidelines for Integrated Power Electronics Modules

By

Ying Feng Pang

Dissertation submitted to the faculty of the Virginia Polytechnic Institute and State University in partial fulfillment of the requirements for the degree of

Doctor of Philosophy

In

Mechanical Engineering

Dr. Elaine P. Scott, Chair

Dr. Robert L. West, Committee Member

Dr. Jan Helge Bøhn, Committee Member

Dr. Scott T. Huxtable, Committee Member

Dr. Jacobus Daniel van Wyk, Committee Member

Dr. Marwan U. Bikdash, Committee Member

January 20, 2005

Blacksburg, Virginia

Keywords: thermal analysis, thermal modeling, thermal management, integrated cooling, integrated power electronics module

Copyright 2005, Ying Feng Pang

Assessment of Thermal Behavior and Development of Thermal Design Guidelines for Integrated Power Electronics Modules

Ying Feng Pang

Abstract

With the increase dependency on electricity to provide correct form of electricity for lightning, machines, and home and office appliances, the need for the introduction of high reliability power electronics in converting the raw form of electricity into efficient electricity for these applications is uprising. One of the most common failures in power electronics is temperature related failure such as overheating. To address the issue of overheating, thermal management becomes an important mission in the design of the power electronics to ensure the functional power electronics.

Different approaches are taken by academia and industry researchers to provide efficient power electronics. In particular, the Center for Power Electronics System (CPES) at Virginia Tech and four other universities presented the IPEM approach by introducing integrated power electronics modules (IPEM) as standardized units that will enable greater integration within power electronics systems and their end-use application. The IPEM approach increases the integration in the components that make up a power electronics system through novel a packaging technique known as Embedded Power technology.

While the thermal behavior of commonly used packages such as pin grid arrays (PGA), ball grid array (BGA), or quad flat pack (QFP) are well-studied, the influence of the Embedded Power packaging architecture on the overall thermal performance of the IPEMs is not well known. This motivates the presentation of this dissertation in developing an in-depth understanding on the thermal behavior of the Embedded Power modules. In addition, this dissertation outlines some general guidelines for the thermal modeling and thermal testing for the Embedded Power modules. Finally, this dissertation summarizes a few thermal design guidelines for the Embedded Power modules. Hence,

this dissertation aims to present significant and generalized scientific findings for the Embedded Power packaging from the thermal perspective.

Both numerical and experimental approaches were used in the studies. Three-dimensional mathematical modeling and computational fluid dynamics (CFD) thermal analyses were performed using commercial numerical software, I-DEAS. Experiments were conducted to validate the numerical models, characterize the thermal performance of the Embedded Power modules, and investigate various cooling strategies for the Embedded Power modules. Validated thermal models were used for various thermal analyses including identifying potential thermal problems, recognizing critical thermal design parameters, and exploring different integrated cooling strategies.

This research quantifies various thermal design parameters such as the geometrical effect and the material properties on the thermal performance of the Embedded Power modules. These parameters include the chip-to-chip distance, the copper trace area, the polyimide thickness, and the ceramic materials. Since the Embedded Power technology utilizes metallization bonding as interconnection, specific design parameters such as the interconnect via holes pattern and size, the metallization thickness, as well as the metallization materials were also explored to achieve best results based on thermal and stress analyses.

With identified potential thermal problems and critical thermal design parameters, different integrated cooling strategies were studied. The concept of integrated cooling is to incorporate the cooling mechanisms into the structure of Embedded Power modules. The results showed that simple structural modifications to the current Embedded Power modules can reduce the maximum temperature of the module by as much as 24%. Further improvement can be achieved by employing double-sided cooling to the Embedded Power modules.

Based on the findings from the thermal analyses, general design guidelines were developed for future design of such Embedded Power modules. In addition, thermal modeling and testing guidelines for the Embedded Power modules were also outlined in this dissertation.

To My Parents

Kong Pang and Sz Wui Lee who sow in me the value of education and love me unconditionally

Acknowledgment

First and foremost, I would like to express my deepest gratitude to my academic advisor and mentor Prof. Elaine Scott for providing me with a great research opportunity. Without her unconditional support in guiding me to conduct and complete this research, this dissertation would never have come into existence. I am grateful to have Dr. Robert West, Dr. Jan Helge Bøhn, Dr. Scott Huxtable, Dr. Daan van Wyk, and Dr. Marwan Bikdash from North Carolina Agriculture and Technical State University as my doctoral committee members. I owe them a special note of appreciation for their constant encouragement and expertise throughout my graduate studies.

I am indebted to the National Science Foundation and Center for Power Electronics Systems (CPES) at Virginia Tech for funding this research (under award number EEC-9731677) and providing research facilities. I wish to thank all the colleagues and friends at CPES including the wonderful staffs for their insightful discussions, guidance, and helps during my stay at CPES. I will always cherish our friendships. Special thanks are due to Ben Poe, Jamie Archual, Cathy Hill, and Eloise McCoy, as well as the friends in Thermal Inversion Computational and Optimization Lab (TICOL): Dion Minter, Sandra Smith, Marie Madden, Scott Gayzik, Caroline Comas, Manu Mital, and Ashvin Mudalia.

Many thanks to all the people I have come to know at Virginia Tech and Blacksburg, especially Bob and Esther Youngs, whose friendship and companionship I will always enjoy. I owe my sincere appreciation to my family and relatives who have supported and encouraged me over the years. I am grateful to Ming Luo for his inspired love during all these years. Finally, I want to extend my profound appreciation to my beloved parents for their love, affection, and invaluable support.

Table of Contents

Abstract ii
Dedication iv
Acknowledgment v
Table of Contents vi
Nomenclature viii
Acronyms ix
List of Figures x
List of Tables xiv
1. Introduction 1
    1.1. Background—Roles of Power Electronics 1
    1.2. Motivation 2
    1.3. Current Packaging Technology for Power Electronics 9
    1.4. Research Goal and Approach 11
    1.5. Dissertation Outline 13
2. Literature Review 15
    2.1 Packaging Technology for Multi-chip Modules 15
    2.2 Component Level Cooling Technologies 22
    2.3 Tools for Thermal Prediction and Thermal Test Method 28
    2.4 Thermal Design Rules for Multi-chip Modules 30
    2.5 Summary 31
3. Thermal Modeling of IPEMs 32
    3.1 IPEM Structure and Packaging Scheme 33
    3.2 Basic Finite Element Thermal Modeling of IPEM 36
    3.3 Finite Element Models for Numerical Validation 40
    3.4 Experimental Setup for Validation of Numerical Models 40
    3.5 Evaluation of Numerical Results Against Experimental Data 45
4. Thermal Behavior Assessment of Integrated Power Electronics Modules (IPEMs) .48
    4.1 Study I—Thermal Characterizations 48
    4.2 Study II—Effect of Chip-to-chip Distance and the Copper Trace Area 52

4.3 Study III—Selection of DBC Ceramic and Ceramic Carrier Materials 55
4.4 Study IV—Metallization Layer 57
4.5 Study V—Significance of Polyimide Layer 61
4.6 Study VI—Evaluation of Integrated Cooling Mechanisms for IPEMs 62
5. Results and Discussions 71
5.1 Thermal Characterization 71
5.2 Effect of Chip-to-chip Distance and the Copper Trace Area 75
5.3 Selection of DBC Ceramic and Ceramic Carrier Materials 78
5.4 Metallization Layer 78
5.5 Significance of Polyimide Layer 86
5.6 Evaluation of Integrated Cooling Mechanisms for IPEMs 87
5.7 Summary 104
6. Thermal Design Guidelines for IPEMs 106
6.1 Design for Thermal Performance Concept 106
6.2 Types of Design Guidelines 110
6.3 Design Guidelines for Thermal Modeling of Heat Transfer in Embedded Power Modules 112
6.4 Testing Guidelines and Procedures 116
6.5 Thermal Design Guidelines for Embedded Power Modules 119
6.6 Summary 122
7. Conclusion 124
7.1. Contributions 124
7.2. Recommendations 130
Bibliography 132
Appendix A: Thermal Couplings in ESC 139
A.1 DC/DC IPEM 140
A.2 PFC IPEM 142
Appendix B: Publications 145
Appendix C: Data Sheet for Papst-Motoren Axial Fan 148
Vita 149

Nomenclature

A	area, m^2	t	time, s
I	current, A	T	temperature, °C
K	thermal Conductivity, W/m-K	V	voltage, V
l	thickness, m	X^+	sensitivity Coefficient
Q	power loss, W	β	model Parameter
R	resistance, °C/W	σ	uncertainty, °C

Subscripts

M	measured
N	nominal
P	predicted
S	perturbed (for sensitivity analysis)
∞	ambient

Acronyms

AC	alternative current
CFD	computational fluid dynamics
CPES	center for power electronics systems
CTE	coefficient of thermal expansion
DBC	direct bonded copper
DC	direct current
ESC	electronic system cooling
IGBT	insulated gate bipolar transistor
IPEM	integrated power electronics module
IPM	intelligent power module
MOSFET	metal oxide semiconductor field effect transistor
PFC	power factor correction
SiC	silicon carbide

List of Figures

Figure 1.1 Functionality, Size, and Cost Driving the Development of Consumer Electronics 3
Figure 1.2 Moore's Law 4
Figure 1.3 Power Trend for Intel Microprocessor 5
Figure 1.4 Heat Density Trends and Projections for Information Technology Products 6
Figure 1.5 Thermal Power Dissipation Summary for Current and Future Automotive Electronic Systems 7
Figure 1.6 Heat Flow in Conventional Multi-chip Package 10
Figure 1.7 Structural Schematic of Embedded Power Module 11
Figure 1.8 Increased Performance with the Diversity and Number of Components through Integration and Miniaturization 13
Figure 2.1 Different Package Schematic 16
Figure 2.2 Schematic of Pin Grid Array Package and Its Heat Paths 17
Figure 2.3 Schematic of Ball Grid Array Package and Its Heat Paths 17
Figure 2.4 Interconnection Schematic for (a) Wire-bonding and (b) Flipped Chip Technology 19
Figure 2.5 Concept of Embedded Power Technology 22
Figure 2.6 Three Major Phases of Heat Transfer at Component Level 23
Figure 3.1 Conceptual Structure of Embedded Power Module 33
Figure 3.2 Pictures of DC/DC and PFC IPEM 36
Figure 3.3 Solid Models of (a) DC/DC IPEM and (b) PFC IPEM with Location of Interfaces Modeled as Equivalent Thermal Resistances 39
Figure 3.4 Numerical Model for Validation Purposes 41
Figure 3.5 Illustration of Experimental Setup 44
Figure 3.6 Schematic Symbol for a Generic MOSFET Chip 44
Figure 3.7 Electrical Terminals for (a) DC/DC IPEM and (b) PFC IPEM 45
Figure 3.8 Different Effect for Parallel Connection of Parasitic Diodes and MOSFET 45

Figure 3.9 Thermography Images and Simulated Temperature Distributions for DC/DC and PFC IPEM 47
Figure 4.1 Layout for Case 1-6 Studying the Effect of the Chip-to-chip Distance ..53
Figure 4.2 Study on Copper Trace Layout for Case 7-9 with 6 mm Chip-to-chip Distance 54
Figure 4.3 Layouts on Chips Locations for Case 10 and Case 11 with 6 mm Chip-to-chip Distance 54
Figure 4.4 Schematic of ALOX™ Substrate 56
Figure 4.5 Stress Model and Boundary Conditions for Stress Simulations 58
Figure 4.6 Three Studied Interconnect Patters: (a) 6 Interconnect Via Holes, (b) 9 Interconnect Via Holes, and (c) Rectangular Interconnect Pattern 59
Figure 4.7 Illustration of Structural Enhancement of PFC IPEM 63
Figure 4.8 Illustration of Double-sided Cooling for an Active IPEM 64
Figure 4.9 Schematic of Thermal Clad™ Substrate 65
Figure 4.10 Prototypes for Double-sided Cooling Experiments 66
Figure 4.11 Locations of Thermocouples on the Prototype 67
Figure 4.12 Placement of the Module during Experiment 68
Figure 4.13 Illustration of Copper Cap for the PFC IPEM 69
Figure 4.14 Illustration of Channels on Top of Hotspots for the PFC IPEM 70
Figure 5.1 Thermal Characterization of DC/DC IPEM 72
Figure 5.2 Thermal Characterization of PFC IPEM 73
Figure 5.3 Results for Case 2-6 in Study 1 Compared with Case 1 (Baseline) 76
Figure 5.4 Thermal Improvements for Case 7-9 in Study 2 Compared to Case 1 (Baseline) 76
Figure 5.5 Thermal Improvements for Case 10 and Case 11 in Study 3 Compared to Case 1 (Baseline) 77
Figure 5.6 Temperature Contour for Case 9 in Study 2 on Table 4 77
Figure 5.7 Results Comparison for Different Ceramic Materials 79
Figure 5.8 Temperature Rise and Maximum von Mises Stress for Three Different Interconnect Patterns 79

Figure 5.9 Stress Distribution on Top of the Silicon Die and Bottom of Metallization 80
Figure 5.10 Temperature Distribution on the Metallization for 6 Holes Pattern 81
Figure 5.11 Temperature Rise and Maximum von Mises Stress for Different Metallization Thicknesses 82
Figure 5.12 von Mises Stress Distributions on Metallization for Baseline Thickness, 4x Thickness, and 16x Thickness 82
Figure 5.13 Trade-offs Between Thermal Performance and Thermomechanical Behavior for Different Materials 83
Figure 5.14 Possible Locations for Restraints Specification in Stress Model 85
Figure 5.15 von Mises Stress Distribution on Top Silicon Layer 87
Figure 5.16 Significance of Polyimide Thickness on the Temperature Rise of Heat Sources for PFC IPEM 87
Figure 5.17 Temperature Distribution of Baseline Model and Structurally Enhanced PFC IPEM Models 89
Figure 5.18 Results Comparison of Different Combinations of Ceramic Substrate for Double-sided Cooling 89
Figure 5.19 Temperature Rise of the Heat Source at Different Range of Heat Transfer Coefficient 90
Figure 5.20 Comparison of the Effect of the Best Combined Studied Parameters 92
Figure 5.21 Temperature Rise of Obtained Data During Repeated Experiments 93
Figure 5.22 Measured Temperature for Experimental Study I 94
Figure 5.23 Measured Temperature for Experimental Study II 94
Figure 5.24 Measured Temperature of Experimental Study III 95
Figure 5.25 Schematic of 1-D DC/DC IPEM Structure 96
Figure 5.26 Effective Area for Thermal Resistance Calculation in Equation 5.2 96
Figure 5.27 One-dimensional Thermal Resistance Network for Case I 98
Figure 5.28 One-dimensional Thermal Resistance Network for Case II 98
Figure 5.29 One-dimensional Thermal Resistance Network for Case III 98
Figure 5.30 Infrared Image of DC/DC IPEM for Case 1 100

Figure 5.31 Temperature Distribution of IPEM Model With and Without Copper Cap 102
Figure 5.32 Temperature Distribution of the Water Within the Copper Cap 103
Figure 5.33 Effect of Inlet Flow Velocity on the Thermal Performance of the IPEM 103
Figure 5.34 Heat Transfer Coefficient on the Channel Wall 105
Figure 6.1 Block Diagram of the Engineering Design Process 107
Figure 6.2 Generic Thermal Design Flow Process 109
Figure 6.3 Concurrent Engineering Design Flow Process for Embedded Power Modules 110
Figure 6.4 Dimensionless Sensitivity Coefficient for Each Input Parameter in the Numerical Model 118
Figure 6.5 Impact of Metallization Design Parameters on Temperature Rise of the Module 121
Figure A1.1 Locations of the Simplified Interface Conditions in DC/DC IPEM Model 141
Figure A2.1 Locations of the Simplified Interface Conditions in PFC IPEM Model 144

List of Tables

Table 3.1: DC/DC Components Dimensions and Material Characteristics at 300K 35
Table 3.2 PFC IPEM Components Dimensions and Material Characteristics at 300K 35
Table 3.3 Calculated Power Loss for the Power Chips in DC/DC and PFC IPEM 40
Table 3.4 Material Characteristics of Heat Spreaders and Heat Sinks Used in Numerical Models Validation 42
Table 3.5 Measured Power Loss of the Chips in DC/DC and PFC IPEM for Numerical Validation Experiments 42
Table 3.6 Comparison Between Simulated and Experimental Data 46
Table 4.1 Summary of the Case Studies 49
Table 4.2 Parameters Specifications in Investigating the Effects of Chip Locations on the Thermal Performance of DC/DC IPEM 55
Table 4.3 Models Developed for Studying Different Ceramic Materials 56
Table 4.4 Power Losses Specified in Study III 57
Table 4.5 Total Contact Area for the Metallization Layer on the Heat Source for Different Interconnect Patterns 59
Table 4.6 Investigated Cases to Study the Significance of Metallization Thickness 60
Table 4.7 Generic Material Properties at 300K for the Study on Metallization Materials 61
Table 4.8 Material Properties of Thermal Clad™ 65
Table 5.1 Comparison of R_{ja} of Different Chips in DC/DC and PFC IPEM 73
Table 5.2 Prediction Errors Using Thermal Resistance Matrix 74
Table 5.3 Combination of (Translational and Rotational) Restraints Specified for the Stress Model 85
Table 5.4 von Mises Stress on Silicon and Metallization Layer with respect to Different Restraints 86

Table 5.5 Calculated Thermal Resistance for the Layers Illustrated in Figure 5.25 97
Table 5.6 Predicted Junction Temperature 99
Table 5.7 Predicted Temperature Rise and Junction-to-ambient Thermal Resistance 101
Table 6.1 Description and Nominal Values of Parameters Used in Sensitivity Analysis 117
Table A.1 Thermal Coupling Types 139

Chapter 1

Introduction

Power electronics is an enabling technology and widely used in computers, automobiles, telecommunications, motors, lighting, and alternative energy. With its importance in performing in our daily life functions, it is crucial to have high-reliability power electronic systems. Higher temperatures make the electronic components unreliable and more likely to fail. Therefore, keeping the power electronics components within the operating temperature range is essential. More importantly, good thermal management not only can reduce the thermally-induced failures but also enhance the performance of the power electronics components. Consequently, reliability, durability, and cost become very crucial issues in power electronics. Overheating of electronics can cause severe catastrophes in our daily life.

1.1 Background—Roles of Power Electronics

The rapid proliferation of the power electronics industry has created an urgency for obtaining high-performance power electronics systems. The main tasks of power electronics is to control and convert electrical power from one form to another. The four main forms of conversions are:

- AC (alternating current) to DC (direct current) conversion
- DC to AC conversion
- DC to DC conversion, and
- AC to AC conversion

The converter that changes an AC voltage to an DC voltage is called a rectifier. Some of the applications for a AC to DC converter include variable speed drives, battery charges, and DC power supplies. For example, in telecommunication equipment, the AC to DC converters function either as stand-alone power supplies or as chargers for back-up battery. The converter that changes a DC voltage to an AC voltage is called an inverter. Some of the applications of an inverter include emergency lightning systems, AC

variable speed drives, uninterrupted power supplies (UPS), and frequency converters. Whether using solar, wind, or hydroelectric power to provide charging for the batteries, an inverter is a required component to run AC devices such as televisions in remote applications. Other examples include running security cameras powered by solar panels and satellite up-links powered by wind turbines.

A DC to DC converter is also called a switched-mode power supply that accepts a DC input voltage and produces a DC output voltage. Typically, the produced output voltage is at a different voltage level than the input. Typical applications for a DC to DC converter are DC drive, battery charger, and DC power supply. For example, DC power supplies are used for powering high performance microprocessors in computer systems. In addition, a DC/DC converter is also used to charge the battery in automotive applications. Finally, an AC to AC converter is usually used for controlling the speed of a traction motor. In addition, AC to AC conversion is also used for connecting small combustion turbines to the utility system to produce energy.

Throughout the world, electric power is used at an average rate of 12 billion kilowatts every hour of every day of every year. With high performance power electronics systems, the electricity needed to run the electrical applications such as computers, lightning, and audio system in your car is processed, filtered, and delivered with maximum efficiency. Consequently, failure of the power electronics can cause great inconveniences to our life.

1.2 Motivation

The development of electronics is progressing towards the integration of more functionality and miniaturization in both military and commercial products. However, the cost is driving most of the commercial products while striving for more functionality and smaller space as illustrated in Figure 1.1.

1.2.1 Thermal Factors in Computers and Telecommunication Electronics

The introduction of personal computers and the socialization of the Internet have exponentially accelerated our dependence on power electronics supplying power for

conducting our daily routines. Many industries such as the banking industry and small business industries have changed from traditional techniques of doing business to computerization. The creation of computers has made a huge advancement in modern human life. While the information age has been made possible largely by the invention of computers and computer technology, the failure of power electronics in the computers due to overheating can only bring disaster to individuals as well as having a significant economic impact on society.

The refrigerator-size Bendix G-15 created in 1956 was a fairly sophisticated, medium size computer for its day. It used a magnetic drum for internal memory storage and had 180 tube packages and 300 germanium diode packages for logical circuitry. Cooling was merely by internal forced air. Neither a separate power supply nor air conditioning was required. Today, there are about 42 million transistors within a Pentium 4 microprocessor dissipating about 90 W of heat. Moore's Law (Figure 1.2) states that the transistor density on integrated circuits will double every 18 months. This exponential growth and ever-shrinking transistor size would result in better performance as well as the increase in the chip heat loss accordingly. As stated in the thermal design guidelines for Pentium 4 [1], a typical aluminum extruded heat sink may not be adequate to cool the entire range of thermal design power. To avoid potential failure, more advanced cooling techniques are necessary to keep the processor within the operational thermal specifications.

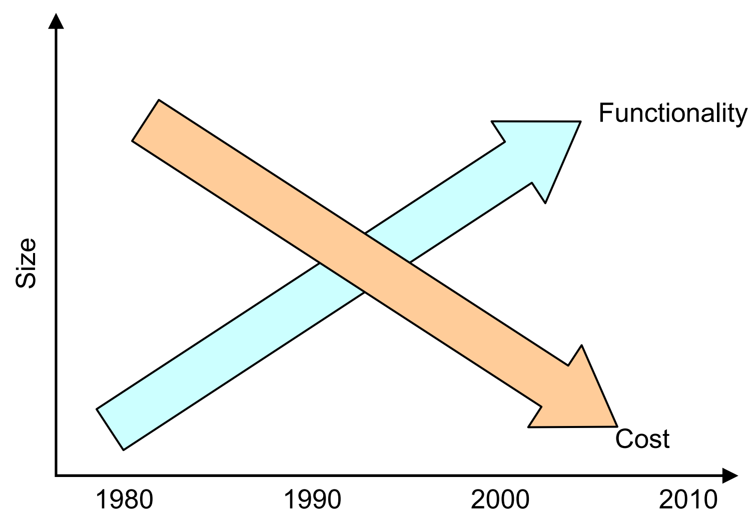

Figure 1.1 Functionality, Size, and Cost Driving the Development of Consumer Electronics

Heat management for the processor chips is a big issue. The power consumption and the dissipation of heat generated in the processor becomes a significant technical challenge. Figure 1.3 illustrates the heat dissipation of Intel's microprocessors for the past 30 years. With the increase in power dissipation, the need to cool local hotspots becomes extremely challenging in the thermal management of the microprocessors.

In recent years, with the massive expansion of the Internet, the need for additional power in communications equipment has forced the development of innovative cooling schemes for existing and new equipment. While the equipment size has shrunk over the past decade, the energy efficiency of the equipment has not dropped at the same rate. Especially for large scale equipment in data center, the heat load has increased rapidly. Although the power density consumed and the heat dissipated within the size of the telecommunication hardware products has increased significantly, this increase in power and heat densities continues to be driven primarily by the technologies of the semiconductor industry.

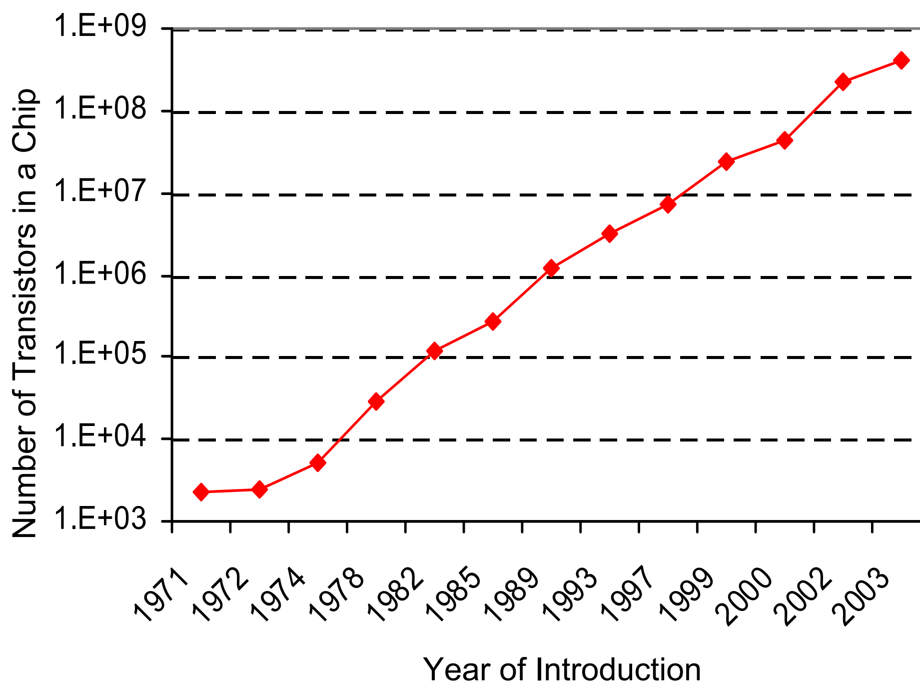

Figure 1.2 Moore's Law [2]

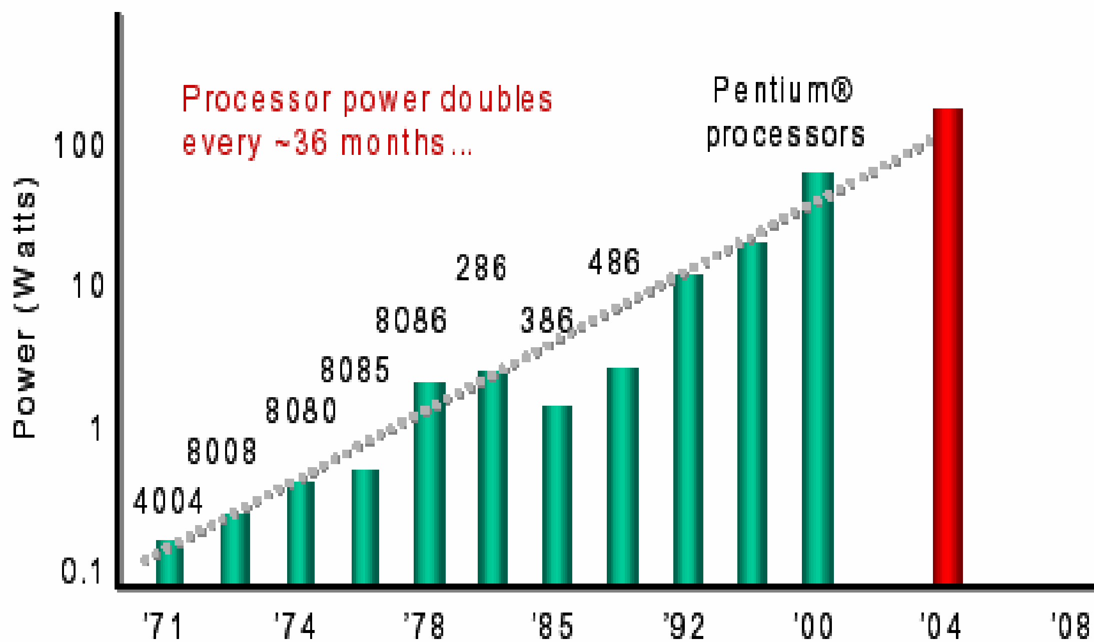

Figure 1.3 Power Trend for Intel Microprocessor [3]

Uptime Institute [4] presented the heat density trends and projections for information technology products as shown in Figure 1.4. The figure clearly shows the rapidly increase in the heat load per product footprint for the products such as tape storage systems, workstations, server and disk storage systems, as well as mainframe communication equipments. With such high heat dissipation, the primary focus of the thermal management for such equipment is to provide adequate air flow at a temperature that meets the limited operating temperature of the components within the equipment.

1.2.2 Thermal Factors in Automotive and Motors Electronics

Power electronics is a major growth area within the automotive industry. Automotive vehicles require sophisticated power management to support demands for higher fuel efficiency, improved performance and increased electric loads. In particular, electronic ignitions, power semiconductor voltage regulators, automatic motor controls, and audio systems are some of the common applications. The power electronics associated with these systems must be reliable over a wide temperature range. The

stability of these power automotive power systems depends on the reliability of the power electronic converters as well as the power electronic components in the systems.

The trend of more of the functional systems of today's automobiles being generated or controlled by electronic systems, continue to hold in the future as more mechanical functions are converted to electric and electrical functions. These vehicles will use high-power motor controls and drive electronics that will likely dissipate kilowatts of heat, thus resulting in an increase of thermal management issues within automotive electronics. Myers [5] presented the thermal power dissipation summary for many current and future automotive electronic systems as illustrated in Figure 1.5. The ability for automotive electronics to withstand high ambient temperature with high power dissipation presents the greatest challenge to the thermal management of these systems.

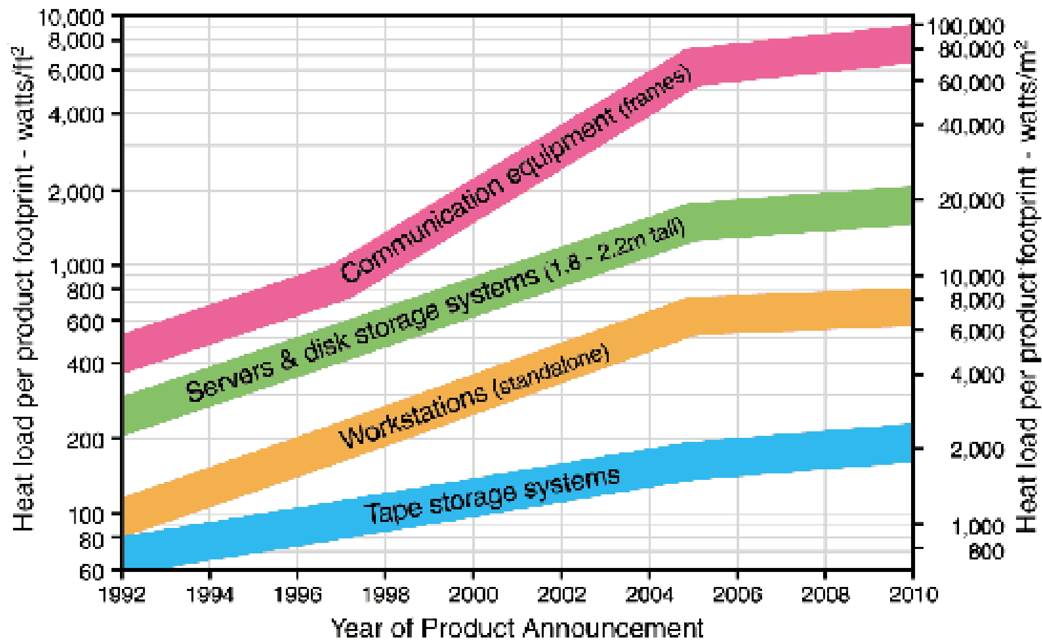

Figure 1.4 Heat Density Trends and Projections for Information Technology Products [4]

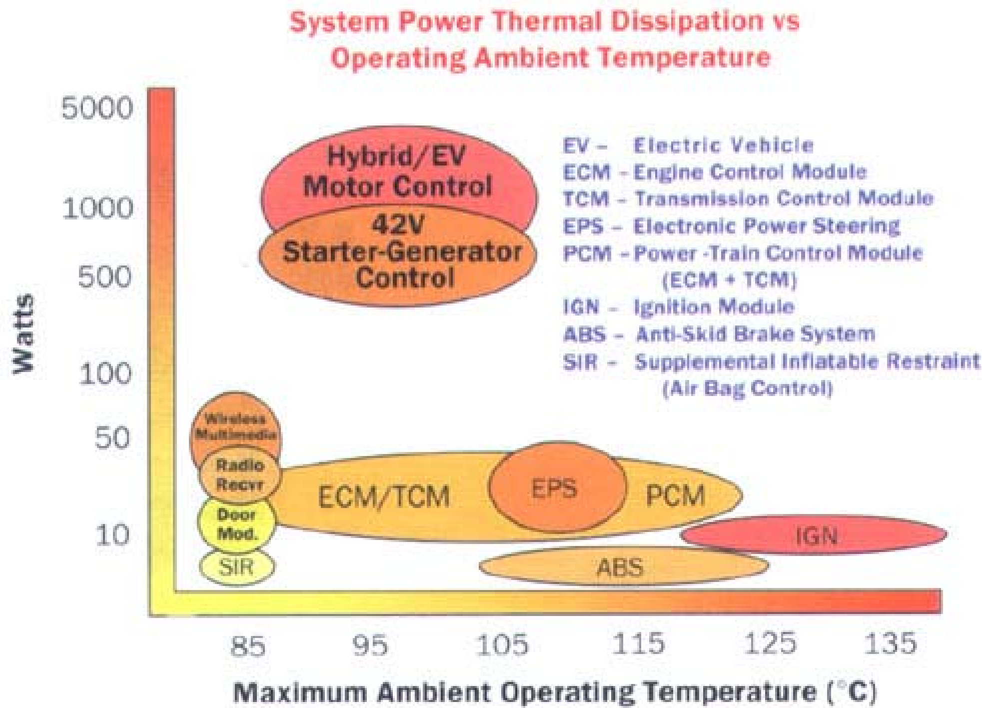

Figure 1.5 Thermal Power Dissipation Summary for Current and Future Automotive Electronic Systems [5]

The worldwide market for electronic motor drives will grow from $12.5 billion in 2000 to $19.1 billion in 2005, according to a new market research study by Drives Research Corporation [6]. The present trends toward energy efficiency, global automation, precision control, and production flexibility predict a continued growth for the electronic motor drives. Some applications for electronic motor drive include combat vehicles, commercial transit such as hybrid electric and fuel cell vehicles, electric oil field drilling equipment, machining systems, and conveyor applications.

Reliable motor drives are essential to provide high performance to the desired functions as mentioned. However, almost all of the motor drives face harsh temperature, humidity, and vibration condition during operations. One of the main approaches to high reliability is to provide good thermal management to the motor drives. While both the motor and the power electronics in the controls produce heat, the thermal management of the motor drives can be improved with optimized design of mechanical components, heat sink design, and components placement layout.

1.2.3 Thermal Factors in Lightning and Power Generation

Compact fluorescent lamps, high-intensity discharge (HID) lighting, high-brightness LEDs, dimming and control systems for all types of lighting are some examples of the applications of power electronics to lighting. Lamps are especially sensitive to the supplied wattage and therefore they should be operated only at the wattage they were designed for and with the type of current they were designed for. Both under powering and over powering the bulbs can damage them and cause overheating. In addition, at the end of the service life of high-intensity discharge lamps, the lamps may overheat due to the rectifier effect. Igniters can also overheat in the event of a short circuit in the associated ballast. One solution is to use a ballast with an integrated temperature switch or a thermal protector to avoid damage due to overheating.

The blackout of August 14, 2003 affecting some 50 million people was a sharp reminder of the essential nature of power failure. Flights were grounded, traffic lights were out, subway and train systems were down, people were stuck in elevators, wireless telecommunication network was down, and water could not be pumped. To prevent such tragedy to happen again, all transmission lines, transformers, and electrical equipment should be monitored to ensure the thermal limits are not exceeded. As you can imagine, overheating of power electronics can cause severe failure in delivering the power to individual home, business offices, and hinder our transit infrastructure, communication network, as well as the water supply. As a result, the loss of electricity, lightning, and telecommunications can cause serious inconvenience.

Driven by the recent surge in Internet usage coupled with the data center construction craze, our nation's dependence on power is growing exponentially. There is just not enough generating capacity to meet consumer demand. As a result, other power generation sources emerge as an alternative energy to satisfy the nation’s demand. The emergence of new developments in microturbine, fuel cell, solar, hydro and wind power can help meet the nation’s energy needs.

Raw power output of alternative energy sources such as wind, solar, and fuel cell needs to be converted into high quality alternating current required by the existing grid

infrastructure. To do so, advanced power electronics, particularly power inverters, are intended to convert the raw power output of the alternative energy source as well as manage the interconnection between the power supply and the grid. Therefore, reliable power electronics are required for the integration of the alternative energy systems as part of the power grid.

1.3 Current Packaging Technology for Power Electronics

A tremendous level of progress, technologically and demand-wise, of electronic devices and systems has been achieved during the past decade. The progress surge has come from the increased functionality and miniaturization of electronics at all levels. The increased number of transistors and shrinking microprocessors size is a good effort in increasing the functionality and miniaturization of the component size. Similarly, the 1U rack-mount system for servers is the example of high performance and space minimization where all the components are fit into a 1.75" height chassis in this slim design.

The increasing interest in high-density power electronics modules is driven by the requirement to handle large numbers of power chips interconnections, high density heat loss, and the desire to pack greater functionality into a compact volume. One of the concepts to achieve these results is through the development of multi-chip modules. To further increase the functionality of electronics components, thus the electronic systems, today's advanced packaging technologies offer integration of chips in a module to achieve the desired increase functionality and minimal size.

The integration of multiple chips into a single multi-chip module package are important to many applications where considerations of size, weight, and electrical performance are required. Examples of commercially available multi-chip modules include multi-chip module (MCM), ball grid array (BGA), and insulated gate bipolar transistor (IGBT) intelligent power module (IPM) where the chips are attached onto a substrate and interconnected using wire bonds. However, a consequence of this integration is the increased necessity for thermal management.

The need to integrate more functionality into the module and higher switching frequency has brought about a coupling of high power densities with tight circuit layout that minimize delays in signal propagation. For every performance improvement in electronic components and systems, there is a corresponding increase in the operating heat generated by the devices. In today's advanced packaging technologies such as system-on-a-chip, thermal management must be designed to handle maximum power dissipation, power density, and hot spots at both the silicon and module levels.

What are the limitations of current practice? First of all, because of this miniaturization and power increase, greater attention is being placed on thermal management's role in the module's packaging design and interconnection. With the current technology for multi-chips packages, almost all of the heat has to be extracted through the solder layer that connects the chips to the substrate as illustrated in Figure 1.6 due to the high thermal resistances of the wire bonds. Secondly, the package is properly encapsulated to protect the chips and the wire bonds from mechanical damage during the handling. Most commonly used encapsulants are silicone and epoxy based. Although silicone offers excellent moisture resistance and epoxy provides improved adhesion, these materials are usually low in thermal conductivity. As a result, the heat generated within the package can hardly be transferred through this layer of material to the ambient.

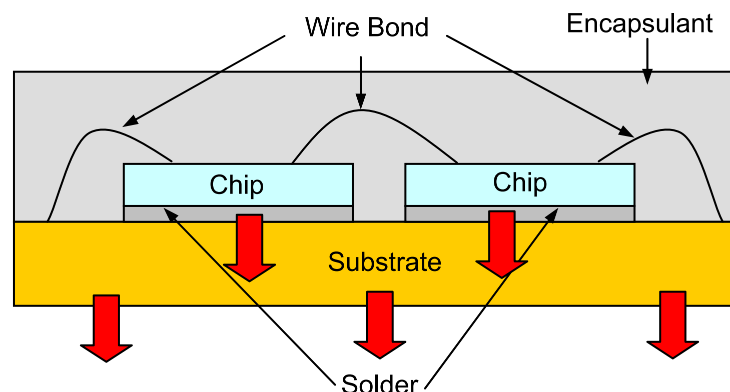

Figure 1.6 Heat Flow in Conventional Multi-chip Package

In searching for solutions to overcome these limitations, new and emerging technologies are introduced. The development of flip chip technology allows for innovative interconnection rather than wire bonds. The interconnection between the die and carrier in flip chip packaging is made through a conductive "bump" that is placed directly on the die surface. The bumped die is then "flipped over" and placed face down, with the bumps connecting to the carrier directly. However, the underfill in a flip chip package makes rework much more difficult, which is a severe limitation to flip chip technology.

1.4 Research Goals and Approach

The Center for Power Electronics Systems at Virginia Tech developed a novel planar integration technology called Embedded Power. The Embedded Power technology features metallization interconnections on co-planar power chips, which are embedded in a flat ceramic carrier. The metallization is for the interconnection of multiple power chips through metallurgical contact to aluminum pads on the power chips. The power chips are then directly soldered onto a substrate. The substrate employed in these prototypes is direct-bonded-copper (DBC) substrate. DBC substrate provides high current interconnect, a good thermal path, and high voltage isolation. In addition, the DBC substrate also provides a platform for soldering multiple power chips. In general, an Embedded Power module consists of three layers as illustrated in Figure 1.7: the base substrate, the embedded power (EP) stage, and the soldered component attached on the top.

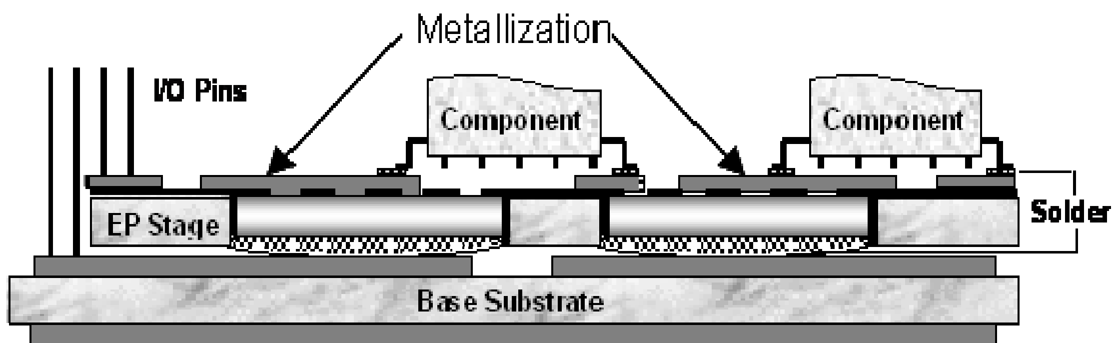

Figure 1.7 Structural Schematic of Embedded Power Module

While the electrical performance can be greatly improved with the proximity of the interconnections, the closeness of the heat generating chips still causes hotspots within the Embedded Power multi-chip module. Removal of generated heat from any given chip within the module is essential to the effort of establishing long-term reliability for a given device. To ensure the reliability of the Embedded Power multi-chip module, this research addresses the thermal performance of the module.

Part of this research is to thoroughly analyze and evaluate multi-chip modules packaged using Embedded Power technology such as integrated power electronics modules (IPEMs), thus providing a strong background for a new and innovative cooling strategy to be engineered. This research studies material and physical properties for the Embedded Power modules. In addition, studies on integrated cooling strategies were examined by implementing double-sided cooling and advanced cooling methods. The final part of this research includes developing general thermal design guidelines for the Embedded Power modules. These guidelines can help in guiding the future design of the IPEMs as well as providing thermal management guidelines for the system designers.

In designing for thermal performance, the goal is to (i) allow the module to operate at harsh environment such as high ambient temperature by reducing the overall thermal resistance of the module as well as (ii) lengthen the life of the module. To develop a reliable, cost-effective thermal solution, different cooling strategies for the module should be considered. Therefore, modules can be cooled with active and passive cooling solutions and can bring flexibility to the end users in different applications for highest performance.

It is believed that the performance of multi-chip modules can be greatly improved by using the introduced Embedded Power technology for integrating multiple chips into a package. The electrical and thermal performance can be improved through integration and miniaturization such as increased diversity and the number of miniature components as shown in Figure 1.8. While the assembly of large numbers of heterogeneous components can form a system capable of robust interaction with its environment, the integration of components is limited by the heat transfer capability.

With the in-depth study on the thermal behavior and the heat transfer phenomena for the Embedded Power modules, failure on the modules can be predicted and avoided as necessary for better long-term reliability. Furthermore, essential thermal management strategies can be developed and implemented to enable higher performance modules. Specifically, the introduction of the thermal design guidelines can facilitate in future design of the Embedded Power modules, thus reducing the design cycle time.

1.5 Dissertation Outline

This dissertation consists of seven chapters including necessary background, motivation, and the objectives of the research effort in Chapter 1. Chapter 1 also discusses limitations of the current practices as well as the impact of the research. Chapter 2 reviews different packaging schemes for multi-chip modules as well as thermal management for multi-chip modules. In addition, Chapter 2 discusses current practice on the packaging of the multi-chip modules and its effect on the thermal management for the multi-chip modules. Finally, a review in the area of thermal design guidelines is presented in this chapter too.

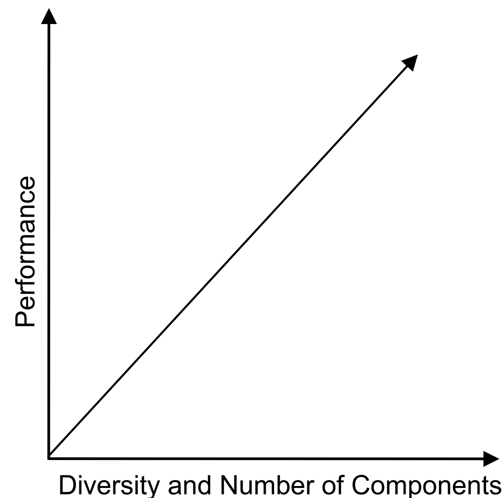

Figure 1.8 Increased Performance with the Diversity and Number of Components through Integration and Miniaturization

Chapter 3 presents detailed modeling of the Embedded Power module including its structure and the thermal properties of the materials used for the Embedded Power module. This chapter discusses the modeling approach as well as the validation of the modeling tool with experimental results for obtaining an accurate and acceptable numerical thermal model for future studies. With the validated thermal model in Chapter 3, the thermal models were then used for various studies addressed in Chapter 4. In depth studies on the thermal behavior of the Embedded Power modules were conducted based on various thermal design parameters such as material properties, sizes, and shapes. Both numerical and experimental approaches were employed for these studies. In addition, different integrated cooling strategies were also explored for improving the thermal performance of the Embedded Power modules.

Chapter 5 discusses the results of the studies in Chapter 4. Based on the results presented in Chapter 5, an in depth understanding on the thermal behavior of the Embedded Power modules allows for enhanced thermal management for the Embedded Power modules. Consequently, better thermal performance can be achieved. Chapter 6 presents the general thermal design guidelines for the Embedded Power modules. The chapter also discusses the concepts for necessary concurrent design process incorporating thermal design as well as various approaches in developing design guidelines.

Finally, Chapter 7 contains a summary of the conclusions of this research and the contribution of this work towards new packaging technology for power electronics.

Chapter 2

Literature Review

The need for thermal management in electronics is inevitable in the foreseen future with the anticipated significantly higher power dissipation than what is consumed in today's electronics. Increased demand for higher frequency and higher power dissipation has increased the need for better thermal solutions. The purpose of electronics cooling is to ensure that the electronic systems behave reliably under the most diverse environmental and operational conditions.

2.1 Packaging Technologies for Multi-chip Modules

The present trend in electronic packaging is going towards high-density packaging such as three-dimensional interconnects that allows stacking the chips and the substrates in x-, y-, and z- direction. These packaging technologies enable the use of different chip attachment technologies for the assembly of one or more chips into a single module. This package technology promises tremendous size reduction while improving the performance of the electronics. Multi-chip packages have become industry's practice to increase functionality in one high-density package. Different multi-chip packaging technologies offer different advantages and thermal performances. In this section, several commonly used packaging technologies for multi-chip modules are reviewed.

Extensive research in the past has focused greatly on the heat transfer in different conventional packages such as ball grid array (BGA) packages, dual-in-line packages (DIP), thin quad flat packages (TQFP), and pin grid array (PGA) packages. Figure 2.1 shows the package schematic for BGA packages, DIP packages, PQFP packages, and PGA packages. Although the pin configurations for these packages are different, the most commonly used interconnection techniques at the chip level are wire bond and solder. Figure 2.2 shows the heat paths within the wire-bonded PGA packages. The BGA package is a potential low-cost packaging solution to achieve miniaturization in electronics. The BGA packages with wire-bond and flip chip die-to-substrate

interconnect are gradually replacing the traditional plastic quad flat packages. Mulgaonker et al. [7] showed that thermal performance of the plastic ball grid array (PBGA) compared well with ceramic pin grid array packages (CPGA), ceramic quad flat pack (CQFP), and the ceramic BGA. The heat is transferred from the die through thermal paths within the substrate and through the solder bumps into the printed wiring board. The heat is then transferred out from the printed wired board to the ambient through system level cooling as illustrated in Figure 2.3.

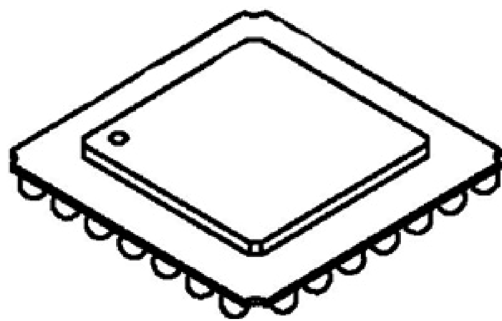

(a) BGA Package

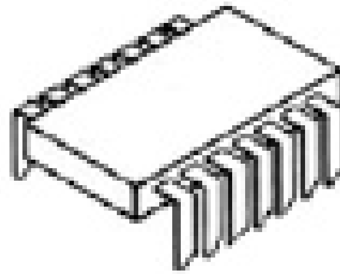

(b) DIP Package

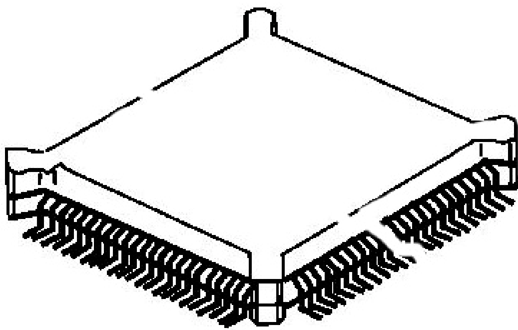

(c) PQFP Package

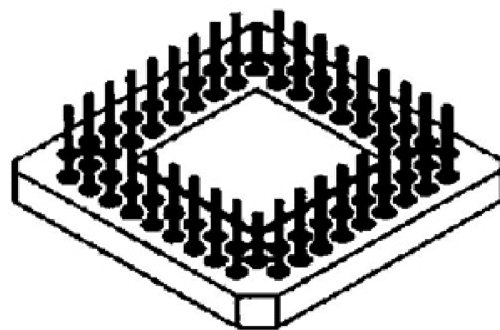

(d) PGA Package

Figure 2.1 Different Package Schematic

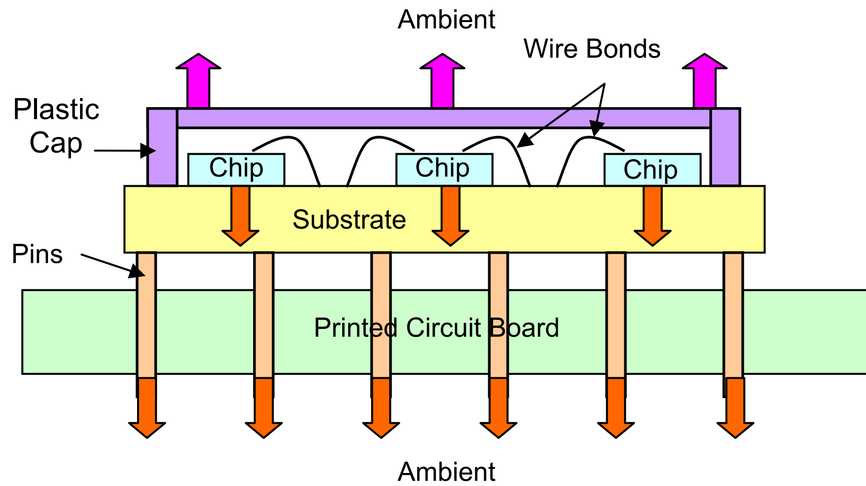

Figure 2.2 Schematic of Pin Grid Array Package and Its Heat Paths

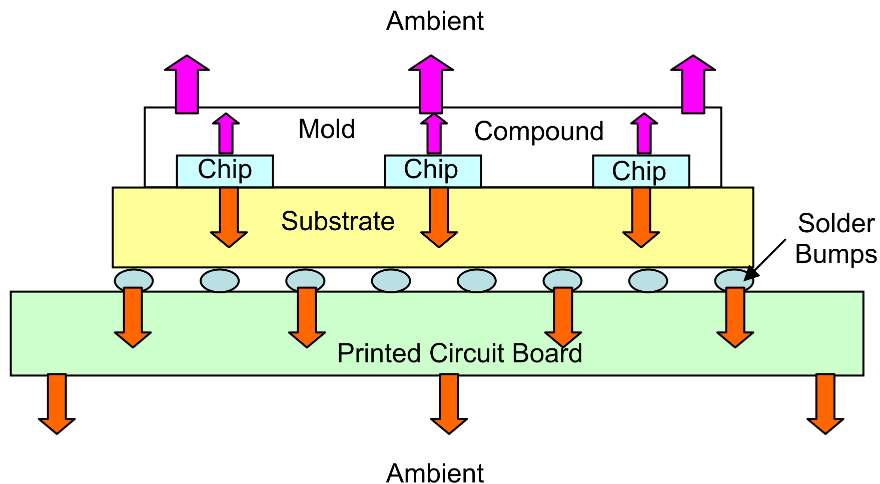

Figure 2.3 Schematic of Ball Grid Array Package and Its Heat Paths

Mita et al. [8] proposed a high density package by mounting two chips on both top and bottom sides of a small substrate by using tape automated bonding (TAB) technology to form a chip on chip ball grid array (COCB) unit. Stiffeners are attached to both sides of the COCB unit to maintain a flat outer surface for the unit. The individual COCB unit can also be stacked to create a three dimensional module with heat spreaders in between each COCB unit. The respective COCB unit is connected with electrical

conductive adhesive or soldering and the heat spreaders are attached to the stiffeners by adhesive. The COCB also showed a better lower package thermal resistance when comparing to traditional plastic molded package where the molded resin has a significantly high thermal resistance.

Yuan [9] compared the thermal performance and characteristics of flip chip and wire bond ceramic multi-chip modules. He concluded that the flip chip packages offer excellent thermal performance compared to the wire bond packages. He also found that the significant parameters affecting the thermal performance of the wire bond packages are the substrate thermal conductivity, substrate thickness, and the card thermal conductivity. On the other hand, the significant parameters affecting the thermal performance of the flip chip packages encapsulated with aluminum cap are the cap material and the card thermal conductivity.

Kim [10] presented a folded stacked package for wireless and portable products that allows dies to be placed side by side on a flexible substrate and folded to produce a low-profile, compact package. The thermal analysis of a four-die folded staked package showed that the junction to ambient of the package can be as high as 47 °C/W and about 96% of the heat is dissipated through the board. Furthermore, Balde [11] reviewed several three dimensional assemblies of stacked chips and other thin packages. He discussed the advantages and disadvantages of different commercial packages such as leaded stacked packages, staked bare die using wire-bonding packages, staked bare die using via interconnections packages, die staking with interposers packages, the monolithic molded block approach, and frame wire-bonding assemblies. He then introduced the folded flex assemblies as a new option in high density packaging especially for memory modules and medical products. To achieve flexible interconnections, Meyer et al. [12] used flexible foils to connect the ICs and surface-mount devices.

Fan et al. [13] evaluated some of the key technologies that major semiconductor manufacturers have adopted for discrete and multi-chip MOSFET module packaging for power conversion applications. These included SO-8 based packages, chip scale, flip

chip, and ball grid array based packages as well as micro-lead frame based packages. In the high thermal performance SO-8 based packages, copper straps and solder bumps are the commonly used to replace wire-bonds. The larger contact area between the copper strap and the chip can provide 10-20% better thermal performance as well as increasing the amount of heat to be transported through the top of the chip. By replacing wire-bonds with solder bumps at the backside of the chip to connect from the chips to the PCB in the chip scale, flip chip, and ball grid array packages, the heat dissipation from the backside of the chip to the PCB can be greatly improved. Therefore, the junction-to-PCB thermal resistance can be greatly reduced. In the micro-lead frame based packages, device interconnections are achieved with wire-bonds and the lead frame are soldered to the bottom of the package.

To meet the capability of operating at high performance, current packaging technologies for power electronics have moved towards high density interconnects. In these packaging technologies, multiple power chips were integrated into a single compact module by using different interconnect technologies such as wire bonding and thin film overlay. Figure 2.4 shows the schematic of wire-bonding and flipped chip interconnection. Ozmat [14] evaluated three different interconnect technologies: flipped tape automated bond (FTAB) configuration, flipped chip package (FCP) configuration, and high density interconnect (HDI) technology. He concluded that the HDI technology offered a better alternative for high density multi-chip module applications than the FTAB and FCP technologies because the HDI technology offers a direct heat path to the chips.

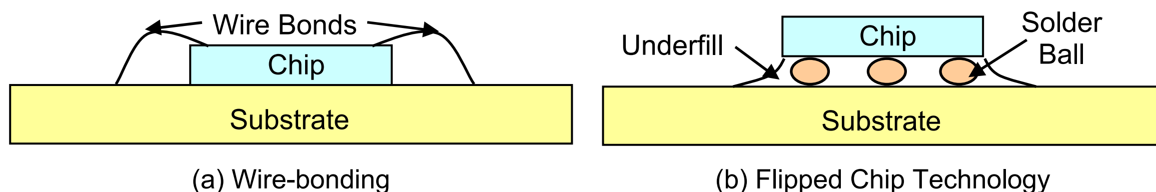

(a) Wire-bonding (b) Flipped Chip Technology

Figure 2.4 Interconnection Schematic for (a) Wire-bonding and (b) Flipped Chip Technology

Sienski et al. [15] presented a three-dimensional interconnect packaging concept where integrated circuits (IC) chips were wire-bonded onto interconnect metal on the diamond substrate. The top and bottom surfaces of the substrate were processed with multi-layer high density interconnects such as copper and polyimide. The two sides were electrically connected through metal-filled vias that penetrate the substrate. The top surface of the high density interconnect was used to connect bond pads. In their study, heat removal from the package was achieved through phase change spray cooling.

In 1997, Ozmat et al. [16] presented a new packaging approach called Harris Thin Pack (HTP) to package high performance power devices. The HTP package contained a combination of multiple discrete power devices and diodes. The key element of HTP package was a dielectric lid that contains patterns of metallization on the top and the bottom surfaces. Finite element analysis and experiments were performed to evaluate the thermal performance of the package. In this package, high performance heat exchangers were incorporated into the package to achieve maximum thermal performance.

In addition, Fisher et al. [17] presented the thin film power overlay technology (POL) for power modules where layers of dielectric and patterned copper on top of a substrate to form a dense interconnect structure. Chips are mounted on top of the interconnection by various methods including wire bonds and solder bumps. This technology enables the chips to be soldered directly to a DBC substrate which acts as the bottom interconnect layer for the chips. Furthermore, POL technology eliminates bond wires. The planarity of the package structure enables double-sided cooling where heat can be removed from the top and bottom sides of the module.

The need for smaller and less expensive power converters for consumer electronics and military power systems has pushed for new packaging technologies. The standardization of power electronics modules can replace complex power electronic circuits and simplify the development and design of large electric power systems. To increase the degree of integration for power modules packages, Stockmeier et al. [18]

presented intelligent power electronics modules such as SKiiP[1]. The intelligent power electronics modules not only integrated power devices but also included a gate drive unit, as well as temperature and current sensors. Other available commercial integrated power modules include products from Fuji [19], Eupec [20], and Toshiba [21].

Lostetter et al. [22] presented the concept of standardized integrated power modules (IPM) by extending multi-chip module laminate (MCM-L) concepts to power electronics packaging. The foundation of the module is a piece of DBC where the bare dies are soldered to the DBC. A nonconductive ceramic or polymer spacer with cavities is used to embed the bare dies, and the bare dies are wire-bonded on the top surface of the bare dies. The entire structure is soldered to a copper or metal matrix composite (MMC) heat spreader for proper thermal management.

Similar to the structure of the POL and IPM, Liang et al. [23-25] presented embedded power technology for integrated power electronics modules (IPEM). The embedded power technology is a deposited metallization based integration technology. The embedded power packaged module consists of the embedded power stage, the electronics circuitry such as the gate drive and the control components, and the base substrate. The concept of the embedded power technology for integrated modules is shown in Figure 2.5. The power chips are embedded in the openings of a ceramic with adhesive dielectric surrounding the chips. An interlayer dielectric is applied on top of the chips and the ceramic with via holes for interconnection to the aluminum pads on the chips. Patterned copper metallization layers are deposited onto the dielectric layer and through the via holes to form interconnections with the aluminum pads on the chips. Different three-dimensional modules can be packaged using the embedded power technology by using different interconnect pattern depending on the desired functions and applications of the three-dimensional packages.

[1] SKiiP is a registered trademark of Semikron Electronic

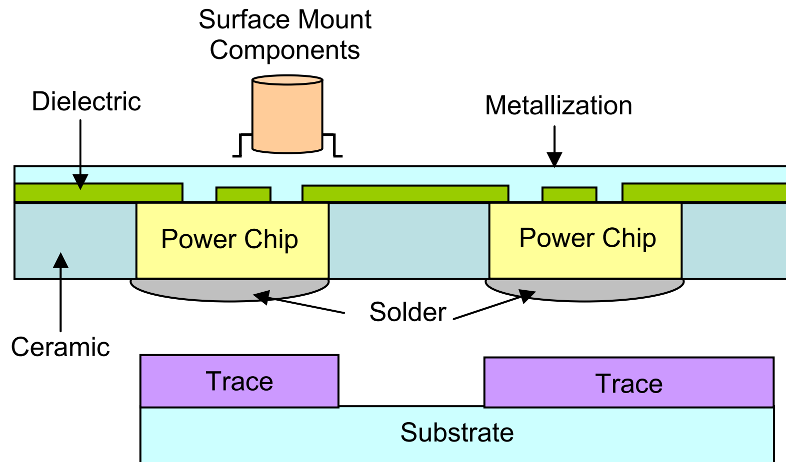

Figure 2.5 Concept of Embedded Power Technology

Most of these multi-chip packaging technologies are used by industry nowadays. Therefore, many studies have been conducted to understand the advantages and disadvantages of these packaging technologies from the view points of electrical performance, thermal performance, reliability, process of integration, and cost. Ginsberg et al. [26] summarized some general considerations for different packaging technologies for multi-chip modules. While other common packaging technologies such as BGA packaging technologies and wire-bonding interconnection are well-studied, there is still much work to be done on embedded power technology. Therefore, an in-depth understanding of the advantages and disadvantages of using embedded power technology and its consequent advantages from the IPEM can greatly promote its practical use in industry.

2.2 Component Level Cooling Technologies

The need to miniaturize and improve the performance of the conventional electronics has pushed the development of multi-chip module in which two or more bare chips are interconnected on a common substrate. The ability to integrate more functionality into a smaller area and the ability to operate at higher frequencies in multi-chip modules have also increased the challenge in the thermal management of the package due to the higher power dissipation. A diverse set of constraints, among them

cooling performance, may ultimately limit the overall performance at which a technology can reliably be operated.

Thermal management design has a significant impact on package form factor and shape. Heat generated inside the package must be transferred to the surface of the package and dissipated from the package to ambient by any available cooling strategies. In summary, the thermal management process can be categorized into three major phases as illustrated in Figure 2.6:

I. Heat transfer within the component package,

II. Heat transfer from the package to a heat spreader or heat sink, and

III. Heat transfer from the heat spreader or heat sink to the ambient environment.

The package type defines the internal heat transfer processes in the first phases and the system level thermal engineer does not usually have control of it. The goal of the packaging engineer in the second and third phases is to design a reliable, efficient thermal connection from the package surface to the heat spreader or heat sink and to the ambient environment. To achieve this goal, a package level thermal engineer is required to have a thorough understanding of heat transfer fundamentals and the knowledge of available interface and good thermal conductivity materials.

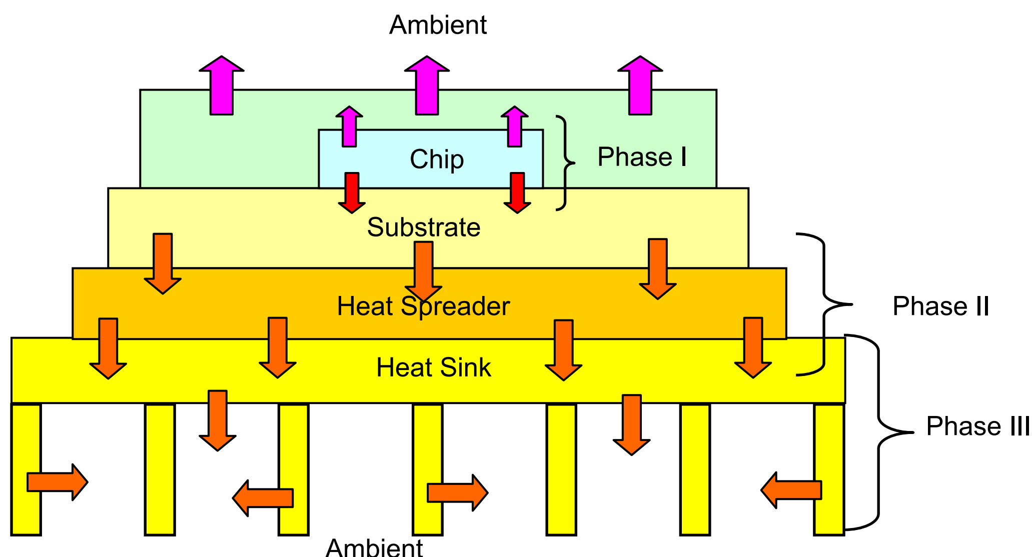

Figure 2.6 Three Major Phases of Heat Transfer at Component Level

2.2.1 *General Thermal Management Overview*

Bergles [27] extensively summarized the use of cooling technologies for electrical, electronic, and microelectronics for the past 50 years. Some of these technologies included conduction cooling, air cooling, and liquid cooling. In conduction cooling, heat is transferred by conduction to the fins which are cooled by convection and radiation. In other cases of conduction cooling, heat is conducted by one end of the heat pipe to the other end where the other end is cooled by convection or radiation. Natural air convection and forced air convection are categorized in the air cooling technique. In liquid cooling, liquid can be forced to flow through a channel with mounted devices and the liquid is cooled in an air or liquid-cooled heat exchanger. The devices can also be submerged in a boiling liquid where heat is rejected to an air or water-cooled condenser. In addition, devices can also be mounted in an enclosure filled with dielectric fluid and cooled by air-cooled or water-cooled heat exchanger.

Price [28] reviewed several thermal management solutions for military electronics systems, including direct and indirect air cooling of printed wiring boards, liquid-cooled flow-through power supply, liquid-cooled and two-phase cold plates, expendable liquid systems, implementation of phase change materials, implementation of thermoelectric coolers, and stirling cycle mechanical cryogenic cooler. These cooling methods are implemented in the design of modular microwave integrated circuits devices. These devices are used in missile electronics, NASA communication arrays, the Discover II Satellite Communications Systems, military infrared detector arrays, target acquisition systems, ground-based night vision systems, and airborne electro-optics forward looking infrared (FLIR) systems.

In addition, Azar [29] presented several active cooling options as well as their advantages and disadvantages. These options included fan and heat sinks or heat pipe combinations, air flow management and enhancement, hybrid cooling, thermoelectric, thermosyphon, closed loop liquid cooling, direct immersion, refrigeration, and cryogenics. While these advanced cooling technologies can greatly improve the thermal performance of the electronics, the common constraints of these technologies are the cost of packaging and the reliability of the system.

2.2.2 *Thermal Management for Multi-chip Modules*

The introduction of multi-chip modules has brought new challenges to the thermal management techniques in electronics. The high density integration in the multi-chip modules results in higher heat flux densities at the component-level packaging technologies. In addition, the wide variety of materials used in the modules and the varying coefficients of thermal expansions (CTE) involved in the multi-chip modules present more difficult problems in thermal management. While the purpose of the thermal management is to ensure that the circuit components are maintained within their functional temperature limits, the generated heat within the modules is usually dissipated through conduction, convection, and radiation.

Heat generated within the multi-chip modules is usually transported by conduction to the external surfaces of the package. From there, the heat is then transferred to external heat sinks by conduction or convection. Very often the heat is removed through the back side of the components because the top side of the components is encapsulated for safety and protection purposes. Thus, the thermal resistance from the chip to the top surface of the package is significant higher than the thermal resistance from the chip to the back side of the package.

While most of the heat is conducted through the back side of the chip through the solder interconnects to the substrate, Patel [30] presented a backside cooling solution for high power flip chip multi-chip modules. The design used a high thermal conductivity (2.8 W/m-K) thermal compound with an innovative referencing scheme for interfacing the chips to the heat sink. The heat sink was used for convective heat flow.

Lee [31] presented several thermal enhancing techniques for flip chip plastic ball grid array (BGA) packages. He studied 26 different thermal enhancing methods. These included the effect of attaching a copper heat spreader with different thicknesses to the back side of the die, effective area covered by the interface material, attachment of aluminum lid, and the attachment of heat sink. He concluded that attaching a copper heat spreader on the back side of the die can significantly increase the heat flow projection. Furthermore, using high thermal conductivity molding compound can also reduce the

junction-to-ambient thermal resistance. On the other hand, Liang et al. [32] presented multi-chip modules encapsulated with crimped metal cap which provides lower thermal resistance on the top side of the module compared to molding compound.

To improve the heat transfer from the heat source to an external surface of a package, Pittler et al. [33], Chu et al.[34], Blodgett et al.[35], and Oktay et al. [36] presented the development of the thermal conduction module (TCM). The TCM has a helium-based module cap which provides a thermal conduction path from the back of each chip, via one contacting piston per chip, to the cap. The cap is in contact with a water-cooled cold plate. The chip temperatures are established by the external and internal thermal resistances to heat flow from the chip to the cap, to the cold plate, and to the board on which the modules are held by special connectors. They concluded that the power dissipation limits can be extended by over 50% with the TCM combines the advantages of conduction cooling used at the chip and module levels with that of the forced convection liquid cooling at the system level.

Mudawar [37] reviewed several different high heat flux thermal management schemes. These included avionic air cooling, micro-channel and mini-channel cooling, jet impingement cooling, and spay cooling. In addition, he also listed the saturated thermophysical properties of different liquid coolant used in liquid cooling. These commonly used coolants include FC-72, FC-87, PF-5052, and water. He concluded that phase change plays a key role in attaining attractive cooling performances although phase change systems are generally more complicated to implement. Lee et al. [38] demonstrated the capability of using a liquid-filled cooling environment to enhance the thermal performance of a multi-chip module package. The package was externally cooled by either free-air or forced-air. High thermal properties of dielectric liquids showed promising 2-4 times improvement in the thermal performance compared to air.

In addition, Chen et al. [39] investigated the thermal performance of a stacked multi-chip module using direct liquid cooling with single phase FC-72 as the working fluid. Experimental and numerical studies were conducted. They concluded that using liquid cooling can further increase the package power loss. Furthermore, Shaw et al. [40]

implemented direct low-pressure water spray-cooling on the surface of the diodes within a variable-speed motor drive. The surfaces of the exposed devices and interconnects were coated with 25 micron of Parylene as a dielectric layer.

The use of a thermoelectric cooler for spot cooling had also shown to be an effective way to improve the thermal performance of electronics equipments back in 1961 [41]. They have been used for over three decades for electronics cooling. Fleurial et al. [42] presented novel thermal management approach that used thermoelectric cooler located under each of the power devices to cool only the key high power devices. Simons et al. [43] reviewed the application of thermoelectric cooling to the cooling of electronic equipment. They concluded that the heat loss from multi-chip modules are simply too high for current thermoelectric modules to provide enhancement effectively. In other application, Solbrekken et al. [44] proposed to convert the waste heat from the CPU to generate electricity using a thermoelectric module drive the cooling fan.

Advanced materials are commonly used as passive thermal management strategies for electronics. The continuing increase in packaging density and power levels has resulted in a need for high thermal conductivity materials. In addition to the thermal properties, the matching of the coefficient of thermal expansion (CTE) of adjacent materials in the package is also crucial in minimizing thermal stress for potential failure. Zweben [45] presented an overview of composites used in and thermal management and evaluated their thermal conductivities and CTE values. These composites included silicon carbide particle-reinforced aluminum, carbon fiber-reinforced copper, carbon fiber-reinforced aluminum, diamond particle-reinforced copper, and beryllia particle-reinforced beryllium.

Jha [46] introduced a new thermal management material named CUVAR. CUVAR is an extruded composite of copper and Invar powder and can be used as heat sinks or substrates for direct bonding the silicon devices. Invar restrains thermal expansion and copper provides high thermal conductivity. However, exposure of CUVAR to temperature higher than 700°C could cause degradation in its physical properties. Davidson et al. [47] presented a copper-diamond composite material with

higher thermal conductivity and closer CTE with silicon and gallium arsenide as substrate material for multi-chip module.

2.3 Tools for Thermal Prediction and Thermal Test Method

Temperature is an important parameter that must be controlled in electronics to ensure long term reliability of the electronics. However, the heat transport in electronic systems is, in most cases, not immediately well understood. Therefore, different techniques are employed to improve the understanding of the heat transfer in electronics systems. Commonly used techniques include analytical and computational approaches as well as experimentation.

Accurately predicting the operating temperature of critical electronic parts often presets an overwhelming challenge. Ellison [48] presented analytical and computational approaches of solving heat transfer problems in electronic equipment. He confined the numerical approach to conduction, radiation, and convection by natural and forced airflow and presented two computer programs named Thermal Analyzer for Multilayer Structures (TAMS) and TNETFA. Eid [49] outlined the methodology of performing multi-dimensional thermal modeling using a spreadsheet.

Many commercial computational fluid dynamics and heat transfer tools for thermal design of electronics components and equipment are available in the market. Mak et al. [50] introduced an approximate analysis method incorporated in ANSYS for thermal finite element analysis of a surface mount plastic package mounted on a printed circuit board. This approximate numerical technique employs a point matching method at the board mounting locations where the temperature and heat flow continuity requirements are enforced. In addition, Zahn [51] benchmarked the capabilities of two CFD software tools, IcePak and Flotherm, to predict flow fields and heat transfer in a package level, laminar flow, and natural convection environment.

Although numerical modeling are widely used for the thermal analysis of electronics components and systems, Joshi et al. [52] concluded that the key challenges in thermal modeling include the solution methodology, the uncertainty of input parameters, and the measurement uncertainties in providing meaningful validation for computational

simulations. To identify the capabilities of current algorithms used for CFD modeling, Eveloy et al. [53] reviewed the potential shortcomings of the fluid flow modeling currently employed for printed circuit board thermal analysis especially the turbulence models in the CFD codes. Therefore, computational approach can not always correctly describe the heat transfer in electronic equipment especially when convection and fluid flow is involved. For the same reason, experimentation is needed to benchmark the computational program as well as provide insight to the thermal behavior of the electronic equipment.

Experiments are conducted at all levels of the design cycle to ensure system integrity and adherence to design specifications. Common goals for performing experimentation include component characterization, validation of numerical models, and operational integrity. Experimental measurement can provide reliable information for knowing the junction temperature and consequently the thermal behavior of the electronic package. Hence, it is necessary to generate important and accurate data in order to achieve the design objectives.

Azar [54] outlined important steps to successful measurement in electronic enclosures. He also reviewed tools necessary for a successful analysis and their limitations and domain of application identified. Kromann [55] used experimentation to perform thermal characterization of an alumina-tungsten multilayer multichip module. He showed that the experimental measurement variability was small. Other researchers have also conducted experimentation for the purpose of validation [56-58]. To understand these experimental methods, the Joint Electron Device Engineering Council (JEDEC), under the Electronic Industries Association (EIA), is creating thermal measurement standards for integrated circuit packages by which the performance of different packages housing similar devices, or different devices in similar packages can be compared [59].

Uncertainty analysis can identify the uncertainties in measurements and evaluate their effect on the accuracy of the results. Moffat [60] presented a procedure for

estimating the uncertainties in the experimental results as well as outlined possible sources of errors.

2.4 Thermal Design Guidelines for Multi-chip Modules

The thermal design guidelines for single-chip electronics are well established. The standard guidelines for determining the thermal resistance of a single chip package are well documented by JEDEC [59]. On the other hand, there is no standardized method available to determine the thermal resistance for multi-chip packages. A common parameter used for the comparison of various single-chip thermal designs is the junction-to-ambient thermal resistance, R_{ja}. However, this single parameter cannot effectively describe three-dimensional heat flow in multi-chip modules. Researchers have presented methods to determine the equivalent thermal resistance for each die in a multi-chip module [61, 62].

Liang et al. [63] addressed the thermal issues affecting the thermal performance of the multi-chip modules. These included the spreading resistance, the non-symmetrical heating in the module, the substrate materials, and the thermal vias. In addition to component level thermal design guidelines, Lall et al. [64] presented thermal design guidelines for predicting the maximum temperature of a heating component on a conducting board with uniform surface conductance on the top and bottom surface.

Although design guidelines are not well-established for the thermal design of electronics especially multi-chip modules, the design guidelines for very large scale integration (VLSI) design are well developed. For example, Watanabe et al. [65] presented design guidelines for HfSiON gate dielectrics for 65 nm CMOS generation. In addition, geometry constraints such as minimum allowable values for certain widths, separations, extensions, and overlaps of geometrical objects patterned in the various levels of a system are widely used in the VLSI design [66]. VLSI circuit layout design-rule checking to reduce errors in the VLSI designs is also well studied [67]-[69].

2.5 Summary

The evolution of electronic packaging technology has posed greater challenges for the thermal design. Miniaturization with increased integration in functionality and components, as well as higher heat loss from the semiconductor continues to be a major concern. Traditional and novel cooling strategies have been studied over the past few decades for different applications, both in consumer electronics and military electronics. Various tools and methodology are used to predict the thermal performance of the semiconductor in electronics as well as the electronics equipment. In summary, increase in the power dissipation in electronics will continue to drive the need for novel thermal management strategies. The importance of thermal management to the ultimate success of future electronics will not diminish.

Although Embedded Power technology is a rather new technology, it resembles flip-chip packages in taking the advantage of the area under the package for the solder interconnections. Therefore, we can presume that the main heat path within the Embedded Power module is from the chip through the solder layer to the substrate as illustrated in Figure 2.4 (b). In addition, the metallization bonding technique in the Embedded Power technology resembles the power overlay technology where layers of dielectric and patterned copper on top of a substrate to form a dense interconnect structure. Thus, we believe that the planarity of the metallization layer can be used for double-sided cooling as suggested by the literature in [17].

Chapter 3

Thermal Modeling of IPEMs

Thermal modeling is important at the electronics design stage where different developments and explorations can be performed without expensive and time consuming modifications. It also allows engineers to understand the thermal behavior of the electronics components and their interrelationship between the electronics components as well as the thermal dynamics of the system. The implementation of thermal modeling in the design process can ensure good thermal management for the electronics components in the electronics systems.

Traditional power electronic modules are based on standard industry semiconductor package configurations. Heat is conducted from the chip through the wire bonds and solder to the bottom of the package base, and then through an interface material into a heat spreader and heat sink for either air-cooled or water-cooled applications. Heat is also conducted through some thick compound material or electrical insulated layer to the top of the package. However, almost all of the heat is conducted through the package base rather than to the top of the package due to the higher thermal resistance of the compound material or the insulation layer.

On the other hand, the heat transfer in planar multi-layer structures is usually more complicated than in the traditional power electronics structures since it is three-dimensional with spatially distributed thermal resistances and capacitances. Therefore, good analysis tools are required to analyze the planar multi-layer structured power electronics modules and to predict the temperature distribution of these structures. This chapter presents the details of the finite element thermal modeling of IPEMs and the validation of the numerical models against the experimental results.

3.1 IPEM Structure and Packaging Scheme

In power electronics, it is believed that the next level of improvement can be achieved by integrating discrete components into a single multi-chip module. To understand the thermal behavior of planar multi-chip packaged power electronics modules, two active integrated power electronics modules, direct current to direct current (DC/DC) and power factor correction (PFC) IPEMs, were studied in this research. Active IPEMs integrated typical active discrete components such as MOSFETs and diodes for front-end DC/DC converters into a high density package.

The IPEMs described in this research were designed for a 1 kW DC/DC converter for distributing power system (DPS) applications with 400 V input bus voltage and 5 A root-mean-square (RMS) current operating at 200 kHz switching frequency. The IPEMs were packaged using Embedded Power technology. This technology features the building-up of interconnects on co-planar power chips that were embedded in a ceramic frame. In other words, the Embedded Power technology replaces the wire bonds with deposited copper metallization layers for electrical connections. Through this advanced interconnect technology, the electrical and mechanical performances of the modules were improved by the elimination of the resistance, noise, and fatigue failure of the wire bonds. Figure 3.1 shows the conceptual structure of Embedded Power module presented by Liang [23].

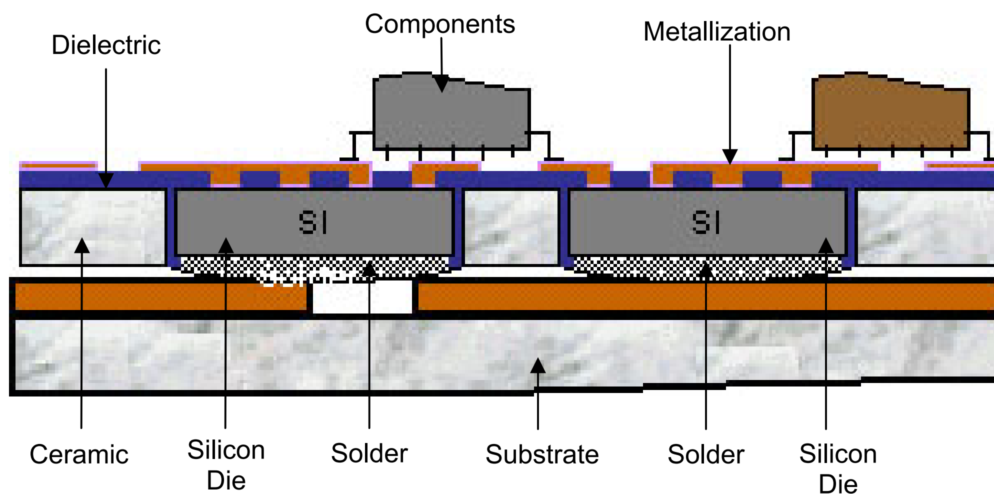

Figure 3.1 Conceptual Structure of Embedded Power Module

The DC/DC IPEM consists of two MOSFET bare chips soldered to a direct-bonded-copper (DBC) substrate. While the DBC substrate consists of three layers with a ceramic substrate sandwiched between two layers of copper, the DBC substrate provides a good current interconnection, high electrical isolation, and a good thermal path for the MOSFET chips. The top copper layer of the DBC substrate was etched to desired patterns as interconnect platform for the chips. To integrate multiple chips into one compact module, a ceramic carrier with openings was used to frame the MOSFET chips. The silicone gel, with a thermal conductivity of 0.2 W/m-K, filled the gap formed between the DBC ceramic and the ceramic carrier due to the etched copper traces. The epoxy, with a thermal conductivity of 1.4 W/m-K, filled the gap between the MOSFET chips and the ceramic carrier to secure the position of the MOSFET chips.

An inter-layer dielectric using polyimide was coated onto the top and bottom of the ceramic carrier using polymer screen-printing method. The flat surface of the ceramic carrier also provides a platform to deposit copper metallization layer on top of the MOSFET chips for electrical interconnection. The patterned metallization with via holes were designed based on the aluminum pad pattern of the chips. Finally, a hybrid gate driver was assembled to the module for controlling the circuitry of the module. The DC/DC IPEM has a footprint of 28.5 mm x 27.3 mm. Table 3.1 lists the physical dimensions and the material characteristics of the components in the DC/DC IPEM.

Similarly, the PFC IPEM was also packaged using Embedded Power technology. Instead of MOSFET chips, there are two CoolMOS[1]™ chips and two silicon carbide (SiC) diodes in the PFC IPEM. Other components such as the embedded capacitors and the embedded current sensor are also part of the PFC IPEM. In addition, a commercial gate driver was also attached to the PFC IPEM. The footprint of the PFC IPEM is 34.2 mm x 29.7 mm. For safety purposes, the top surface of the active IPEMs was encapsulated with silicone gel for electrical isolation. The physical dimensions and the material characteristics of the components in PFC IPEM are listed in Table 3.2. Both DC/DC and PFC IPEMs are shown in Figure 3.3.

[1] CoolMOS is a trademark of Infineon Technologies

Table 3.1 DC/DC IPEM Components Dimensions and Material Characteristics at 300K

Item	Material	Characteristic Dimensions (mm)	Characteristic Thickness (mm)	Thermal Conductivity (W/m-K)
MOSFET (IXFD21N50)	Silicon	8.84 x 7.19	0.425	118
DBC Ceramic Substrate	Alumina (Al_2O_3)	28.45 x 27.32	0.635	26
DBC Base	Copper	28.45 x 27.32	0.3	395
DBC Traces	Copper	N/A	0.3	395
Hybrid Gate Driver	Alumina (Al_2O_3)	21.08 x 8.51	0.635	26
Ceramic Frame	Alumina (Al_2O_3)	27.32 x 25.4	0.625	26
Dielectric Layer	Polyimide	N/A	0.125	0.3
Epoxy Interface	Epoxy	N/A	0.3	1.4
Gap Filler	Silicone Gel	N/A	0.254	0.2
Chip Attached	Solder	N/A	0.127-0.475	51

Table 3.2 PFC IPEM Components Dimensions and Material Characteristics at 300K

Item	Material	Characteristic Dimensions (mm)	Characteristic Thickness (mm)	Thermal Conductivity (W/m-K)
CoolMOS™ (SPW20N60C3)	Silicon	5.83 x 4.52	0.234	118
SiC Diode (SDP06S60)	Silicon Diode	1.5 x 1.4	0.368	490
DBC Ceramic Substrate	Alumina (Al_2O_3)	27.95 x 23.14	0.625	26
DBC Base	Copper	27.95 x 23.14	0.3	395
DBC Traces	Copper	N/A	0.3	395
Commercial Gate Driver	Alumina (Al_2O_3)	4.9 x 3.9	0.635	26
Ceramic Frame	Alumina (Al_2O_3)	25.45 x 23.14	0.625	26
Dielectric Layer	Polyimide	N/A	0.125	0.3
Epoxy Interface	Epoxy	N/A	0.51	1.4
Gap Filler	Silicone Gel	N/A	0.254	0.2
Chip Attached	Solder	N/A	0.267-0.4	51

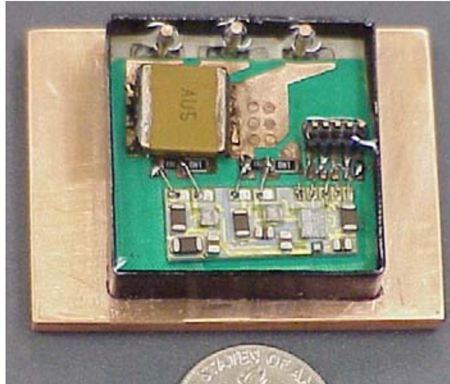

(a) DC/DC IPEM

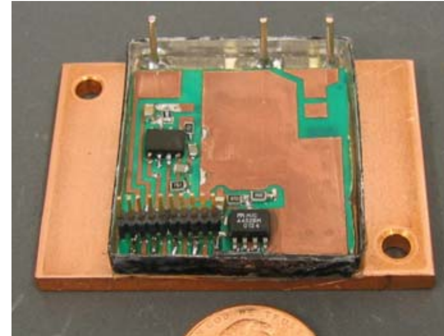

(b) PFC IPEM

Figure 3.2 Pictures of DC/DC and PFC IPEM

3.2 Basic Finite Element Thermal Modeling of IPEM

The finite element models were created using commercial software, I-DEAS[2]™. I-DEAS™ provides a solid modeler to model solid geometry and electro-system cooling (ESC) solver for thermal simulations. ESC allows conjugate heat transfer analysis with comprehensive 3D computational fluid dynamics (CFD) solutions. In addition, ESC combines finite element modeling (FEM) based analysis with control volume formulation to achieve accurate solutions. The fluid flow and thermal model are solved iteratively. More information on the capabilities of ESC can be found in [70].

The ESC solver allows for conductive, convective, and/or radiative analyses. In this study, radiation was assumed negligible, and both conductive and convective modes were used. Conduction is a process of heat transfer from a solid-solid interface due to the atomic or molecular activity. A general conduction rate equation is known as Fourier's Law and can be expressed as follows:

$$q'' = -k \cdot \left(i\frac{\partial T}{\partial x} + j\frac{\partial T}{\partial y} + k\frac{\partial T}{\partial z}\right), \quad (3.1)$$

where q" is the heat flux, k is the thermal conductivity, and T is the temperature. It can be observed from Eq. 3.1 that the heat flux is a directional quantity.

[2] I-DEAS is a trademark of UGS Corp.

The process of heat transfer from a solid-fluid interface due to fluid motion is known as convection. The overall effect of convection heat transfer is known as Newton's law of cooling and can be expressed as follows:

$$Q = h \cdot A \cdot (T_w - T_a), \quad (3.2)$$

where Q is the quantity of the heat convected, h is the heat transfer coefficient in W/m^2-K , A is the convecting surface area, T_w is the temperature of the convecting wall, and T_a is the ambient fluid temperature.

Any component level thermal analyses must consider the details of the power electronics package. Understanding the physical structure of the package is the first step in the analyses process. The basic numerical models of the active DC/DC and PFC IPEM are shown in Figure 3.3. The finite element models included 2D linear triangle shell elements and 3D linear tetrahedron solid elements. To improve the accuracy of the simulation results, all available details were included in the models. Due to the thin layer of the interface materials, interface conditions within the modules were specified as equivalent thermal resistances. The details of obtaining these equivalent thermal resistances at the interfaces can be found in Appendix A.

Unknown interface conditions were modeled as estimated values based on engineering judgment. These interfaces included solder layers, epoxy layers, and polyimide layers. The calculated equivalent thermal resistance values for these interfaces are presented in Appendix A. Figure 3.3 (b) shows the locations of these interfaces within the PFC IPEM. Note that the interfaces in the DC/DC IPEM are similar to the PFC IPEM shown in Figure 3.3 (b). The hybrid gate driver in the DC/DC IPEM was modeled as a homogenous block with its thermal conductivity equivalent to alumina. On the other hand, the commercial gate driver in the PFC IPEM was not considered in the thermal model since it has negligible heat load. Overall, the hybrid gate driver in DC/DC IPEM, the commercial gate driver, the embedded capacitors, and the current sensor in the PFC IPEM add negligibly to the heat load in the IPEMs, and were therefore not considered further.

Heat generation in the power chips was assumed to be uniform on the top surface of the chips. The main heat paths within the active IPEMs were from the heat sources to the copper traces to the DBC ceramic, and from the DBC ceramic to the DBC copper base. From there, the heat dissipated through conduction from the DBC copper base to the copper heat spreader and to the heat sink. Heat was then transferred to ambient air through convection. Other heat paths included from the heat source to the top copper metallization layer connected to the DBC traces. Although there was possible heat path from the top copper metallization layer to the top encapsulated gel and to the ambient air, the encapsulated gel has rather high thermal resistance that prevented top side cooling. Therefore, the top surface of the active IPEMs was modeled as adiabatic surface in the finite element models.

The power dissipations of the power chips during actual operation of the DC/DC converter were unavailable. Therefore, calculated values based on operating conditions were used in most of the cases studied in this research. The calculated values are listed in Table 3.3. However, specific power dissipations for each investigated case will be specified in the individual case study discussed in Chapter 4.

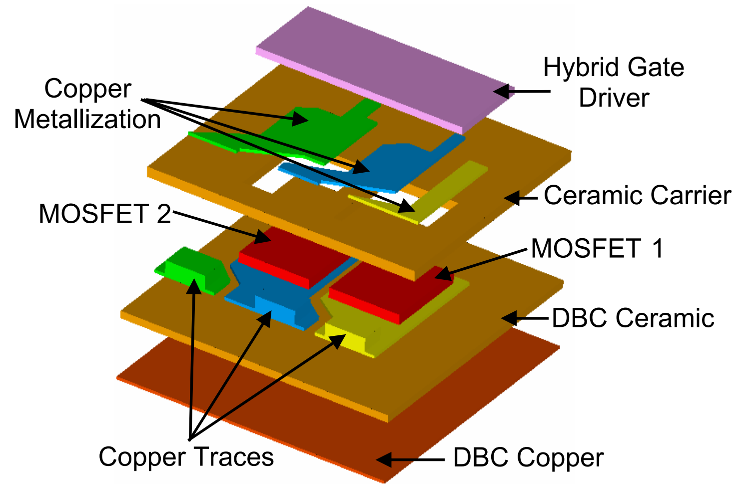

(a) DC/DC IPEM

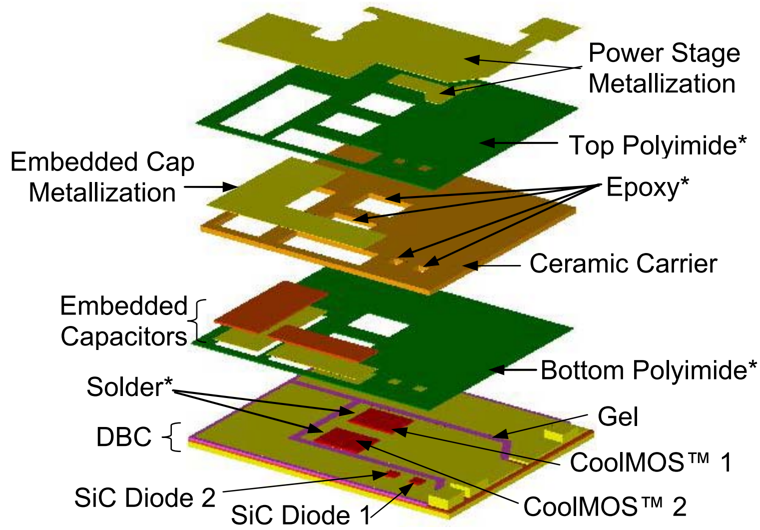

(b) PFC IPEM

Figure 3.3 Solid Models of (a) DC/DC IPEM and (b) PFC IPEM with Location of Interfaces Modeled as Equivalent Thermal Resistances

Table 3.3 Calculated Power Loss for the Power Chips in DC/DC and PFC IPEM

Power Chip	Power Loss (W)
MOSFET 1	12
MOSFET 2	7
CoolMOS™ 1	7.8
CoolMOS™ 2	7.8
SiC Diode 1	4.52

3.3 Finite Element Models for Numerical Validation

Numerical models for DC/DC and PFC IPEMs were validated with experimental data. Figure 3.4 illustrates the finite element model created in I-DEAS™ for validation purposes. The model included the DC/DC or PFC IPEM with a copper heat spreader, a heat sink, and a wind tunnel used in the experiments. The components and material characteristics of the IPEMs are listed in Table 3.1 and Table 3.2, and the component dimensions and the material characteristics of the copper heat spreader and the heat sink are listed in Table 3.4. To validate the thermal models, boundary conditions in the finite element models were defined based on the information from the well-designed experiment described in section 3.4. The power losses measured from the experiments are listed in Table 3.5.

3.4 Experimental Setup for Validation of Numerical Models

Despite the advancements in finite element modeling capabilities and ease of use, a fully numerical design study is an overwhelming task without the guidance of experimental measurements. Thus, two experiments were conducted to validate the numerical models with the thermal tests of the DC/DC and PFC IPEMs. In each of the validation experiments, the test component was attached to a copper heat spreader and to an aluminum heat sink during the experiment. With the IPEM attached to the heat sink, the IPEM and the heat sink were placed at the center of the wind tunnel.

Figure 3.5 shows the experimental setup for the three experiments performed in this research. A wooden box was constructed using 19 mm thick ply wood as an insulated wind tunnel. The dimensions of the wind tunnel are 150 mm (H) x 150 mm

(W) x 400 mm (L). One end of the wind tunnel was equipped with an outlet axial fan producing constant volume airflow rate of 0.05 m^3/s, while the other end was vented to room temperature. Honeycombs were placed at the inner ends of the wind tunnel to straighten the airflow. The top of the wind tunnel was equipped with an infrared window to allow access for the infrared camera to the test component.

Thermocouples and an infrared camera were used during the experiments. Surface temperatures of the IPEMs were measured using an infrared camera model Thermacam PM290 with ThermaGRAM, the data acquisition software, for recording and capturing the thermal images. Both the inside of the wind tunnel and the test components were painted black to ensure a uniform and high emissivity for the infrared thermography. Similarly, the measured temperatures from the thermocouples were collected using an Agilent 34970A data acquisition unit. The accuracy of the infrared camera is ±2°C and the uncertainty of the temperature measured with thermocouples is ±0.5°C when calibrated in an ice water bath.

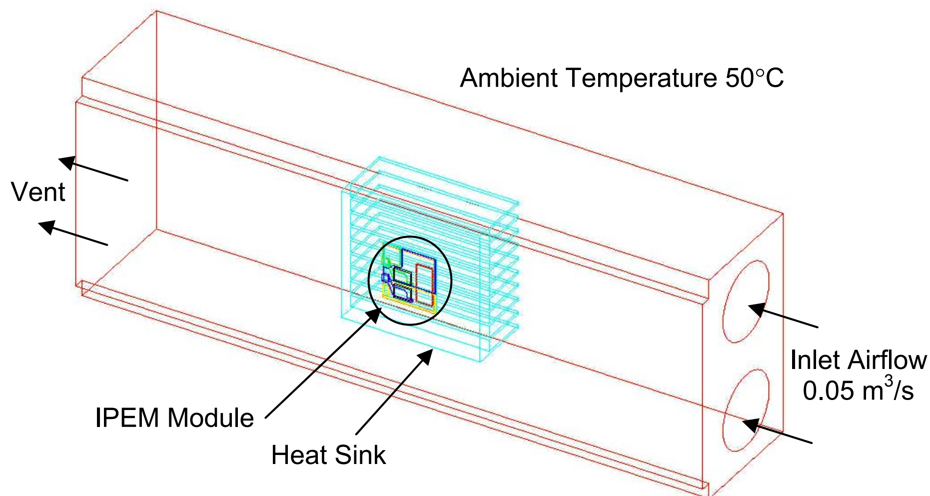

Figure 3.4 Numerical Model for Validation Purposes

Table 3.4 Material Characteristics of Heat Spreaders and Heat Sinks Used in Numerical Models Validation

Component	Material	Characteristic Dimensions (mm)	Characteristic Thickness (mm)	Thermal Conductivity (W/m-K)
Heat Spreader	Copper	50 x 38	5 (DC/DC) 3 (PFC)	395
Heat Sink	Aluminum	73 x 68 (DC/DC) 73 x 73 (PFC)	32.5	164

Table 3.5 Measured Power Loss of the Chips in DC/DC and PFC IPEM for Numerical Validation Experiments

Heat Source	Heat Loss (W)
MOSFET 1	9.55
MOSFET 2	5.9
Hybrid Gate Driver	0.65
CoolMOS 1	14.85
CoolMOS 2	14.85
SiC Diode 1	2.22
SiC Diode 2	3.34

Thermocouples were attached on the heat spreader and at the inlet of the wind tunnel. The thermocouple placed on the heat spreader was used to calibrate the infrared camera and the other thermocouple at the inlet of the wind tunnel was used to measure the ambient temperature. Both thermocouples were connected to a data acquisition system. To attach the thermocouple on the heat spreader, thermally conductive silicone paste (OT-201 from Omega) was placed onto the bead of the thermocouple and a small piece of Kapton[3]™ tape was used to attach the bead to the surface of the heat spreader. The thermal conductivities of the silicone paste and the Kapton™ tape are 2.83 W/m-K and 0.12 W/m-K respectively.

To avoid disturbance of the heat flow within the IPEMs, no thermocouples were embedded into the IPEMs. Therefore, the data from the infrared images were critical since these images provided the only source for the temperature distribution of the

[3] Kapton is a registered trademark of Dupont

IPEMs. To calibrate the infrared camera, the thermocouples readings were adjusted based on the calibration of the thermocouples in the cold bath. Then, the data from the infrared images were corrected according to the adjusted thermocouple readings from the ice bath by adding the difference between the data from the infrared images at the calibration point and the adjusted thermocouple reading from the ice bath to the data from the infrared images. Consequently, the data from the infrared images were corrected by the difference between the thermocouple readings and the infrared images at the calibration point.

In order to avoid the complicated interface circuitry required to activate the actual circuit to dissipate heat, the measurement circuit was made active and the initial voltage drop across the chips was measured and the heating current was switched on for a sufficient amount of time to achieve steady state conditions. Each MOSFET chip has a parasitic diode characteristic and a MOSFET characteristic in its structure as shown in Figure 3.6. Both the parasitic diode and the MOSFET characteristics can provide heat losses. When heating the DC/DC IPEM, each MOSFET chip was powered up separately and the current flow through the parasitic diode within the MOSFET chip was measured. The N and O terminals were connected to power up the MOSFET 1 chip and terminals P and O were connected to power up the MOSFET 2 chip (Figure 3.7 (a)). Thus, the power loss from the MOSFET chips was obtained from $P=V\cdot I$, where P is the power loss, V is the measured voltage drop across the chip, and I is the current flow through the chip.

To activate the CoolMOS™ chips in the PFC IPEM, the voltage drop across the MOSFET characteristic was measured. This is because the parasitic diode characteristics within the two CoolMOS™ chips have a negative temperature coefficient (NTC) characteristic when connected electrically in parallel as shown in Figure 3.8 (a). The negative temperature coefficient exhibits a decrease in electrical resistance with increasing temperature. Thus, one CoolMOS™ chip will be continuously heated up since the electrical resistance is lower while the other CoolMOS™ chip will not be activated. To heat up the CoolMOS™ chips under a positive temperature coefficient characteristic (PTC) as illustrated in Figure 3.8 (b), the terminals N and O shown in Figure 3.7 (b) were connected with the addition of 15 V applied to the gate driver. With the PTC

characteristic, the electrical resistance rises within the MOSFET during an over current situation so that excessive current is not allowed to flow. As a result, the excessive current in the circuit will pass through the second CoolMOS™ chip and the chips will be heated up until both the CoolMOS™ chips are in equilibrium condition. Fortunately, the two SiC diodes showed a PTC characteristic when connected electrically in parallel. Thus, the terminals O and P were connected to power up the two SiC diodes (see Figure 3.7 (b)).

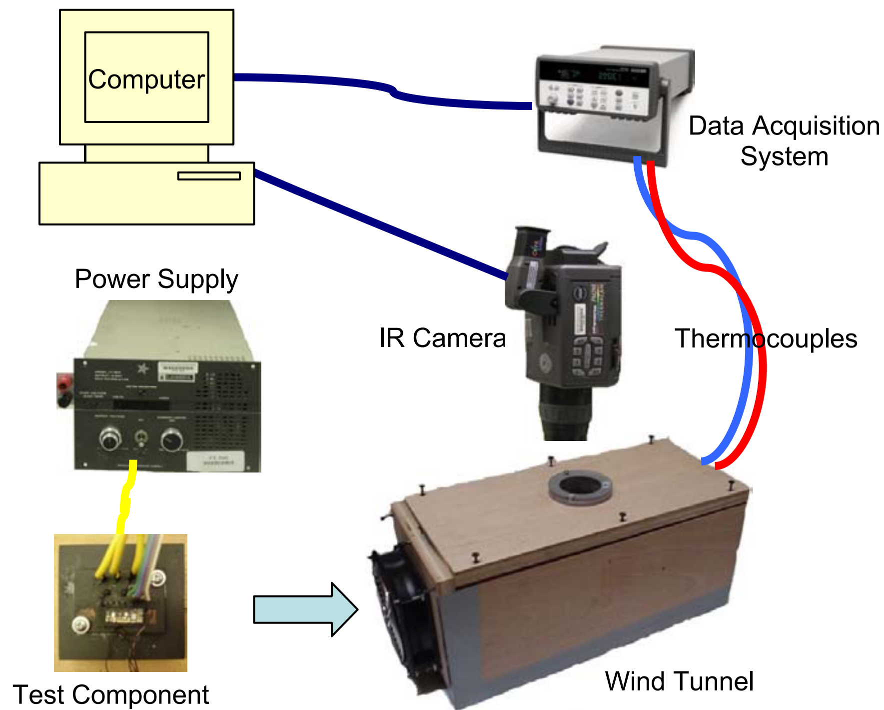

Figure 3.5 Illustration of Experimental Setup

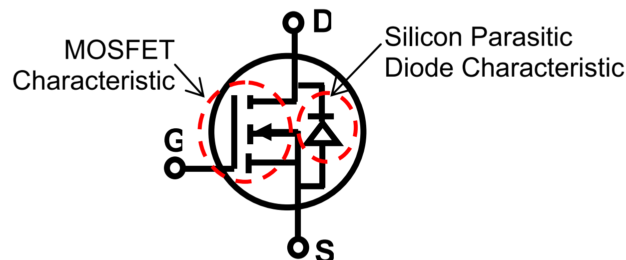

Figure 3.6 Schematic Symbol for a Generic MOSFET Chip

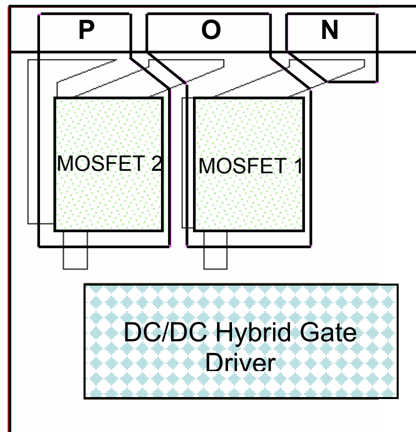

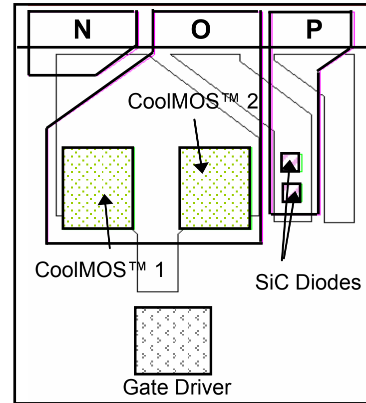

(a) DC/DC IPEM (b) PFC IPEM

Figure 3.7 Electrical Terminals for (a) DC/DC IPEM and (b) PFC IPEM

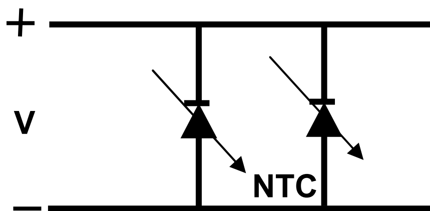

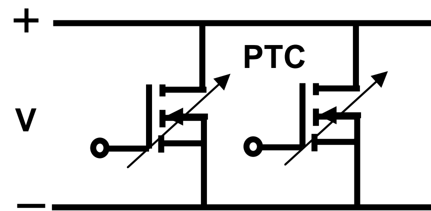

(a) Parallel Connection of Parasitic Diodes Characteristic

(b) Parallel Connection of MOSFET Characteristic

Figure 3.8 Different Effect for Parallel Connection of Parasitic Diodes and MOSFET

3.5 Evaluation of Numerical Results Against Experimental Data

Both the DC/DC and PFC IPEM models were validated. Table 3.6 shows the comparison between the simulated and experimental data with respect to the chip temperatures. In addition, Figure 3.9 shows the infrared images and the simulated temperature distributions of the DC/DC and PFC IPEM. The difference in the maximum temperatures of the chips between the numerical results and the experimental data were within 1.5°C, which resulted in a maximum of 5% difference. With the ambient temperature at 24.2°C, the difference between the numerical results and the experimental

data at the maximum temperature of the module was calculated based on the temperature rise expressed in Eq. 3.3:

$$\%\text{Difference} = \left| \frac{T_{exp} - T_{sim}}{T_{exp} - T_{\infty}} \right| \times 100\% , \quad (3.3)$$

where T_{exp} is the measured temperature from experiments, T_{sim} is the simulated temperature, and T_{∞} is the measured ambient temperature.

The validation shows that the thermal modeling program, ESC, can model the conjugate heat transfer phenomena within a reasonable error. In addition, it is also important to match the temperature distribution from the numerical models with the experimental data within a reasonable difference. In this case, the temperature distributions agreed within 10% difference.

Table 3.6 Comparison Between Simulated and Experimental Data

Heat Source	Max. Simulated Temperature (°C)	Max. Measured Temperature (°C)	Error (%) Relative to Ambient Temperature of 24.2°C
MOSFET 1	45	44	4.6
MOSFET 2	43	42	4.8
CoolMOS 1	86.1	85.8	0.5
CoolMOS 2	86.9	86.6	0.5
SiC Diode 1	78.1	78.9	1.5
SiC Diode 2	84.9	83.8	1.9

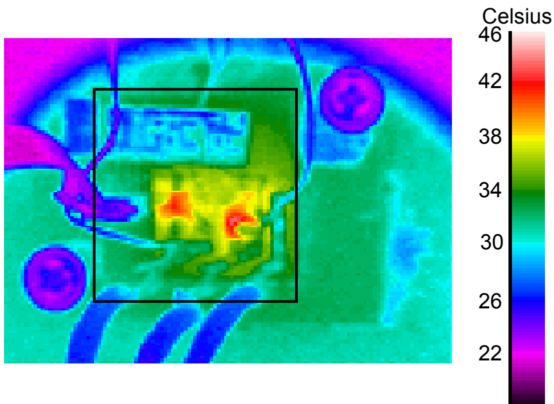

(a) Thermography Image of DC/DC IPEM

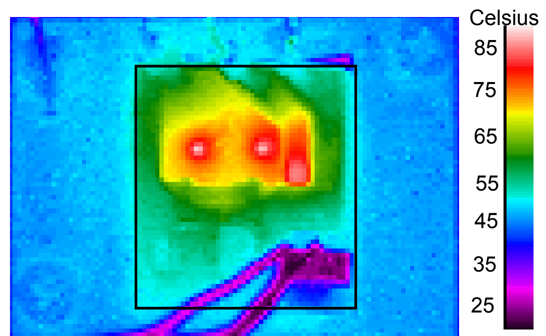

(b) Thermography Image of PFC IPEM

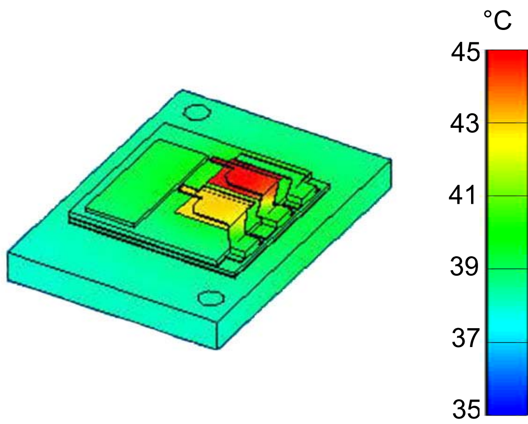

(c) Simulated Temperature Distribution of DC/DC IPEM

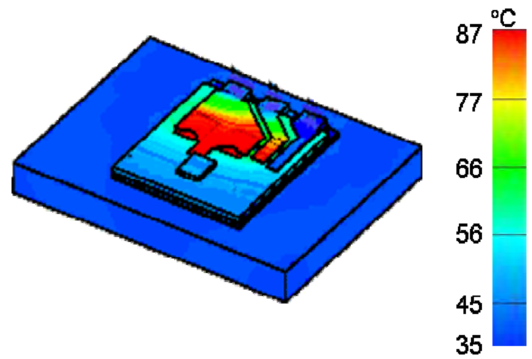

(d) Simulated Temperature Distribution of PFC IPEM

Figure 3.9 Thermography Images and Simulated Temperature Distributions for DC/DC and PFC IPEM

Chapter 4

Thermal Behavior Assessment of Integrated Power Electronics Modules (IPEMs)

The increased heat generation in electronic components can greatly reduce the reliability of the components and increase the chances of malfunction to the components. A good understanding of the thermal behavior of these components can help in deciding on an effective thermal management schemes. To understand their thermal behavior, various methods should be conducted to analyze the thermal performance of the components. These analyses can be conducted using finite element thermal modeling as well as experiments.

Since the finite element models and the thermal boundary conditions varied from case to case, this section discusses the specific details for each case as well as the variations in finite element models from the baseline model discussed in section 3.2. In addition, corresponding experiments for these studies are also discussed. Six studies were performed in this research to examine various design parameters of the IPEMs that would possibly affect the thermal performance of the modules. Table 4.1 describes and lists the objectives of these six studies.

4.1 Study I—Thermal Characterizations

Thermal characterization provides data on the thermal performance of electronic components. The most common thermal characterization parameter used in characterizing electronic components is the thermal resistance. This parameter is a measure of heat flow from the chip to some defined point on the isothermal surface or ambient under specific environmental conditions. Experimental characterization method was presented here to obtain the junction-to-ambient thermal resistance, R_{ja}, of the DC/DC and PFC IPEMs.

Table 4.1 Summary of the Case Studies

Study	Description	Objective
I	Thermal Characterization of IPEMs	To understand the overall thermal performance of the IPEMs
II	Chip-to-chip Distance and Copper Trace Area	To understand the mutual effect among the heating chips
III	DBC Ceramic and Ceramic Carrier Materials Selection	To identify better ceramic materials for use to enhance the heat transfer within the IPEMs
IV	Metallization Interconnect Patterns, Thickness, and Materials	To understand the metallization design parameters on the ability of transferring heat within the IPEMs
V	Polyimide Thickness	To understand the effect of the polyimide thickness on the heat transfer within the IPEMs
VI	Integrated Cooling Mechanisms	To evaluate and introduce integrated cooling strategies for improving the thermal performance of the IPEMs

4.1.1 Experimental and Numerical Characterization

The chips were analyzed at different power levels ranging from 0 W to 30 W experimentally. The experiments were the same as the experiments described in section 3.4. However, only the characterized chip was heated up during the experiments rather than heating all the chips in the module at the same time as described in the previous section. Heat generated in the chips took a finite amount of time to propagate from the junction to the environment surrounding the chips. Therefore, careful attention was given to the amount of time that power was applied to the device to achieve a reasonable steady state condition. The relationship between the temperature rise of the chips and the power loss were then explored. The validated numerical model of the DC/DC and the PFC IPEM discussed in section 3.3 was also used to characterize the IPEMs numerically in conjunction to the experiments.

4.1.2 Evaluation of Thermal Resistance Matrix for Multi-chip Modules

A common figure-of-merit used for the comparison of various thermal designs is the junction-to-ambient thermal resistance, R_{ja}. However, this single parameter cannot effectively describe the three-dimensional heat flow in multi-chip modules. Sofia [62] presented a methodology using the superposition method to superimpose the temperature

fields for different chips within the multi-chip modules. He also mentioned that this method is most accurate for applications which are dominated by conduction.

In this method, independent heat sources can be characterized and measured independently. For a single heat source, the thermal resistance equation can be expressed as $R = \Delta T/Q$, where R is the junction-to-case thermal resistance, Q is the heat loss, and ΔT is the temperature rise of the heat source. The ΔT can be expressed as $\Delta T = T_{hs} - T_{ref}$, where T_{hs} is the temperature of the heat source and T_{ref} is the reference temperature. The reference temperature is referred to a chosen isothermal surface. As Sofia [62] stated, there is no practical way for specifying the isothermal surface. Therefore, any thermal resistance based on the fixed temperature surface is specific to the cooling conditions under which the thermal resistance is determined.

The temperature difference between the heat sources and the case in a multi-chip module is radically affected by the heat dissipation from the neighboring components, the heat paths within the module, and the cooling conditions. By using the superposition method, the junction-to-case thermal resistance for each heat source within the multi-chip module can be described in a matrix form in Eq. 4.1,

$$[R] = \frac{[\Delta T]}{[Q]}. \tag{4.1}$$

For a multi-chip module with 'N' number of heat sources, the [R] will be an N x N matrix. The [Q] and [ΔT] matrices will be column vectors. The elements in [ΔT] represent T_i-T_{ref} for i=1st to Nth heat source. For example, a two heat source module will yield a 2 x 2 thermal resistance matrix in Eq. 4.2:

$$\begin{bmatrix} R_{11} & R_{12} \\ R_{21} & R_{22} \end{bmatrix} \cdot \begin{bmatrix} Q1 \\ Q2 \end{bmatrix} = \begin{bmatrix} \Delta T_1 \\ \Delta T_2 \end{bmatrix} = \begin{bmatrix} T_1 - T_{ref} \\ T_2 - T_{ref} \end{bmatrix}, \tag{4.2}$$

where ΔT_1 is the maximum temperature rise of heat source 1 with only the heat source 1 dissipating heat plus the maximum temperature rise of heat source 1 with only the heat source 2 dissipating heat. Similarly, ΔT_2 is the maximum temperature rise of heat source 2 with only the heat source 1 dissipating heat plus the maximum temperature rise of heat source 2 with only the heat source 2 dissipating heat.

Similarly, the elements in the matrix $\begin{bmatrix} R_{11} & R_{12} \\ R_{21} & R_{22} \end{bmatrix}$ can be expressed by the following:

$$R_{11} = \frac{T_{11} - T_{ref}}{Q_1}, \tag{4.3}$$

$$R_{12} = \frac{T_{12} - T_{ref}}{Q_2}, \tag{4.4}$$

$$R_{21} = \frac{T_{21} - T_{ref}}{Q_1}, \tag{4.5}$$

$$R_{22} = \frac{T_{22} - T_{ref}}{Q_2}, \tag{4.6}$$

where T_{11} is the temperature of heat source 1 with heat dissipation from heat source 1, T_{12} is the temperature of heat source 1 with heat dissipation from heat source 2, T_{21} is the temperature of heat source 2 with heat dissipation from heat source 1, and T_{22} is the temperature of heat source 2 with heat dissipation from heat source 2.

The purpose of this study is to examine the possibility of applying this methodology to IPEMs as well as examine the error of prediction in predicting the junction temperatures of the chips in a multi-chip module with a different heat dissipation rate since the heat transfer within the IPEMs is mainly dominated by conduction. The numerical model used in this study was the validated DC/DC IPEM model described in section 3.3 with different boundary conditions. Therefore, the validated interface conditions and the material properties in the module were not changed in all the cases discussed in this section.

In this study, the bottom surface of the DBC was defined as an isothermal surface of 50°C to satisfy the imposed fixed reference temperature in Eq. 4.1 and Eq. 4.2 although the bottom surface might not be an isothermal surface under the real operating conditions. However, the average temperature on the bottom surface can be taken as the reference temperature during real operating conditions. The T_1 and T_2 are determined by the maximum temperatures of the MOSFET chips in the IPEM.

To determine the thermal resistance matrix for the DC/DC IPEM, two cases with individual heat dissipation of 10 W for both chips were simulated. Different combinations of heat dissipation for the two chips were also simulated. These results were used to compare with the predicted results from the calculation using the thermal resistance matrix obtained earlier.

4.2 Study II—Effect of Chip-to-chip Distance and the Copper Trace Area

Numerical studies were conducted to study the effect of the chip position in the DC/DC IPEM on the thermal performance of the module. In this study, a simplified numerical model was created. Since most of the heat from the chips were conducted through the bottom surface of the chip to the copper traces, from the copper traces to the DBC ceramic, and to the DBC copper due to the high thermal resistance between the sides of the chips and the ceramic carrier as well as the top of the chips and the metallization interconnects, the model created for this study only consisted of the two chips, the copper traces, the DBC ceramic, and the DBC copper.

The top surfaces of the chips were modeled as adiabatic surfaces. Thus, the heat from the chips was expected to flow to the bottom surface of the bottom DBC copper. The bottom surface of the DBC copper was modeled with a heat transfer coefficient of 100,000 W/m^2-K at ambient temperature of 20°C so that all of the heat was transferred to the ambient through the bottom surface of the DBC copper. The minimum size of the copper trace under each chip in the baseline model was 0.5 mm larger than the chip on all four sides, which resulted in ~26.8% larger copper trace area than the chip area of ~63.5 mm^2.

To study the effect of the chip location and the size of the copper trace on the thermal resistance of the IPEM, eleven cases were investigated. In the first six cases, three comparisons were conducted to examine the influence of power loss level of two chips at 3 mm and 6 mm apart in the x direction as shown in Figure 4.1. The first comparison evaluated the temperature rise of the models dissipating 5 W each from the two chips, with chip distance of 3 mm and 6 mm apart, and with the minimum trace area each. The second comparison compared the models with 10 W heat dissipation from

each chip and the third comparison compared the models with 20 W heat dissipation from each chip.

The model with chip distance of 6 mm apart and 5 W heat dissipation from each chip was studied for Case 7 to Case 9. These three studies were conducted to study the effect of enlarging the copper trace area. In Case 7, the copper trace area was expanded in the x direction by 2 mm as illustrated in Figure 4.2 (a). On the other hand, the copper trace area was expanded in the y direction by 10 mm as shown in Figure 4.2 (b) in Case 8. Finally, the copper trace area was expanded in both x and y directions by 2 mm and 10 mm respectively in Case 9 (Figure 4.2 (c)). The expansion of the copper trace area in the x and y directions were mainly restrained by the overall footprint of the DC/DC IPEM. Based on the current footprint of the DC/DC IPEM, the expansion was limited by 2 mm in the x direction and 10 mm in the y direction in these studies.

Case 10 and Case 11 examined the location of the chips on the copper trace area with chip-to-chip distance of 6 mm. In Case 10, MOSFET 1 was maintained at the same position while MOSFET 2 was moved 10 mm in the –y direction resulted in the chip-to-chip distance of 1.16 mm in the y direction as shown in Figure 4.3 (a). In Case 11, MOSFET 1 was moved 2 mm in the –x direction while MOSFET 2 was moved 2 mm in the +x direction from the position in Case 10. This resulted in the chip-to-chip distance of 1.16 mm in the y direction and 10 mm in the x direction (Figure 4.3 (b)). The heat dissipation from the chips was 5 W each in both cases. All eleven cases in this section are summarized in Table 4.2.

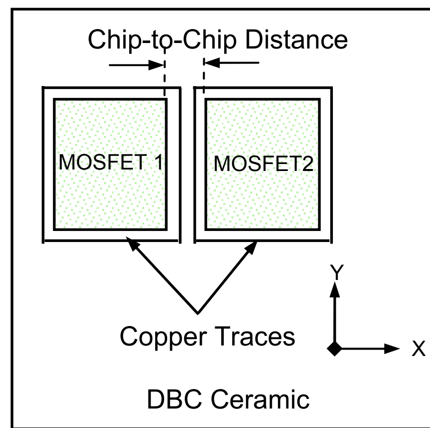

Figure 4.1 Layout for Case 1-6 Studying the Effect of the Chip-to-chip Distance

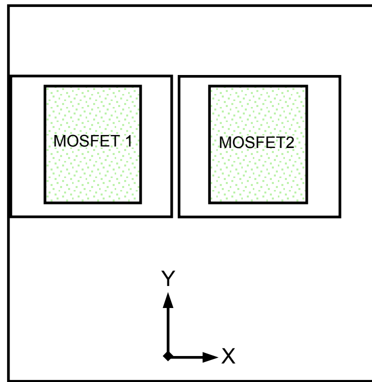

(a) Copper Trace Area Expansion in x Direction by 2 mm

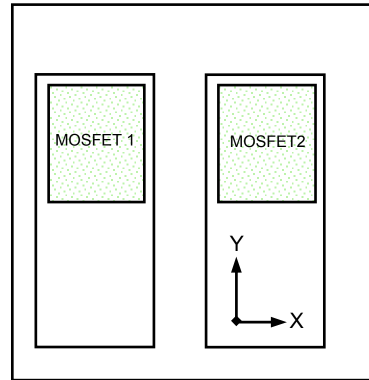

(b) Copper Trace Area Expansion in y Direction in 10 mm

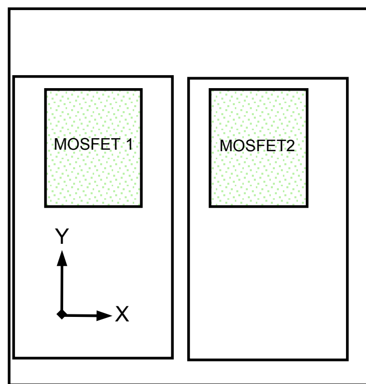

(c) Copper Trace Area Expansion in x Direction

Figure 4.2 Study on Copper Trace Layout for Case 7-9 with 6 mm Chip-to-Chip Distance

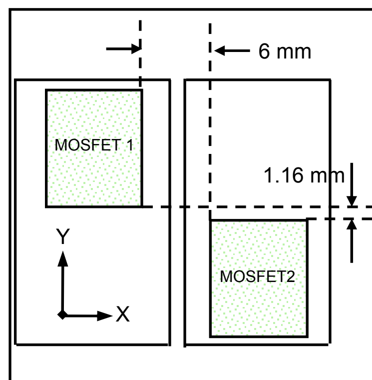

(a) Layout for Case 10—Moved MOSFET 2

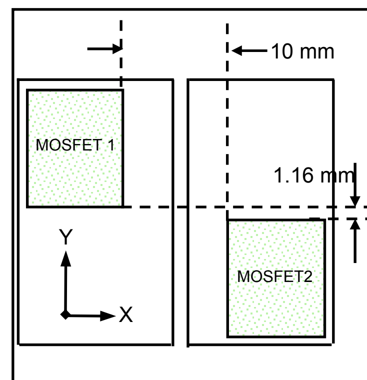

(b) Layout for Case 11—Moved MOSFET 1 and MOSFET 2

Figure 4.3 Layouts on Chips Locations for Case 10 and Case 11 with 6 mm Chip-to-Chip Distance

Table 4.2 Parameters Specifications in Investigating the Effects of Chip Locations on the Thermal Performance of DC/DC IPEM

Case	Power Loss (W)			Chip-to-Chip Distance (mm)		Copper Trace Area Expansion		Moved MOSFET	
	5	10	20	3	6	In ±x Direction at 2 mm	In -y Direction at 10 mm	MOSFET 1	MOSFET 2
Baseline									
1	x			x					
Study 1									
2	x				x				
3		x		x					
4		x			x				
5			x	x					
6			x		x				
Study 2									
7	x				x	x			
8	x				x		x		
9	x				x	x	x		
Study 3									
10	x				x	x	x		x
11	x				x	x	x	x	x

4.3 Study III—Selection of DBC Ceramic and Ceramic Carrier Materials

A number of ceramic substrates are available for active IPEMs to form high density interconnects. In this study, we examined the thermal performance of the PFC IPEM including alumina, aluminum nitride, and ALOX[1]™ substrate materials. Three models with different combinations of ceramic materials were studied and compared to the baseline model (Case 1) using alumina for the DBC ceramic as well as the ceramic carrier. In Case 2, an aluminum nitride substrate replaced the alumina substrate as the ceramic carrier while keeping the alumina DBC ceramic substrate. Similarly, ALOX™ substrate was used in Case 3 to replace the alumina ceramic substrate in Case 1. ALOX™ substrate features a solid aluminum core and 20 μm thick of oxidized

[1] ALOX is a trademark of Micro Components Ltd.

aluminum surface for electrical isolation as shown in Figure 4.4. Finally, aluminum nitride was used for the DBC substrate as well as the ceramic carrier in Case 4. Table 4.3 summarizes the models developed in this study.

Since our interest was in searching for better thermal solutions for the module itself, the heat sink and the enclosure of the electronic system were not modeled. Instead, an equivalent convective condition for a fixed heat sink surface area was defined in the finite element model by defining an overall heat transfer coefficient at the bottom surface of the DBC copper base. Similarly, the top surface of the module was maintained as an adiabatic surface as discussed in section 3.2. The heat sink had a size of 73 mm (W) x 73 mm (L) x 32 mm (H) with a 7 mm thick base plate and ten 1.5 mm thick fins. The heat transfer coefficient on the heat sink was 25 W/m^2-K and the ambient temperature was 50°C. The convection from the heat sink to the ambient is defined by Eq. 4.7,

$$Q = h_s \cdot A_s \cdot (T_{sink} - T_\infty), \qquad (4.7)$$

where Q is the total power loss, h_s is the average heat transfer coefficient on the heat sink, A_s is the total heat convecting area of the heat sink, T_{sink} is the heat sink temperature, and T_∞ is the ambient temperature. We can then define the overall heat transfer coefficient, U, at the bottom surface of the DBC copper, A_{DBC}, using Eq 4.8,

$$h_s \cdot A_s = U \cdot A_{DBC}. \qquad (4.8)$$

The power losses for the heat sources in the model are listed in Table 4.4.

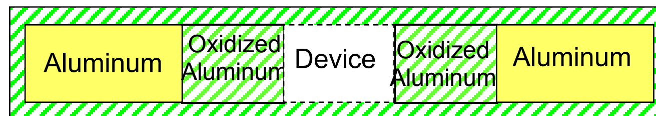

Figure 4.4 Schematic of ALOX™ Substrate

Table 4.3 Models Developed for Studying Different Ceramic Materials

Case	Ceramic Material (DBC Ceramic/Ceramic Carrier)
1 (Baseline)	Al_2O_3/ Al_2O_3 Substrate
2	Al_2O_3/AlN Substrate
3	Al_2O_3/ALOX™ Substrate
4	AlN/AlN Substrate

Table 4.4 Power Losses Specified in Study III

Heat Source	Power Loss (W)
CoolMOS 1	7.8
CoolMOS 2	7.8
SiC Diode 1	4.52

4.4 Study IV—Metallization Layer

In today's power electronics modules, power semiconductor devices such as MOSFET chips and IGBT chips are interconnected via wire bonds. This is not suitable for advanced three-dimensional integration as well as advanced thermal management. Over the last few years, a planar interconnect technique has been developed to enable the construction of three-dimensional integrated power electronics modules such as the metallization bonding used in the IPEMs. While the planar interconnect technique offers some dominant advantages, reliability issues need more attention because thermo-mechanical stress can lead to the degradation of the interconnections. Differences in the coefficient of thermal expansion (CTE) of multi-layers with dissimilar materials expand and contract at different rates on heating and cooling that lead to thermo-mechanical failures. In general, these thermo-mechanical failures include defects, cracks, and peeling of the layers within the module.

To understand the reliability of the metallization layers in Embedded Power modules, thermally induced stresses in the metallization layers have to be evaluated. The cohesive failure of the interface delamination between the chips and the deposited metallization layer can degrade the thermal performance and the reliability of the module. Thus, a proper design of chip-metallization contact should simultaneously satisfy the thermal requirement and the mechanical integrity between the chip and the metallization layer. This section specifically studies (a) the shape and contact areas of the interconnection on the chip, (b) the metallization thickness, and (c) the material properties of the metallization.

To reach a better understanding of the thermal and thermo-mechanical behavior of the metallization layer in Embedded Power modules, the PFC IPEM was chosen as a

study case. Both thermal and thermo-mechanical stress simulations were performed using I-DEAS™. For thermal simulations, the thermal model and the boundary conditions described in section 4.3 were also used in this study. However, aluminum nitride was chosen as the ceramic carrier material in the models investigated in section 4.4.1 and 4.4.2. As for the studies in section 4.4.3, aluminum nitride substrate was used for both the DBC ceramic as well as the ceramic carrier.

The stress simulations were conducted using the structural analysis within I-DEAS. In embedded power modules, more than 70% of the copper deposition is on top of the top polyimide layer. Due to the low Young's modulus of the polyimide, the polyimide can function as a buffer layer to absorb the thermally induced stress. It was shown in [71] that the critical stress was on the top surface of the silicon where the two rigid materials, silicon (chip) and copper (metallization), were in contact. Therefore, only the silicon chip, the top polyimide layer, and the metallization layer were considered in the stress model as shown in Figure 4.5 (a). Since the interconnect area had covered 40% of the SiC diode top area with one 1 mm diameter interconnect via hole on the 1.4 mm x 1.4 mm SiC diode's top surface, no study was done on the interconnect pattern on the SiC diodes. Therefore, the focus of this study was only on the interconnect pattern on the CoolMOS™.

In the stress model, the intrinsic residual stress at 20°C was assumed to be zero since the metallization layer is electroplated onto the top surface of the silicon at 20°C. The temperature of the structure was increased from 20°C to 100°C uniformly. The type of element used for the stress simulations is solid parabolic tetrahedron. A point located at the center of the bottom surface of the CoolMOS™ chip was fully constrained (translational and rotational) in all directions. In addition, a point located at the corner of the chip illustrated in Figure 4.5 (b) was also constrained in the z direction.

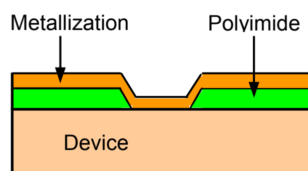

(a) Stress Model

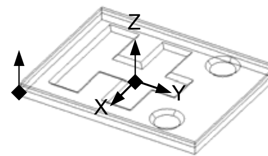

(b) Boundary Conditions

Figure 4.5 Stress Model and Boundary Conditions for Stress Simulations

4.4.1 Metallization Interconnect Patterns

It is believed that large interconnect area between the chip and the metallization layer can provide higher heat transfer. To investigate the effect of the interconnect pattern on the thermal performance and the thermal stress, three patterns shown in Figure 4.6 were selected. These patterns were selected based on the current available interconnect patterns on the chips defined by the chip manufacturers. The first interconnect pattern had 6 interconnect via holes with diameter of 0.6 mm on the CoolMOS™ chip. The second interconnect pattern had 9 interconnect via holes with diameter of 0.6 mm and the third pattern had a rectangular pattern. Table 4.5 summarized the total heat transfer area for each pattern.

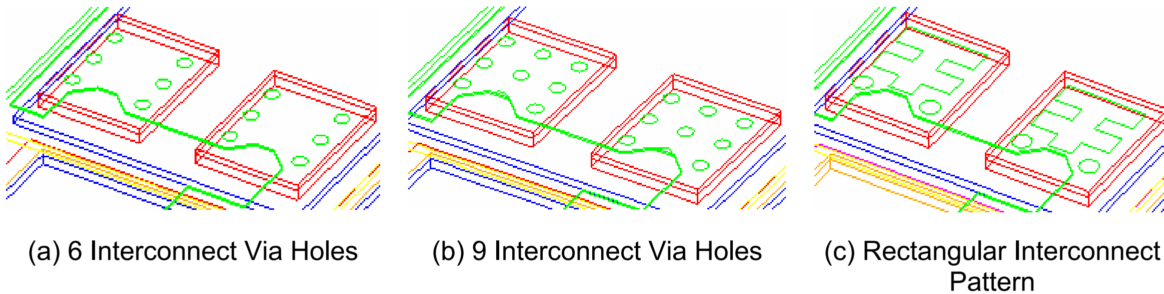

(a) 6 Interconnect Via Holes (b) 9 Interconnect Via Holes (c) Rectangular Interconnect Pattern

Figure 4.6 Three Studied Interconnect Patterns: (a) 6 Interconnect Via Holes, (b) 9 Interconnect Via Holes, and (c) Rectangular Interconnect Pattern

Table 4.5 Total Contact Area for the Metallization Layer on the Heat Source for Different Interconnect Patterns

Case	Interconnect Pattern	Total Contact Area (mm^2)
1	6 Interconnect Via Holes	1.7
2	9 Interconnect Via Holes	2.5
3	Rectangular Pattern	9.4

4.4.2 Metallization Thickness

To study the significance of the metallization thickness on the thermal and thermo-mechanical behavior of the module, nine cases were examined against the baseline model. In this case, the baseline model consists of the rectangular pattern described in section 4.4.1 and a metallization thickness of 0.076 mm. In these 9 cases, the baseline metallization thickness was increased by 20%, 40%, 60%, 80%, 2x, 4x, 8x, 16x, and 32x. These cases are summarized in Table 4.6.

4.4.3 Metallization Materials

Material properties have always played an important role in the thermal and thermo-mechanical behavior of power electronics components. While the Young's Modulus describes the stiffness of the material and the Poisson's ratio describes the ratio of lateral strain and axial strain, the two concerned metallization material properties in this study are the high thermal conductivity and the matching of the coefficient of thermal expansion (CTE) with silicon. Three available materials were considered in this study. These materials were aluminum, molybdenum, copper, and silver in which copper metallization was the baseline model in this case. Table 4.7 lists the thermal conductivities, the CTE, the Young's Modulus, and the Poisson's ratio for these materials.

Table 4.6 Investigated Cases to Study the Significance of Metallization Thickness

Case	Description
1 (Baseline)	Baseline Model with Baseline Metallization Thickness 0.076 mm
2	1.2x Baseline Metallization Thickness
3	1.4x Baseline Metallization Thickness
4	1.6x Baseline Metallization Thickness
5	1.8x Baseline Metallization Thickness
6	2x Baseline Metallization Thickness
7	4x Baseline Metallization Thickness
8	8x Baseline Metallization Thickness
9	16x Baseline Metallization Thickness
10	32x Baseline Metallization Thickness

Table 4.7 Generic Material Properties at 300K for the Study on Metallization Materials

Material	Thermal Conductivity (W/m-K)	CTE (μm/m-C)	Young's Modulus (GPA)	Poisson's Ratio
Aluminum	170	23.5	69	0.33
Copper (Baseline)	395	16.4	110	0.34
Molybdenum	138	6	330	0.32
Silver	410	19.9	76	0.39
Silicon	118	2.22	185	0.28
Polyimide	0.3	10	14	0.35

4.5 Study V—Significance of Polyimide Layer

Polyimide layers were added to the IPEMs for electrical insulation as well as providing planarity for depositing the next layer in the packaging process. The thickness of the polyimide is highly constrained by the available thin-film technology during the IPEMs packaging process. A thick polyimide layer can result in high thermal resistance and increase module thermal resistance. In this study, the effect of the polyimide thickness on the thermal performance of the IPEMs was studied. Current polyimide thickness is 0.127 mm for both layers illustrated in Figure 3.3 (b). The smaller the polyimide thickness, the smaller the particular layer will contribute on the overall package thermal resistance.

In this study, a reduced polyimide thickness of 0.02 mm was investigated. In Case 1, the thicknesses of both polyimide layers were reduced from 0.127 mm to 0.02 mm. To further identify the polyimide layer that has a larger influence on the thermal performance of the active IPEMs, two other cases were studied. In Case 2, only the thickness of the top polyimide layer was reduced while keeping the thickness of the bottom polyimide layer at 0.127 mm. In contrast, only the thickness of the bottom polyimide layer was reduced in Case 3. The thermal model and the boundary conditions described in section 4.3 were also used in this study. In all three cases, an aluminum nitride ceramic substrate was used for the DBC ceramic and the ceramic carrier.

4.6 Study VI—Evaluation of Integrated Cooling Mechanisms for IPEMs

As a general trend in power electronics, packaging is shrinking and more functionality is integrated into closely packed structures, thus increasing the demands on the thermal management of power electronics. Recognizing the inherent need for the thermal design of the active IPEMs, this section presents some of the thermal management options which will lead to the achievement of integrated cooling mechanisms in the active IPEMs.

There are many different approaches for achieving such integrated cooling. These strategies include the employment of integrated heat pipes, radiant cooling, or better interface materials. To achieve integrated cooling in the structure of the active IPEMs, this research investigated several possible integrated thermal management options. We first identified the heat path within the structure of the active IPEMs. With known hotspots and high thermal resistance heat paths, we worked on various ways to reduce the hotspots by reducing the thermal resistances in the major heat paths. The baseline model in this study refers to the model described in section 3.2 in which alumina substrates were used as the DBC ceramic as well as the ceramic carrier.

4.6.1 Structural Enhancement

To create an additional heat path from the hotspot to the ambient, an alumina substrate was added to the IPEM structure from the top of the metallization on top of the SiC diode 1 to the DBC copper trace in the first studied case. In the second case, an alumina substrate was connected from the top of the metallization on the SiC diode 1 to the heat sink. It is important to remember that any modification to the IPEM structure can change the characteristic of the IPEMs in the aspects of the electrical, mechanical and thermal performances. Figure 4.7 shows the structural enhancements investigated in this study.

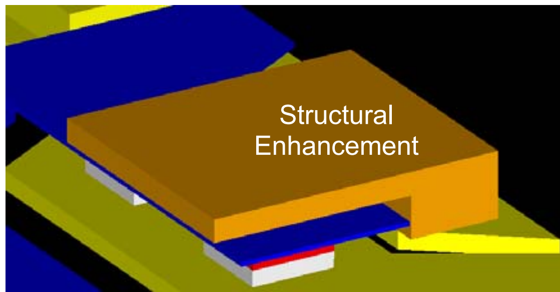

(a) Structural Enhancement from Metallization to Copper Trace

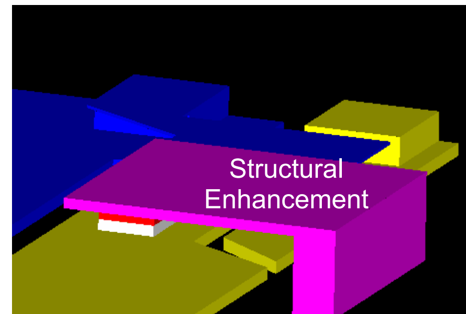

(b) Structural Enhancement from Metallization to Heat Sink

Figure 4.7 Illustration of Structural Enhancement on PFC IPEM

4.6.2 Double-sided Cooling

Thermal design of the integrated cooling mechanisms is full of distinct challenges. The first is to fulfill the ability to integrate the cooling mechanisms into the module but not increase the profile height of the module. The second is to be able to integrate the fabrication process and the assembly of the cooling technology into the fabrication process of the active IPEMs without complicating the number of processing steps. To meet these challenges, different feasible thermal designs and strategies were investigated using thermal simulations. This included the implementation of double-sided cooling on the active IPEMs.

The Embedded Power packaging technology and the metallization interconnects offer a great way of using double-sided cooling to further improve the thermal performance of the active IPEMs. The Embedded Power packaging not only eliminates the use of wire bonds for interconnects but also provide a flat area on top of the module that can easily be used for implementing double-sided cooling. To enable the double-sided cooling on the PFC IPEM, a DBC substrate was soldered to the top metallization layer. The size of the top DBC was 19 mm (L) x 19 mm (W) x 1.2 mm (t) with a 0.635 mm thick aluminum nitride substrate sandwiched between two 0.305 mm thick copper. With the ceramic substrate in the DBC served as an electrical insulator, the top copper layer of the top DBC substrate allowed to be exposed to ambient. Thus, a heat sink could

be brazed to the top as well as the bottom surface of the PFC IPEM. In addition, other advanced cooling methods such as liquid cooling, spray cooling, and jet impingement can also be implemented on the top surface of the module to achieve the double-sided cooling effect. Figure 4.8 illustrates the concept of double-sided cooling for an active IPEM.

To investigate the significance of the top DBC on the double-sided cooling effect, two finite element models were created to examine several commercially available ceramic substrate materials for the top DBC. Again, these ceramic substrates were alumina ceramic and aluminum nitride ceramic substrates. In addition to DBC, Thermal Clad[2]™ substrates were also investigated in exploring better substrate for top side cooling. The Thermal Clad™ substrate is an insulated metal substrate[3]™ (IMS) with three layers: aluminum or copper base, dielectric layer, and circuit layer illustrated in Figure 4.9. The material properties and the thickness of the individual layer in the Thermal Clad are summarized in Table 4.8.

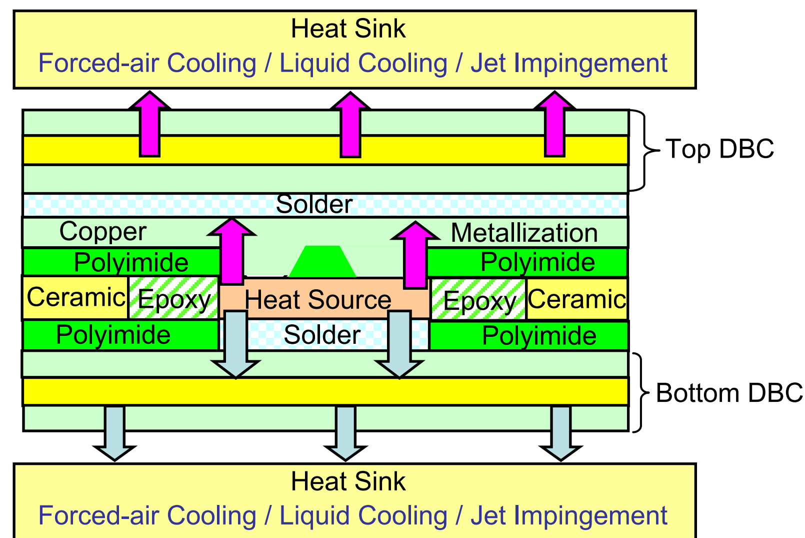

Figure 4.8 Illustration of Double-sided Cooling for an Active IPEM

[2] Thermal Clad is a trademark of The Bergquist Company
[3] IMS is a trademark of Sanyo Electric Co., Ltd.

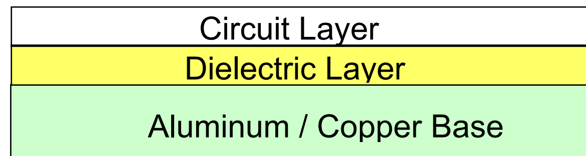

Figure 4.9 Schematic of Thermal Clad™ Substrate

Table 4.8 Material Properties of Thermal Clad™

Layer	Material	Thermal Conductivity (W/m-K)	Thickness (μm)
Circuit	Copper	388	35
Dielectric	Bergquist	3	75
Base	Aluminum	167	1000
	Copper	388	1000

Table 4.9 lists the four models investigated in this study. The finite element models created in this study were similar to the finite element models described in section 4.3. Both the bottom DBC surface and the top DBC surface were modeled as an equivalent convective condition of 25 W/m^2-K for a fixed heat sink surface area at ambient temperature of 50°C. Since the top DBC surface was smaller than the bottom DBC surface, the heat sink brazed on the top DBC was also relatively smaller than the bottom heat sink.

4.6.3 Assessment on Double-sided Cooling Experimentally

In addition to the numerical studies described in section 4.6.2, experiments were also conducted to study the advantages of double-sided cooling for IPEMs. By using the similar experiment setup described in section 3.2, three different cases were studied using DC/DC IPEM. Two prototypes were fabricated for the experiments. The first prototype, Module A, was the original DC/DC IPEM. The second prototype, Module B, had additional DBC substrate soldered onto the top of the DC/DC IPEM. Module B was also used in the third case study by adding additional heat spreaders on both the top and

bottom of the module. Interface material, Sarcon[4]® thermal gap filler pads with thermal conductivity of 7 W/m-K, were placed between the prototype and the heat spreaders to enhance the heat transfer from the module to the heat spreaders. Figure 4.10 shows the prototypes for all three cases.

In all three experiments, one thermocouple was placed at the inlet of the wind tunnel to measure the ambient temperature. To avoid disturbance of the heat flow within the modules, no thermocouples were embedded into the modules. In Case I, two thermocouples were attached on the backside of the module as shown in Figure 4.11 (a). On the other hand, three thermocouples were attached on the backside of the module in the second experiment as illustrated in Figure 4.11 (b). Finally, six thermocouples were used in the third experiment to obtain real-time temperature of the module at different locations (Figure 4.11 (c)). To avoid the effect of heat sink on the heat transfer from the module to the ambient, no heat sink was used in all three experiments. To ensure equal airflow on both the top and bottom surfaces of the module, the module was placed at the center of the wind tunnel supported by an insulated stand as shown in Fig. 4.12.

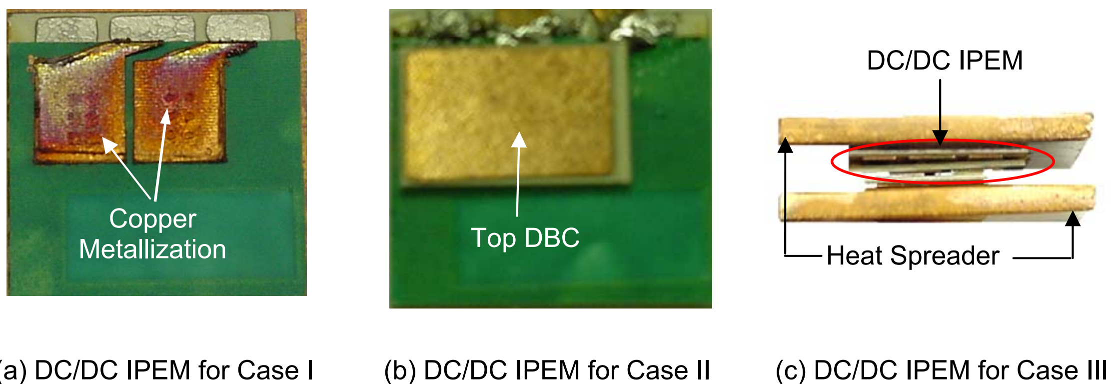

(a) DC/DC IPEM for Case I (b) DC/DC IPEM for Case II (c) DC/DC IPEM for Case III

Figure 4.10 Prototypes for Double-sided Cooling Experiments

[4] Sarcon is a registered trademark of Fujipoly

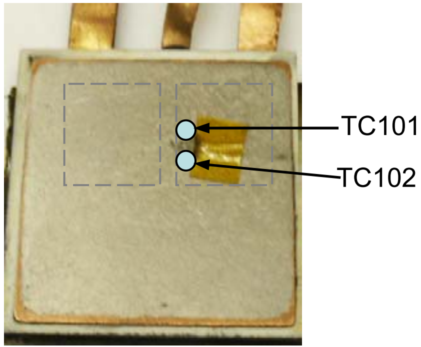

(a) Case I—DC/DC IPEM

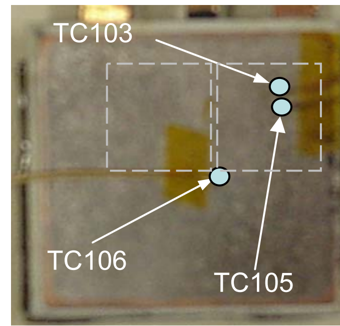

(b) Case II—DC/DC IPEM with Top DBC

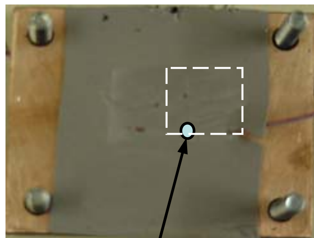

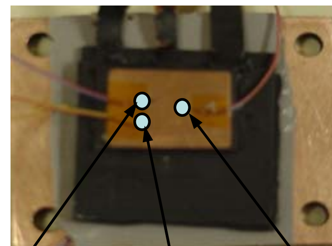

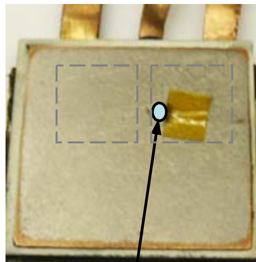

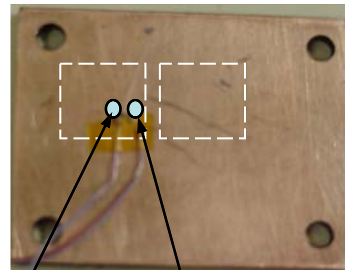

(c) Case III—DC/DC IPEM with Copper Heat Spreader

Figure 4.11 Locations of Thermocouples on the Prototype

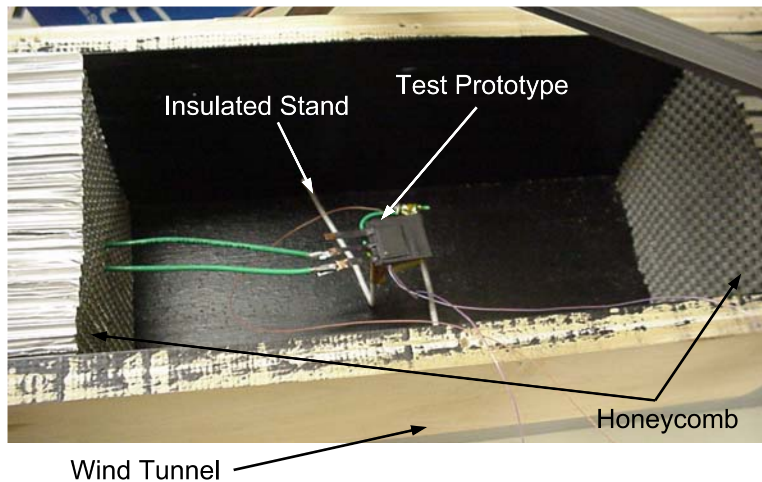

Figure 4.12 Placement of the Module during Experiment

4.6.4 Micro-channel Cooling

With heat loss density continues to rise, micro-channel liquid cooling has become a major consideration in the thermal management of electronic components. Cooling liquid is pumped through the micro-channels to remove the heat from the electronic components. High heat transfer coefficients can be achieved in micro-channel cooling by either increasing the liquid flow rate or decreasing the hydraulic diameter. Micro-channel liquid cooling offers additional benefit of superior liquid thermal properties compared to forced-air cooling. However, this application is limited by the pumping power limit due to the high pressure drop. A preliminary study on the micro-channel cooling was conducted in this research to assess the advantages of using micro-channel cooling for IPEMs.

The advantages of the additional DBC soldered onto the metallization have been discussed in section 4.6.2. However, additional advantage can be obtained by implementing liquid cooling on the top side of the top DBC. To further reduce the temperature rise of the hotspots within the PFC IPEM, implementation of liquid cooling on the top side of the top DBC was studied. To attain integrated cooling mechanism within the module, two different ways of implementing micro-channel on the module were studied using finite element modeling.

The first study employed a copper cap with etched channels in the copper cap for liquid cooling as illustrated in Figure 4.13. This copper cap covered the top side of the module as well as connected to the bottom heat spreader. Six channels with diameter of 1.5 mm and 50 mm long were created in the copper cap and covered the top surface area of the module. In this study, the finite element model was similar to the one described in section 4.3 with the same convection condition on the bottom surface of the DBC. However, the equivalent heat transfer coefficient was defined on the bottom surface of the copper heat spreader rather than the DBC with adjusted value based on the bottom surface area of the copper heat spreader. The size of the heat spreader was 38 mm (L) x 50 mm (W) x 3 mm (t). On the other hand, the top surface of the copper cap was defined with a heat transfer coefficient of 25 W/m^2-K. The ambient temperature was maintained at 50°C. In this study, the liquid flowed in the channels from one side and exited from the other side of the channels. The inlet condition was defined with a pressure rise of 12 kPa while the outlet of the channels was vented to the ambient condition. The specified boundary conditions are illustrated in Figure 4.13. Water was used as the coolant in this study.

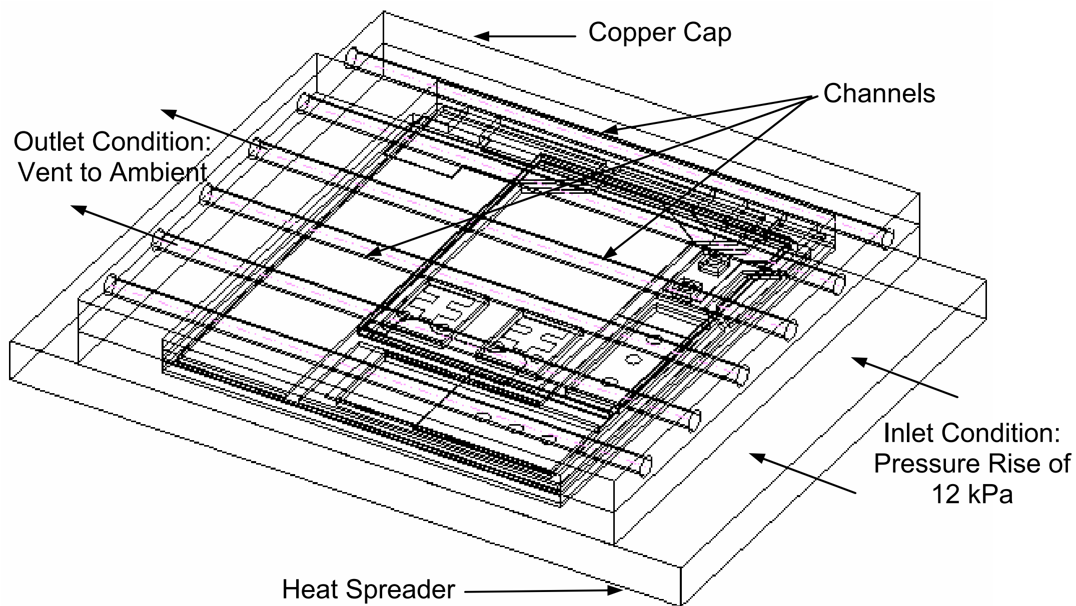

Figure 4.13 Illustration of Copper Cap for the PFC IPEM

To further investigate the effect of liquid cooling on the improvement in the thermal performance of the module, an additional channel layout was also studied. In this second case, the channel layout in Case 1 was modified. Two channels were laid on top of the heat sources, the CoolMOS™ chips and the SiC diode, within the copper cap as illustrated in Figure 4.14. In this case, the inlet liquid condition was modeled with a constant volume flow rate of 0.0003 m^3/s while the outlet was vented to the ambient of 50°C. Again, the channels had a diameter of 1.5 mm. The top surface of the copper cap was defined with a heat transfer coefficient of 25 W/m^2-K.

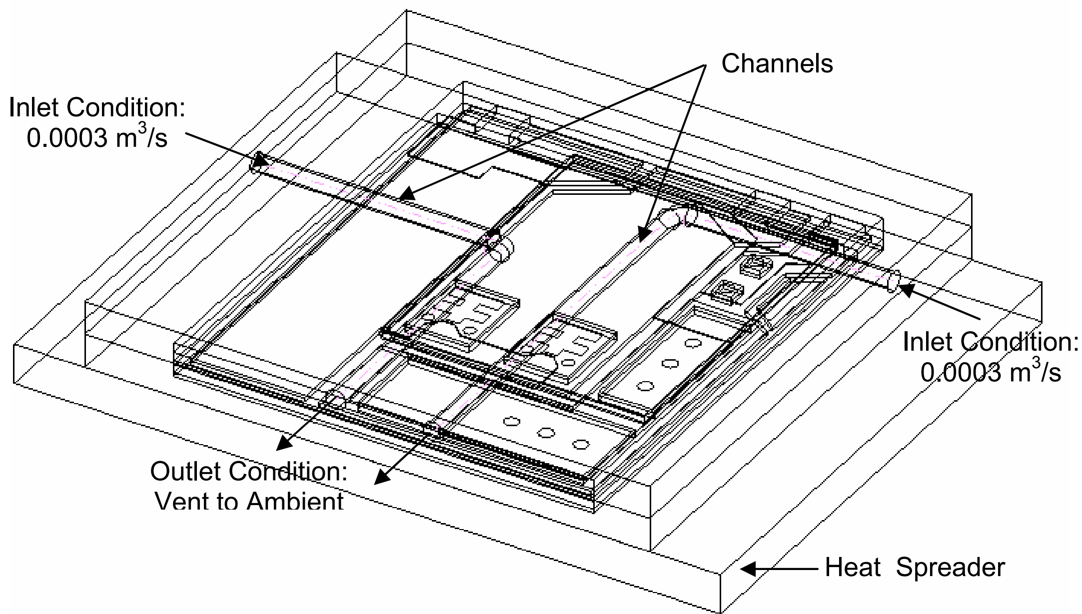

Figure 4.14 Illustration of Channels on Top of Hotspots for the PFC IPEM

Chapter 5

Results and Discussions

Independent of its application, the hottest part in any electronic system most likely is going to be the semiconductor chip. The trend towards increasing heat flux at the module level is continuing. The desire to increase performance by reducing the chip operating temperatures creates a further challenge in the thermal designs. Most of the semiconductor bare chips can be packaged using different packaging technologies such as commonly used QFPA, BGA, and PGA. While the thermal behaviors of these packages are well studied, this research chose to focus on studying the thermal behavior of an innovative packaging technology—Embedded Power.

Since that majority of the thermal resistance of the junction-to-ambient in many common environments is within the package itself, understanding of the role of the package is critical for determining the thermal behavior of the module, especially the effects on the junction temperature. In addition, a good understanding on the package can also help in redesigning the package for better thermal performance, thus reducing the package thermal resistance. While the goals of the studies described in Chapter 4 were to have better understanding on the thermal behavior of the Embedded Power modules, this chapter discusses the results from the studies and provides an insight on the thermal behavior of the Embedded Power modules.

5.1 Thermal Characterization

5.1.1 Experimental and Numerical Characterization

Repeated tests were performed to ensure the reproducibility of the experimental measurements before recording the actual data. Ten readings were taken at each power level. The performance characteristics of the chips in the DC/DC IPEM are presented in the form of chip temperature rise, ΔT, versus power loss. The temperature rise is defined

as $\Delta T = T_{max}-T_{inlet}$, where T_{max} is the maximum die temperature and T_{inlet} is the inlet air temperature.

In the power loss range from 0 W to 30 W, the corresponding maximum temperature rise for the chips of the DC/DC and the PFC IPEM are shown in Figure 5.1 and Figure 5.2 respectively. A line is fitted through the collected data to represent the relationship between the chip temperature rise and the power loss. The slope of the fitted line characterizes the thermal resistance from the chip to the ambient, R_{ja}. Table 5.1 summarizes the R_{ja} of the chips in DC/DC and PFC IPEMs. We can see from Table 5.1 that the R_{ja} of MOSFET 2 is larger than MOSFET 1 while both MOSFET chips have the same material properties. Therefore, it is believed that the location of the chips in the DC/DC IPEM can affect the R_{ja} of the two similar MOSFET chips in a module. Similarly, the R_{ja} of the SiC diodes are larger than the CoolMOS™ chips simply because the conduction area of the SiC diodes is much smaller than the CoolMOS™ chips; thus increasing the thermal resistance of the solder interface between the SiC diodes and the copper trace as well as the epoxy interface between the SiC diodes and the ceramic carrier. From the results summarized in Table 5.1, the users can predict the maximum temperature of the chips with the desired power loss under forced air cooling or for a given maximum operating temperature.

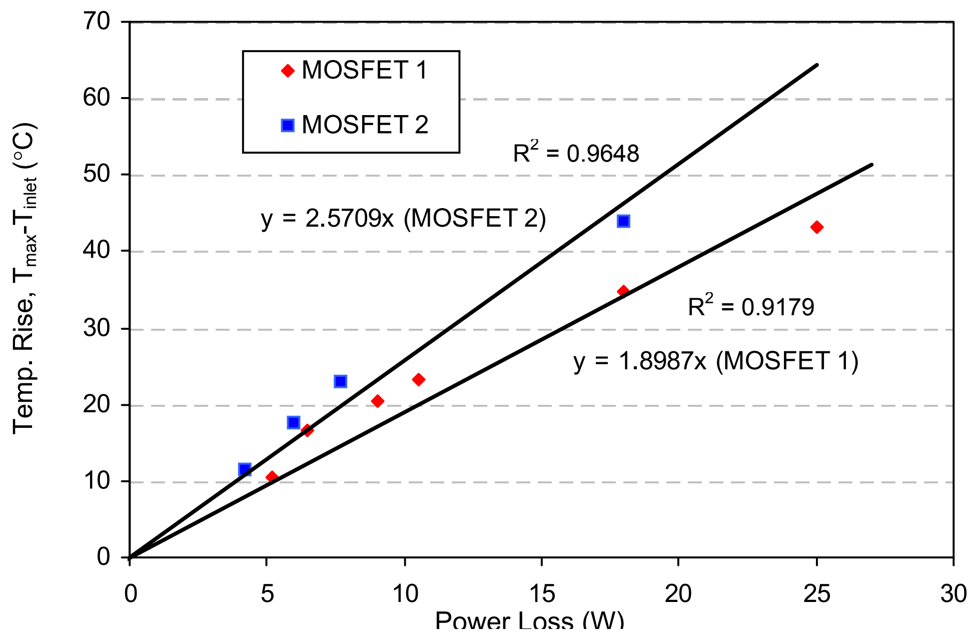

Figure 5.1 Thermal characterization of DC/DC IPEM

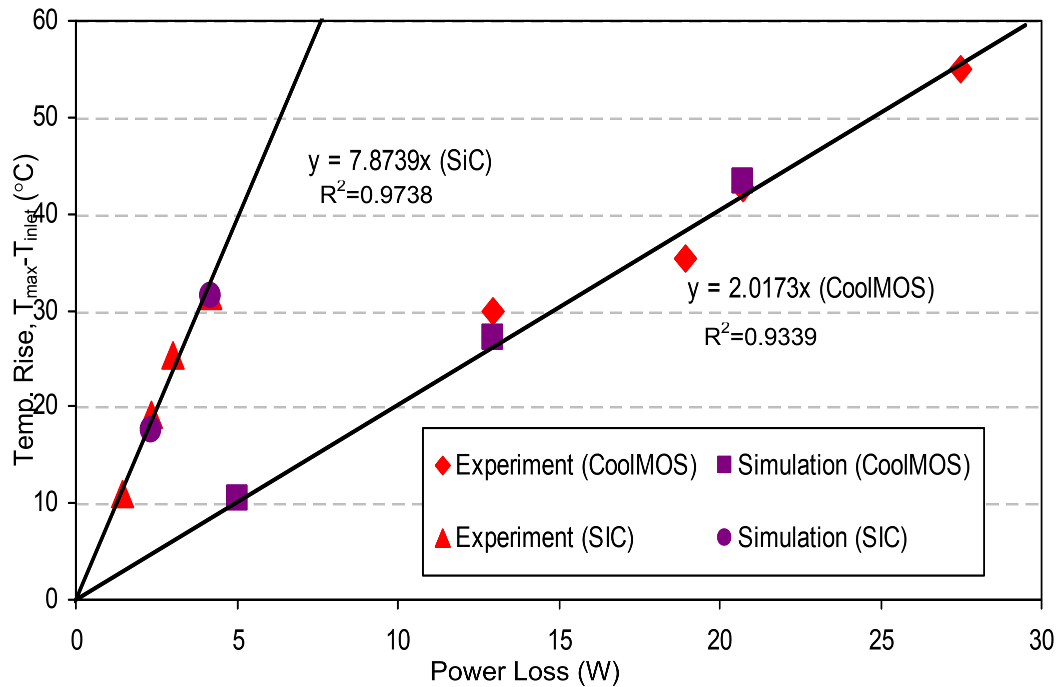

Figure 5.2 Thermal Characterization of PFC IPEM

Table 5.1 Comparison of R_{ja} of Different Chips in DC/DC and PFC IPEM

Description	R_{ja} (°C/W)
MOSFET 1 (DC/DC)	1.9
MOSFET 2 (DC/DC)	2.8
CoolMOS™ (PFC)	2.0
SiC Diodes (PFC)	7.9

5.1.2 Evaluation of Thermal Resistance Matrix for Multi-chip Modules

A preliminary evaluation was conducted using numerical models to study the application of thermal resistance matrix proposed by Sofia [62] in multi-chip modules such as IPEMs. By following the proposed methodology as outlined in section 4.1.2, a resistance matrix for the DC/DC IPEM $[R]=\begin{bmatrix}0.5 & 0.08\\ 0.1 & 0.52\end{bmatrix}$ was obtained. Different combinations of power levels ranging from 7 to 30 watts for both MOSFET chips were also evaluated. Table 5.2 listed the prediction error using the resistance matrix compared to the simulated numerical finite element results. The error was calculated using Eq. 5.1:

$$\%Error = \frac{T_{sim} - T_{matrix}}{T_{sim} - T_{ref}} \times 100\% , \tag{5.1}$$

where T_{sim} is the maximum temperature of the chip from the simulated numerical model, T_{matrix} is the predicted junction temperature of the chip using the resistance matrix, and T_{ref} is the reference temperature. The results show that the predicted errors range from 1.5% to 21% with average of 5.5% depending on the heat dissipation levels of the two heat sources.

It is also observed that the maximum temperature of MOSFET 2 can be predicted more accurately than MOSFET 1. A higher error (21%) was obtained when the heat dissipation from MOSFET 1 was much lower than MOSFET 2 (MOSFET 1:10 W, MOSFET 2:30 W). This is mainly because of the non-symmetrical heat source location in the module and because the positions of the two heat sources in the module skewed more towards MOSFET 1. While maintaining the heat dissipation from MOSFET 1 at 10 W, the thermal resistance matrix under predicted the temperature of MOSFET 1 and over predicted the temperature of MOSFET 2 when increasing the heat dissipation from MOSFET 2. On the other hand, the thermal resistance matrix over predicted the temperature of MOSFET 1 and under predicted the temperature of MOSFET 2 when increasing the heat dissipation from MOSFET 1 while maintaining the heat dissipation from MOSFET 2 at 10 W. It is also observed that keeping the heat dissipation from MOSFET 1 at 30 W while increasing the heat dissipation from MOSFET 2 will increase the prediction error for both MOSFET chips but higher error will occur on MOSFET 2 than MOSFET 1.

Table 5.2 Prediction Errors Using Thermal Resistance Matrix

Heat Losses (W)		Temperature for MOSFET 1 (°C)		Temperature for MOSFET 2 (°C)	
MOSFET 1	MOSFET 2	Simulated	Error Prediction	Simulated	Error Prediction
30	30	66.81	+3.5%	67.19	+8.2%
30	20	66.12	+3%	62.57	+6.6%
30	10	65.53	+1.7%	58.37	-2%
20	30	62.59	-1.5%	66.55	+6.3%
10	30	59.36	-20.9%	65.98	+3.9%
12	7	56.39	+2.7%	54.6	+5.2%

While the resistance matrix works well for symmetrical heat dissipation in multi-chip modules, the resistance matrix can still predict the temperature rise of nonsymmetrical heat dissipation multi-chip modules such as DC/DC IPEM within an acceptable error margin of 5% to 10% in average in the heat dissipation range of 10 W to 30 W. Again, it is important to remember that this method only works for conduction dominant scenarios and the reference temperature should be carefully defined.

5.2 Effect of Chip-to-chip Distance and Copper Trace Area

Six cases were conducted to study the effect of chip-to-chip distance and different power loss levels on the thermal performance of the simplified model of DC/DC IPEM. Figure 5.3 shows the results for case 1 to case 6. The results show that the maximum temperature rise of the chips at different power loss levels is independent of the distance between the two heat sources in the x direction with the minimum copper trace area. In the second study, the copper trace area was expanded in both x and y directions while maintaining the chip-to-chip distance in the x direction to be 6 mm and heat dissipation of 5 W from each MOSFET.

Figure 5.4 shows that expanding the copper trace in the x direction has more of a significant effect than expanding the copper trace area in the y direction. Expanding the copper trace area in the x direction increased the trace area by 48.9% and improved the maximum temperature rise of the MOSFET by 0.8%. On the other hand, expanding the copper trace area in the y direction doubled the trace area but only improved the maximum temperature rise by 0.3%. Overall, expanding the copper trace area in both directions can reduce the temperature rise of the MOSFET by 1.1%, which is the combined improvement in case 7 and case 8.

To further study the influence of the chip-to-chip distance, two different MOSFET locations were investigated and compared to case 1. Figure 5.5 shows that moving MOSFET 2 to the other end of the copper trace does not further reduce the temperature rise of the heat sources from case 8. However, moving the heat sources in the x direction can slightly reduce the maximum temperature rise of the MOSFET by 0.6% compared to case 1.

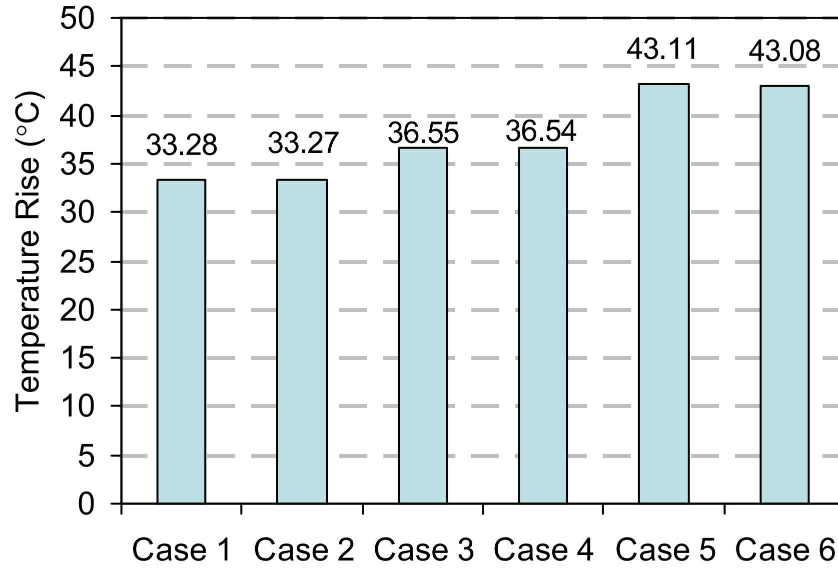

Figure 5.3 Results for Case 2-6 in Study 1 Compared With Case 1 (Baseline)

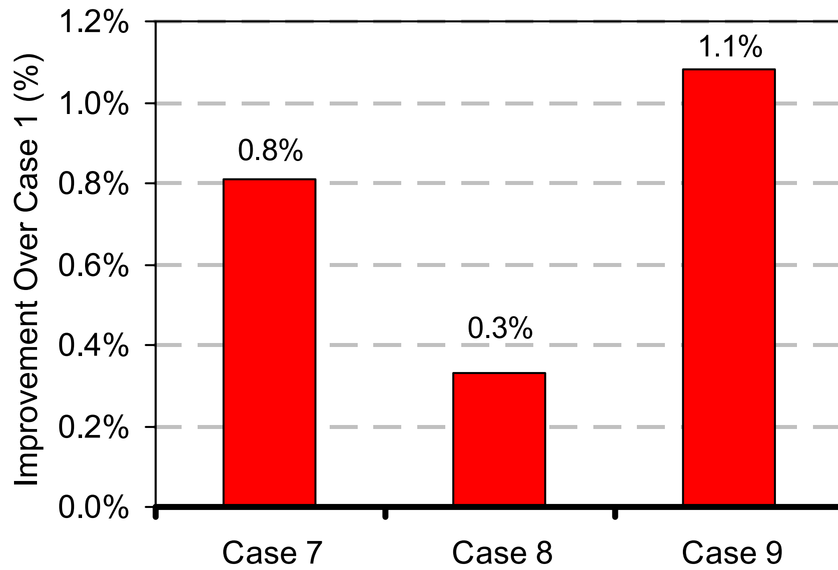

Figure 5.4 Thermal Improvements for Case 7-9 in Study 2 Compared to Case 1 (Baseline)

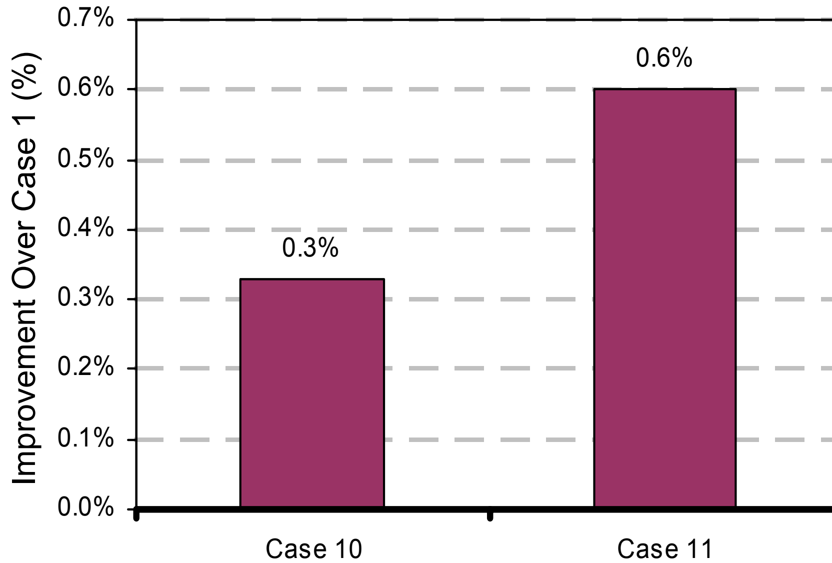

Figure 5.5 Thermal Improvements for Case 10 and Case 11 in Study 3 Compared to Case 1 (Baseline)

From this study, we learn that the chip-to-chip distance in the DC/DC IPEM is an insignificant factor in improving the thermal performance of the module. Although one might think that enlarging the copper trace area would significantly spread the heat from the heat source, the results show that only expanding the copper trace area in the x direction slightly helps in spreading the heat better compared to the copper trace expansion in the y direction as shown in Figure 5.6. Therefore, the total copper trace area does not always improve the heat spreading and the direction of expanding the copper trace area matters.

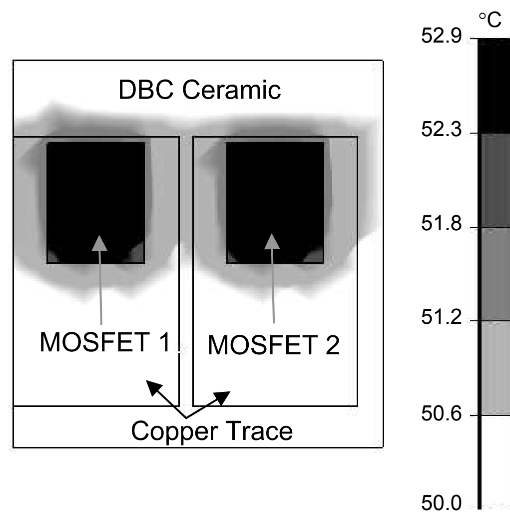

Figure 5.6 Temperature Contour for Case 9 in Study 2 on Table 4

5.3 Selection of DBC Ceramic and Ceramic Carrier Materials

High thermal conductivity ceramic has always promised a better thermal performance in the thermal management of electronics. However, the use of the high thermal conductivity ceramic does not always result in better thermal performance especially in multi-layer structure where the heat path is usually more complex. Therefore, this study investigates the combinations of different ceramic materials for the DBC ceramic and the ceramic carrier. Figure 5.7 compares the results for four cases described in section 4.3. Aluminum nitride and ALOX™ substrates provide ~3% improvement in the thermal performance over the alumina substrate for the ceramic carrier although the thermal conductivity of the aluminum nitride and ALOX™ are about six times higher than alumina. This is mainly due to the high thermal resistance of the epoxy between the device and the ceramic carrier.

Overall, the results show that having high thermal conductivity of the DBC ceramic is more beneficial than increasing the thermal conductivity of the ceramic carrier. This is mainly because most of the heat is dissipated through the DBC substrate to the heat sink. Thus, case 4 with aluminum nitride for both DBC ceramic and ceramic carrier demonstrated the best combination of ceramic materials for the DBC ceramic and the ceramic carrier with 9% improvement over the baseline model (alumina substrate for DBC ceramic and ceramic carrier).

5.4 Metallization Layer

5.4.1 Metallization Interconnect Patterns

In this study, three different patterns were investigated. Figure 5.8 shows the temperature rise of the CoolMOS™ chips and the von Mises stress for each pattern. Although case 2 (9 interconnect via holes) has 50% more area in contact between the silicon die and the metallization than case 1 (6 interconnect via holes), both the temperature rise and the von Mises stress did not show significant improvement over case 1. However, increasing the contact area from 2.4 mm^2 (case 2) to 9.4 mm^2 (~3.9x) of case 3 reduced the temperature rise by 3.9% and reduced the stress on the metallization

by 6.4%. On the other hand, the von Mises stress on the silicon die increased by ~3.5% by replacing case 2 with case 3.

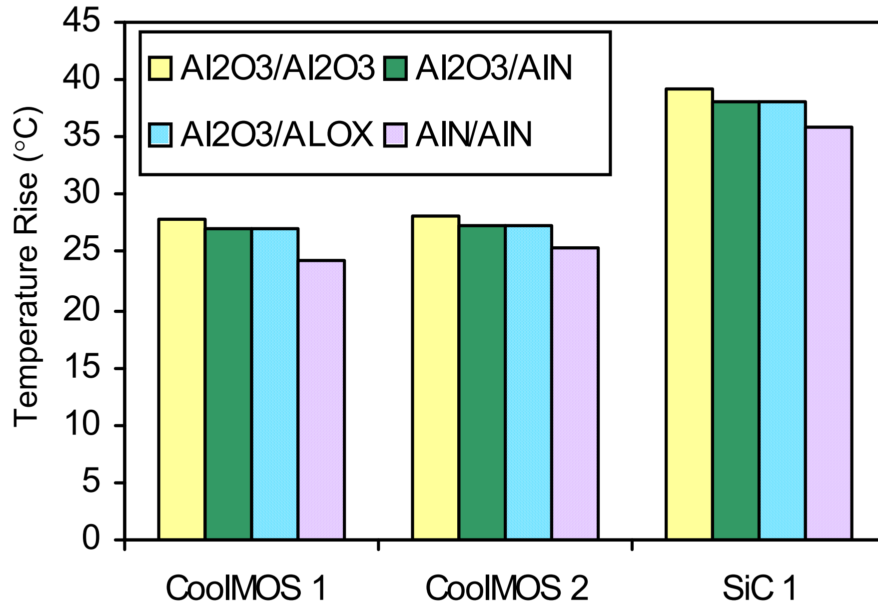

Figure 5.7 Results Comparison for Different Ceramic Materials

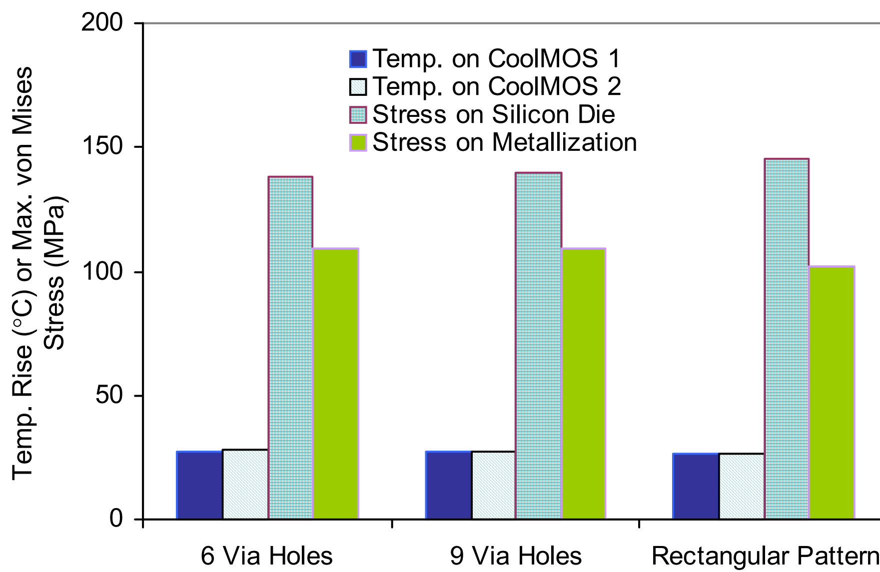

Figure 5.8 Temperature Rise and Maximum von Mises Stress for Three Different Interconnect Patterns

Figure 5.9 shows the stress distributions on the silicon die and the metallization while Figure 5.10 shows the temperature distribution on the metallization layer. It is observed from the stress distributions that higher stress was formed at the edge of the pattern on the silicon die and more towards the center of the pattern on metallization. The temperature distribution shows that the heat was conducted from the silicon die to the metallization through the interconnect pattern. However, the heat spreading resistance was high and thus heat could not transport across the metallization effectively. Overall, the thermomechanical stress is not very sensitive to the patterns with 6 interconnect via holes and 9 interconnect via holes. Therefore, the rectangular pattern (case 3) demonstrates better choice among the three studied patterns thermally and thermo-mechanically.

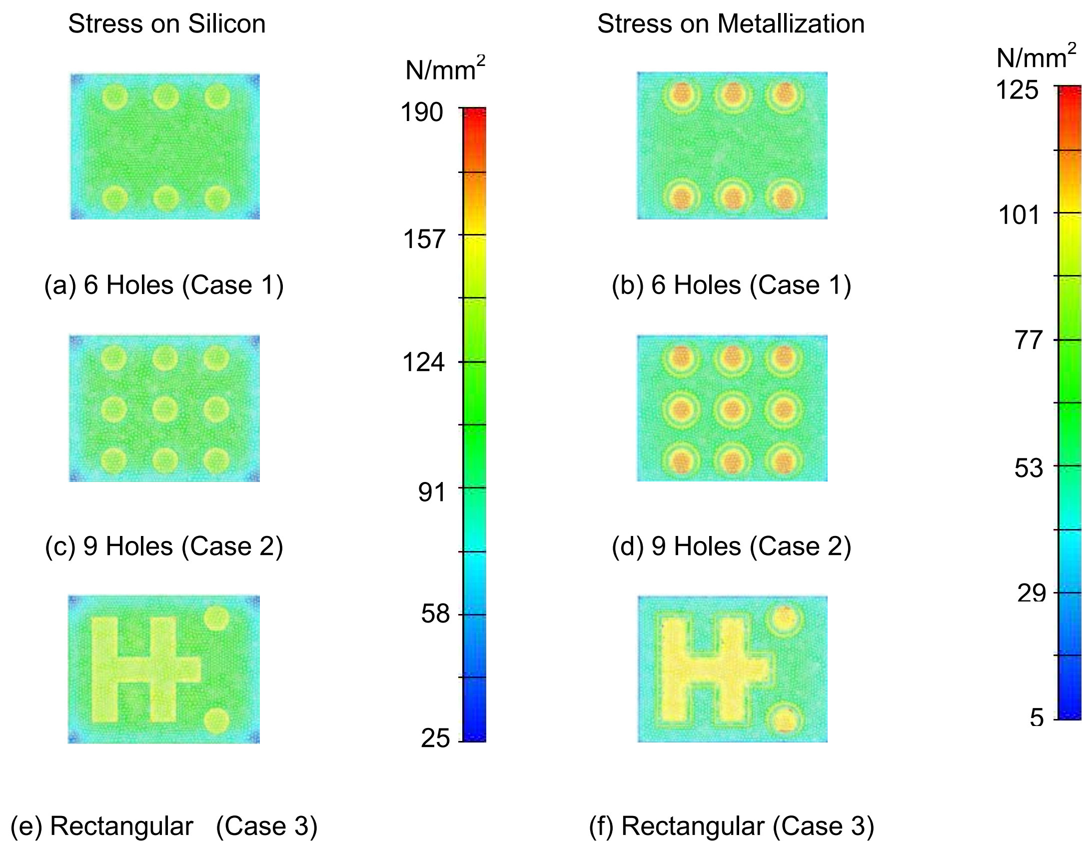

Figure 5.9 Stress Distribution on Top of the Silicon Die and Bottom of Metallization

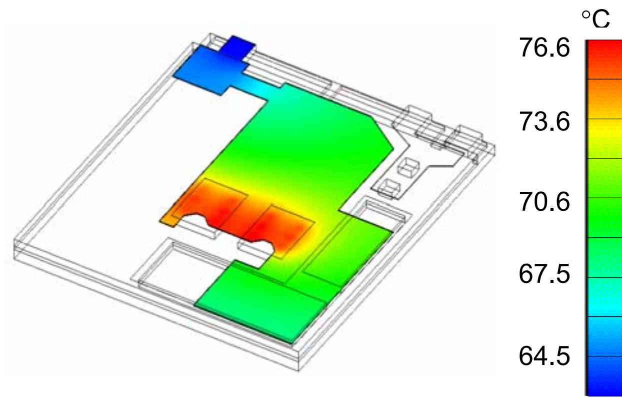

Figure 5.10 Temperature Distribution on the Metallization for 6 Holes Pattern

5.4.2 Metallization Thickness

Different metallization thicknesses were also investigated to understand the effect of the thickness on the thermal performance and thermomechanical stress of the Embedded Power modules. In this study, the original metallization thickness (0.076 mm) was increased by 20%, 40%, 60%, 80%, 2x, 4x, 8x, 16x, and 32x (case 1-case10 in Table 4.6).

Figure 5.11 shows the impact of the metallization thickness on the thermal performance and the thermomechanical behavior of the module. The temperature rise of the module decreases with the increase in the metallization thickness. Despite this, the maximum von Mises stress on the metallization increases with the increase in the metallization thickness. However, the temperatures of the CoolMOS chips are not as sensitive as the temperature of the SiC diode to the change in the metallization thickness. On the other hand, the stresses on the silicon die and the metallization show a significant change only after increasing the metallization thickness by 16x. This metallization thickness, however, is unrealistic from the viewpoint of processing, as well as the necessary electrical interconnect resistance.

Figure 5.12 shows the stress distributions on the metallization with baseline thickness (case 1), 4x increase in thickness (case 7), and 16x increase in thickness (case 9). It can be observed from the stress distributions that the high stress areas shifted from

the center of the interconnect pattern in case 1 (baseline thickness) towards the edge of the pattern with the increase in the metallization thickness.

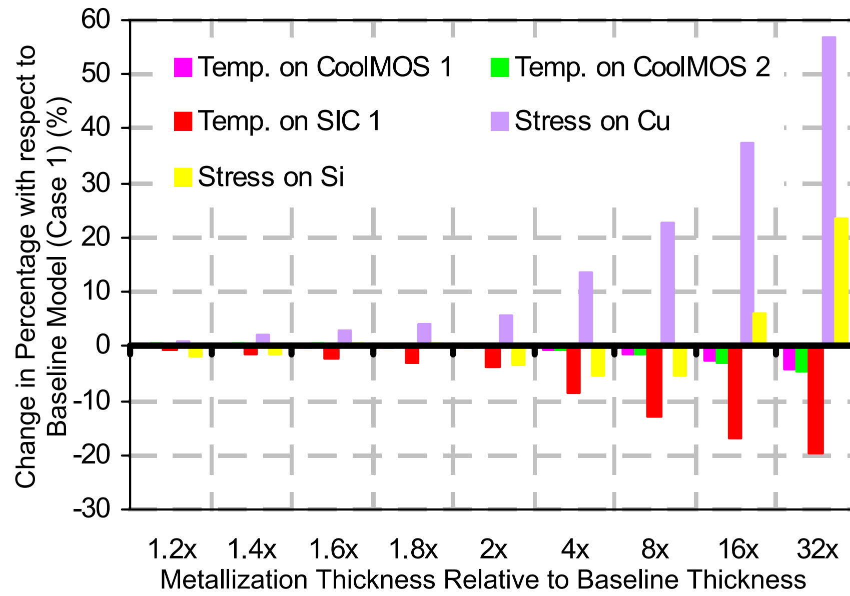

Figure 5.11 Temperature Rise and Maximum von Mises Stress for Different Metallization Thicknesses

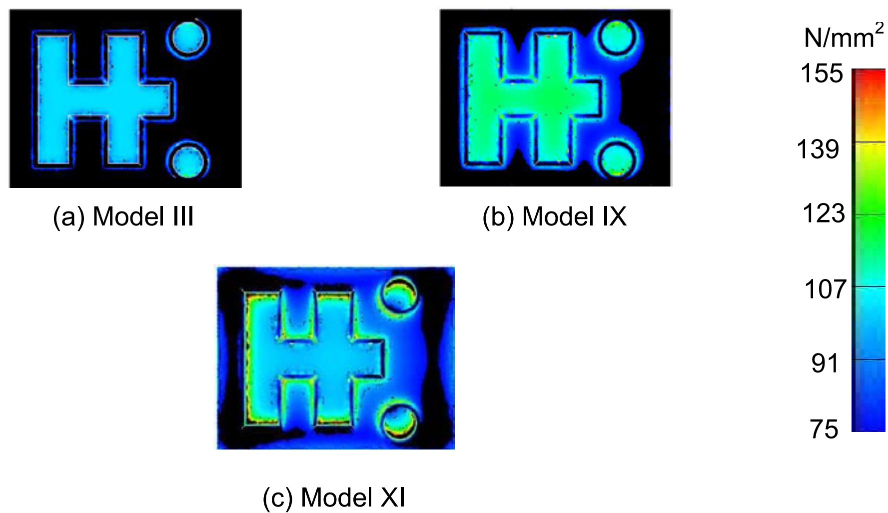

Figure 5.12 von Mises Stress Distributions on Metallization for Baseline Thickness, 4x Thickness, and 16x Thickness

5.4.3 Metallization Materials

The material used for the metallization layer plays an important role in determining the significance of the metallization in transporting heat away from the active devices as well as reliability issues such as possible delamination of the metallization layer. Copper, molybdenum, aluminum, and silver were compared in this study. The material properties for these materials were listed in Table 4.7.

The result in Figure 5.13 shows that using molybdenum as the metallization material results in the lowest stress compared to other materials due to the good match of CTE between other molybdenum and silicon. On the other hand, molybdenum shows the highest temperature rise among the compared materials due to its low thermal conductivity. Compared to copper, molybdenum resulted in 4.7% higher temperature rise but 41% less in stress than copper. Therefore, molybdenum is a good candidate to replace the copper metallization layer from a thermomechanical perspective.

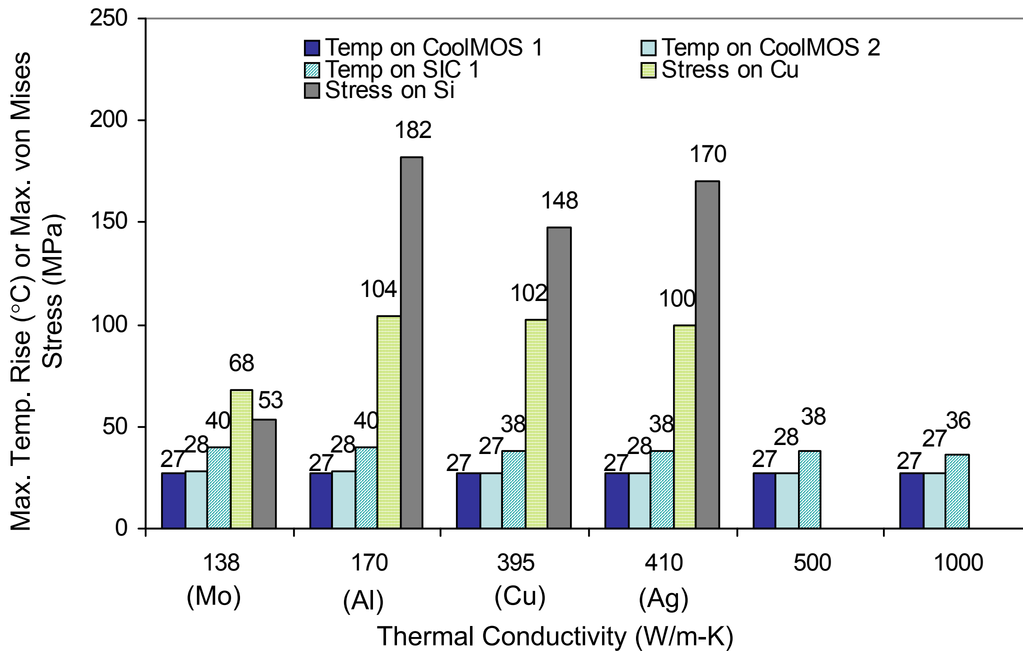

Figure 5.13 Trade-offs Between Thermal Performance and Thermomechanical Behavior for Different Materials

Although silver has the highest thermal conductivity among the studied materials, the improvement in thermal performance would not outperform molybdenum and copper due to its higher CTE mismatch with silicon compared to molybdenum and copper. Overall, the worst material to be used is aluminum because of its low thermal conductivity and highest CTE mismatch with silicon.

Further study was conducted to understand the impact of thermal conductivity of the metallization layer on improving the heat transport through the metallization layer. Thus, the study extended the thermal conductivity values to any material with thermal conductivity values of 500 W/m-K and 1000 W/m-K. Since no specific materials with these thermal conductivity values (i.e., no known CTE values) were specified, the stress analysis was not investigated for these two cases. It is shown in Figure 5.13 that the maximum temperature rise can be further reduced by as much as ~6% when increasing the thermal conductivity from 410 W/m-K to 1000 W/m-K. Figure 5.13 also shows that the temperatures of CoolMOS™ chips were not sensitive to the thermal conductivity of the metallization.

5.4.4 Specification of Restraints on Stress Models

Boundary conditions always play a crucial role in finite element modeling. Inaccurate boundary conditions can result in false simulation results. In the modeling of the thermomechanical behavior, the defined restraints on the finite element model should accurately resemble the actual condition. In the stress model of the IPEM, several possible restraints can be used to mimic the actual condition in analyzing the thermo-mechanical behavior of the IPEM. Therefore, these constraints were explored to examine the influence on the simulation results.

The stress models used in the study of the metallization layer are described in section 4.4. In addition to the restraints described in Figure 4.5, three other restraints were also studied to check the sensitivity of the stress results on different boundary conditions. The points of interest for specifying the constraints include the four corner points as well as the center point on the bottom surface of the silicon. Figure 5.14 shows the possible points for defining the constraints in the stress model.

Three different sets of restraints on the possible locations in the stress model were investigated. While the first restraint set is used in the three studies discussed in section 5.4, the second set of restraint involved constraining point V1 in the x direction, point V2 in both x and y direction, and point V3 in all three directions. In the third restraint set, point V1 is constrained in y and z direction, point V2 is constrained in the z direction, and point V4 is restrained in all three directions. Finally, all four points are constrained in z direction only in restraint set 4. Table 5.3 summarized these four restraint sets.

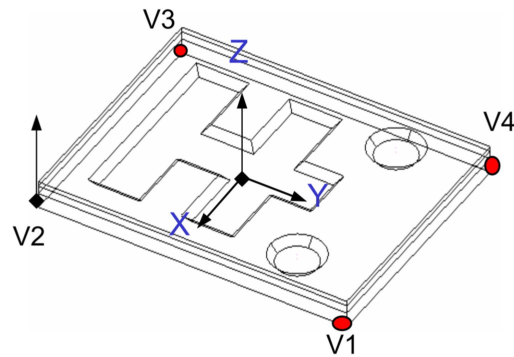

Figure 5.14 Possible Locations for Restraints Specification in Stress Model

Table 5.3 Combination of (Translational and Rotational) Restraints Specified for the Stress Model

Restraint	Restraint at Center Point	Restraint at V1	Restraint at V2	Restraint at V3	Restraint at V4
1	x, y, z		z		
2		x	x, y	x, y, z	
3		y, z	z		x, y, z
4		z	z	z	z

The maximum average von Mises stress on both the silicon and metallization are compared in Table 5.4. Although all these four combinations of restraints are different from each other, the simulated von Mises stress on both the silicon and the metallization layer does not vary within 5%. Further study on the stress distribution also shows that the stress distribution does not change with these different constraints. Figure 5.15 shows the stress distribution on the silicon for the first three restraint sets.

5.5 Significance of Polyimide Layer

Figure 5.16 shows the temperature rise of the heat sources with respect to the change in the thickness of the polyimide layers described above for the all three cases studied in section 4.5. The result shows that reducing both the top and bottom polyimide thickness can further reduce the maximum temperature of the active IPEM by ~5% and the improvement is more evident on the SiC diodes than the CoolMOS™ chips. In addition, reducing the thickness of the top polyimide layer has a more significant improvement than reducing the thickness of the bottom polyimide layer (3.3% vs. 0.6%) on the SiC diode 1. This is mainly because the heat path from the heat generation surface of SiC diode 1 is directly connected to the power stage metallization layer and the heat is then transported from the metallization layer to the ceramic carrier through the polyimide layer since the top surface of the module is insulated. Therefore, having a thin polyimide layer can reduce the thermal resistance between the metallization layer and the ceramic carrier.

Table 5.4 von Mises Stress on Silicon and Metallization Layer with respect to Different Restraints

Restraint	Set 1	Set 2	Set 3	Set 4
On Silicon	128 MPa	132 MPa	128 MPa	131 MPa
On Metallization	109 MPa	110 MPa	109 MPa	109 MPa

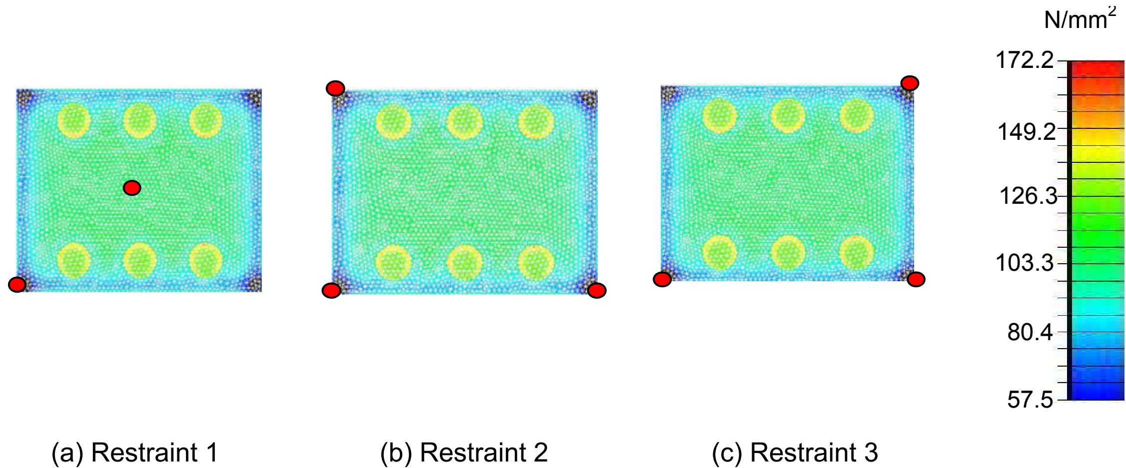

Figure 5.15 von Mises Stress Distribution on Top Silicon Layer

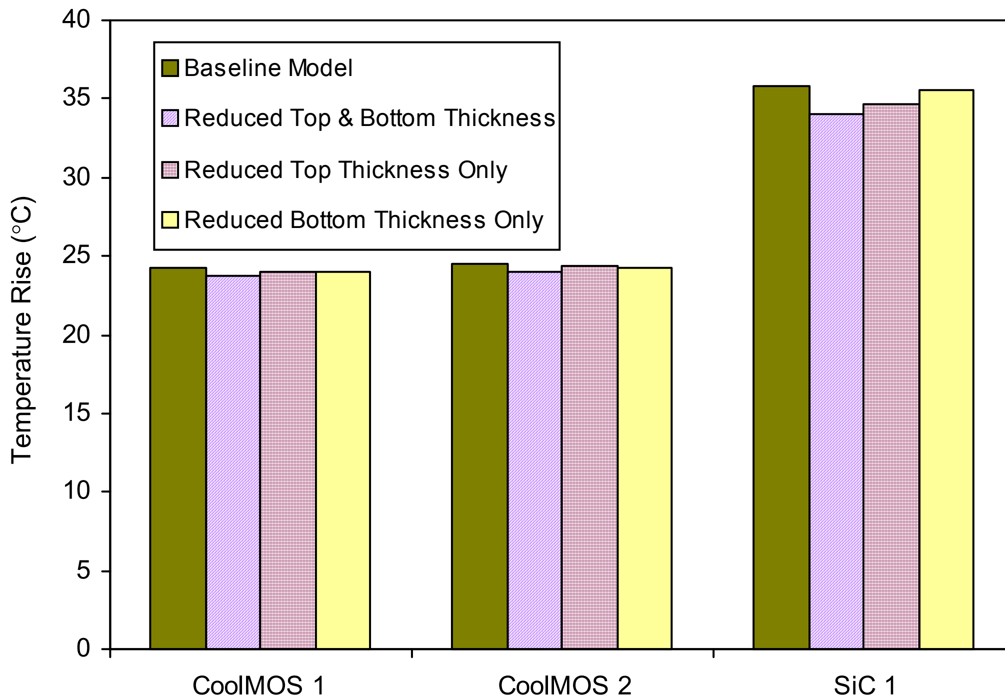

Figure 5.16 Significance of Polyimide Thickness on the Temperature Rise of Heat Sources for PFC IPEM

5.6 Evaluation of Integrated Cooling Mechanisms for IPEMs

5.6.1 Structural Enhancement

Figure 5.17 shows the steady state temperature contours of the two cases described in section 4.6.1. In each case, the hottest spot in the module is the SiC diode

that dissipates 4.52 W. The baseline model shows that the maximum temperature is as high as 89.3°C, a temperature rise of 39.3°C. We were also able to identify the large temperature gradient across the devices to the ceramic carrier. This is mainly due to the low thermal conductivity of the epoxy used to fill the gap between the devices and the ceramic as well as hold the devices in place.

One way to improve the thermal performance of the active IPEM could be shortening the heat path within the module by modifying the structure of the module. Case 1 in this study was the model where an additional heat path was created from the hotspot to the DBC copper trace. This simple modification can improve the thermal performance by 14%, a 5°C reduction in the maximum temperature rise of the active IPEM.

Further improvement can be achieved in case 2 by creating an additional heat path directly from the hotspot to the heat sink. A significant improvement of 24% can be attained in case 2 compared to baseline model. The result comparison of the models is summarized in Figure 5.17. The result also shows that this structural enhancement has more impact on the temperatures of the SiC diodes (especially SiC diode 1) than the CoolMOS™ chips. This is mainly because the additional heat path is created from the SiC diodes to the heat sink by connecting a piece of aluminum nitride ceramic from the hotspot to the heat sink.

5.6.2 Double-sided Cooling

The idea of employing double-sided cooling is to increase the heat exchange area. Optimization of the module was conducted to further reduce the internal thermal resistance of the active IPEM. In this study, employment of different combinations of ceramic materials used in the active IPEM was investigated. The results in Figure 5.18 show that more than 30% of thermal improvement can be achieved with the employment of double-sided cooling. Although the use of Thermal Clad™ for the double-sided cooling can improve the thermal performance by 36%, employing of aluminum nitride for the top DBC ceramic substrate shows an additional 5% improvement over the Thermal Clad™.

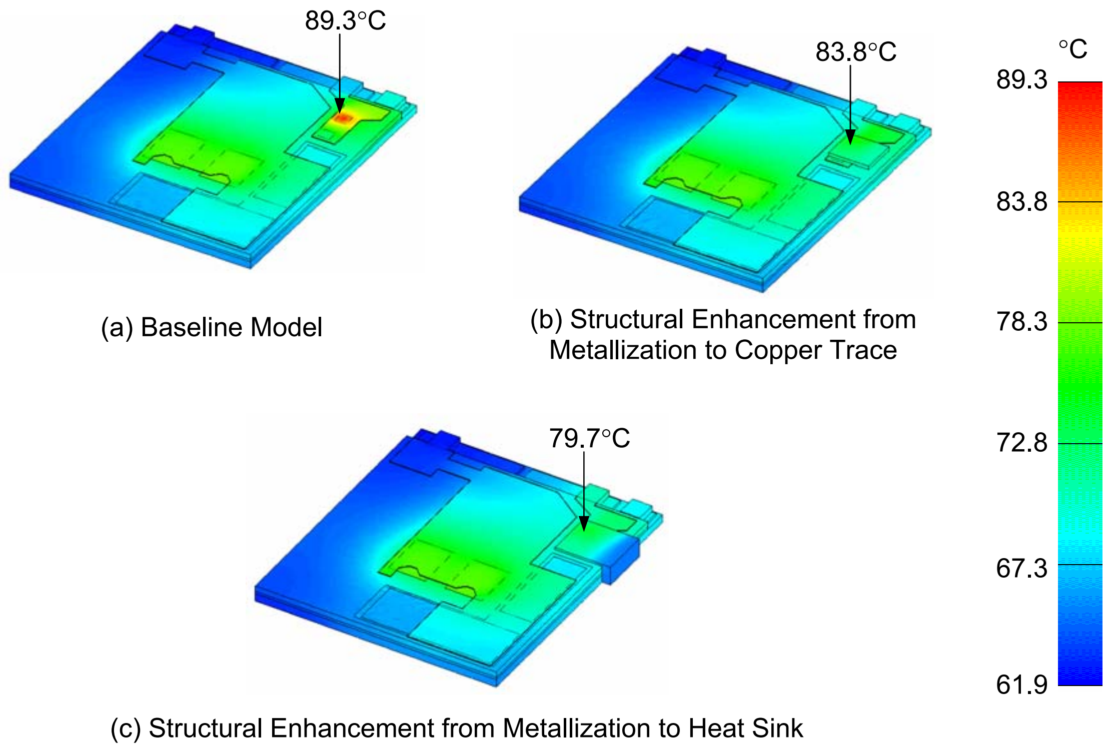

Figure 5.17 Temperature Distribution of Baseline Model and Structurally Enhanced PFC IPEM Models

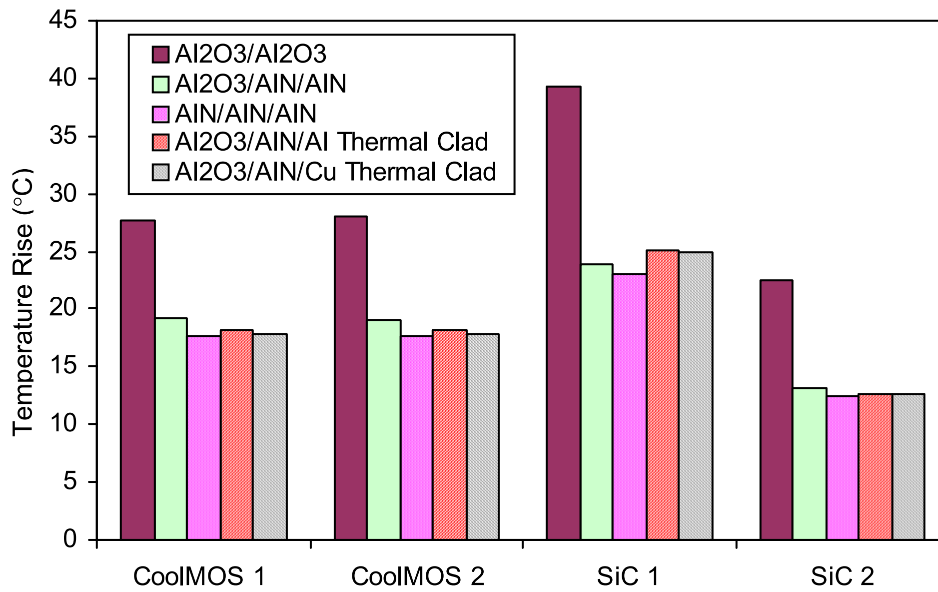

Figure 5.18 Results Comparison of Different Combinations of Ceramic Substrate for Double-sided Cooling

In addition, this study also investigated the effect of having the additional top DBC layer cooled by a wide range of cooling mechanisms in terms of the individual equivalent heat transfer coefficient. In this study, we investigated the temperature rise of the heat sources when applying top side cooling with equivalent heat transfer coefficient of 50 W/m^2-K, 200 W/m^2-K, 1000 W/m^2-K, and 10,000 W/m^2-K. These heat transfer coefficient values represent the typical range of heat transfer coefficients for single phase and two phase forced air convection and liquid cooling with reference to the values published in [72]. Figure 5.19 summarizes the results and it shows that significant improvement can be achieved with two phase cooling.

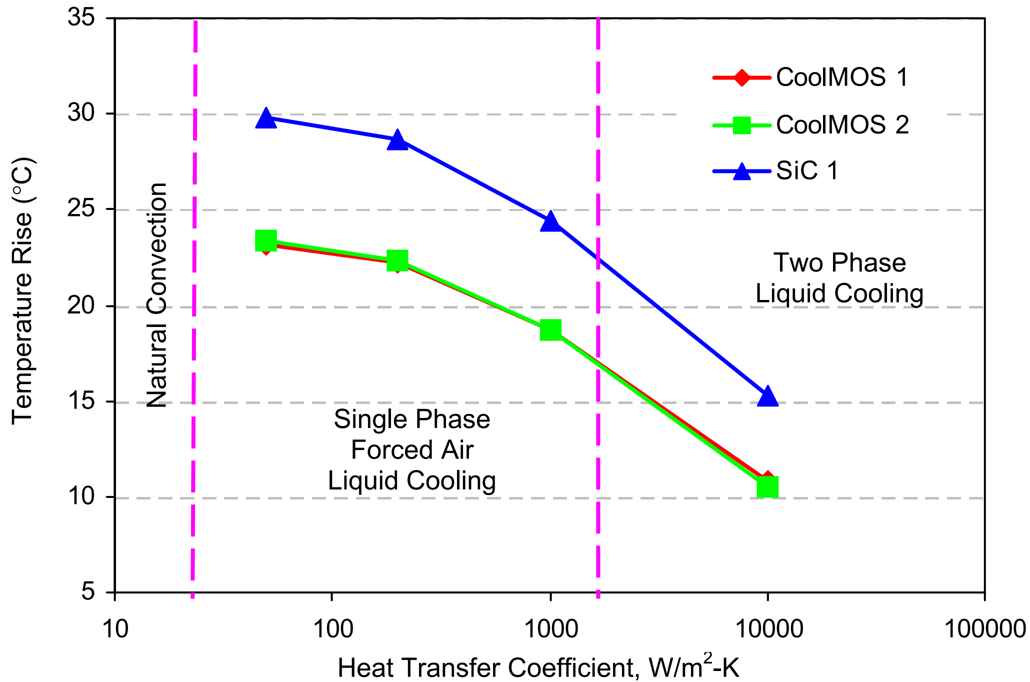

Figure 5.19 Temperature Rise of the Heat Sources at Different Range of Heat Transfer Coefficient

5.6.3 Combined Effect of Ceramic Material and Polyimide Thickness

It is believed that the maximum thermal performance can be achieved by applying the combination of the best results from the parametric studies discussed above. In this study, the application of the best ceramic materials combination with double-sided cooling which included aluminum nitride substrates for all the ceramic in the module and the reduced thickness of the top and bottom polyimide layers were studied as the best case scenario. Although the structural enhancement can improve the thermal performance by 14%, double-sided cooling can improve the thermal performance by more than 30%. Therefore, only double-sided cooling was considered. It is also possible that one parameter has more significant impact than other parameters on the overall thermal performance which will be examined in this section. Results in section 5.6.2 show that the best combination of ceramic materials includes aluminum nitride substrate for the bottom DBC ceramic, the ceramic barrier, and the top DBC ceramic. In addition, the results in section 5.5 shows that reducing both the top and bottom polyimide layers produces the best result.

Based on the results from section 5.6.2 and section 5.5, we summarize that the best combination of ceramic materials selection with double-sided cooling resulted in 41% of improvement and reducing both layers of polyimide resulted in 14% of improvement over the baseline model described chapter 3. Figure 5.20 shows the result of examining the improvement in the best case scenario compared to the cases with changes in the individual parameters. The results show that the effect of the double-sided cooling is much larger than the reduced in the thermal resistance of the polyimide layer. The combination of the best ceramic materials and reduced polyimide thicknesses can improve the thermal performance by 42%, which is only 1% more than the double-sided cooling. Therefore, the best approach to improve the thermal performance of the module is to have effective thermal management practices to transfer heat from the package to ambient.

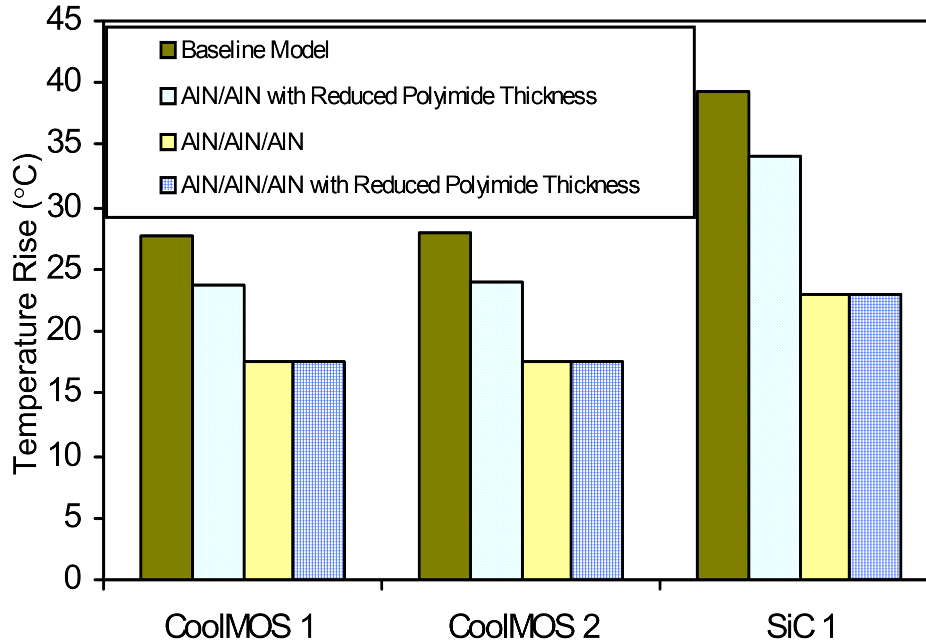

Figure 5.20 Comparison of the Effect of the Best Combined Studied Parameters

5.6.4 Experimental Assessment of Double-sided Cooling

The ability to improve the heat extraction from the heat sources to the ambient has always been the focus of the researchers in electronic cooling. Various thermal management strategies such as high thermal conductivity interface materials, heat pipes, and liquid cooling have been implemented to improve the thermal performance of electronic packages. However, the cost of using these advanced thermal management strategies has always negated the advantages of them. Thus, this work presented a simple and less costly method to improve the thermal performance of power electronic packages. Three experiments were performed to quantify the advantages of using double-sided cooling for the DC/DC IPEM. To ensure the experiments were repeatable, the same test was conducted twice for all three cases. Figure 5.21 shows the repeated results for both the temperature rise data from the infrared images as well as the thermocouple for the second experiment described in section 4.6.3.

Figure 5.22, 5.23, and 5.24 show the measured temperatures from infrared images and thermocouples for the investigated three cases respectively. In addition, Table 5.5 lists the measured power dissipation during the experiments. The recorded data show the

heating from the ambient temperature until steady state temperature and cooling from steady state temperature until ambient temperature. Note that the measured ambient temperatures for all three cases are different.

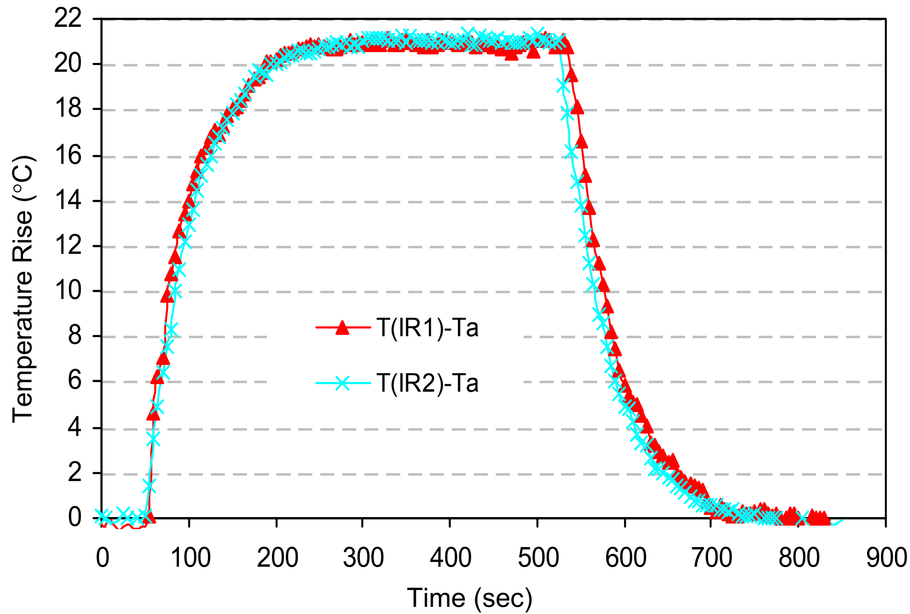

(a) Temperature Rise Data from Infrared Images

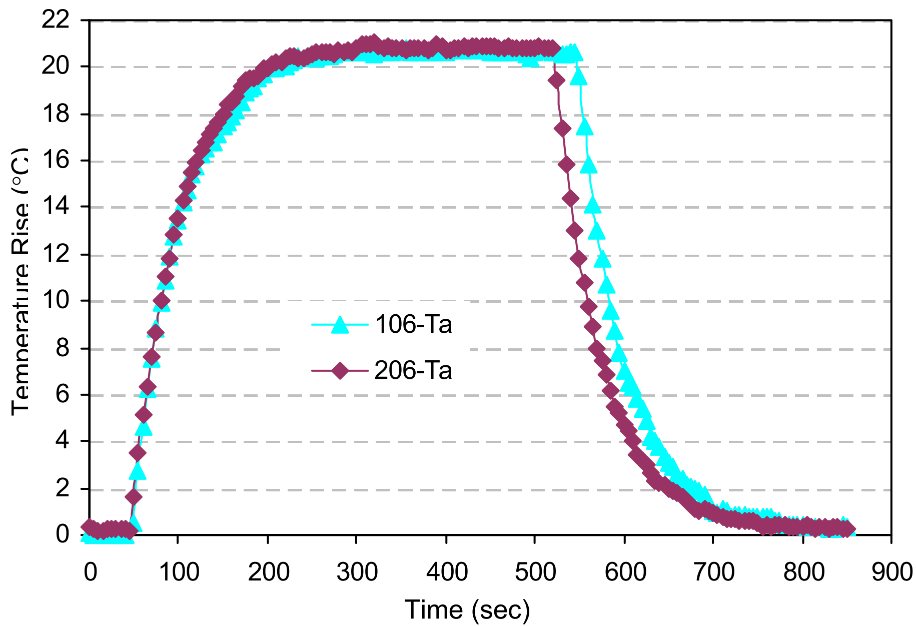

(b) Temperature Rise Data from Thermocouples

Figure 5.21 Temperature Rise of Obtained Data During Repeated Experiments

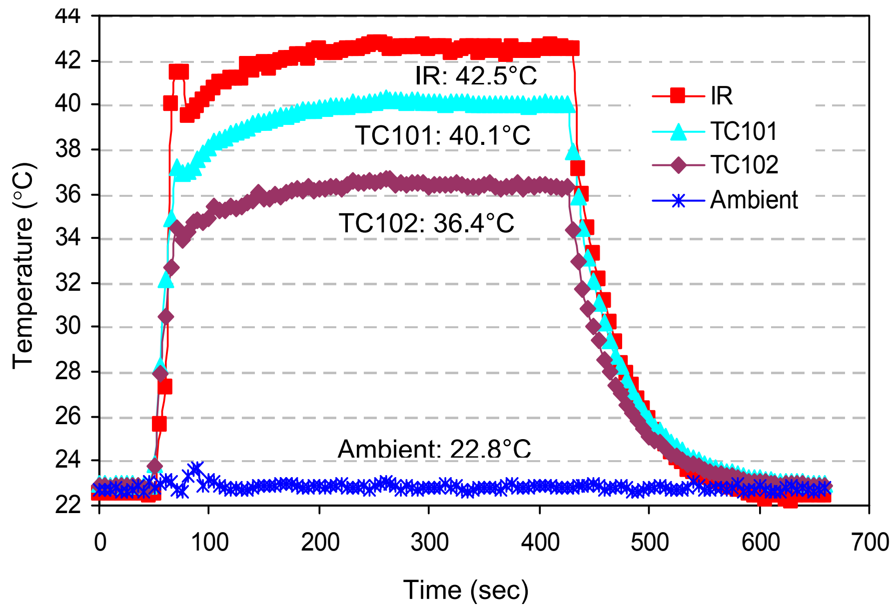

Figure 5.22 Measured Temperature for Experimental Study I

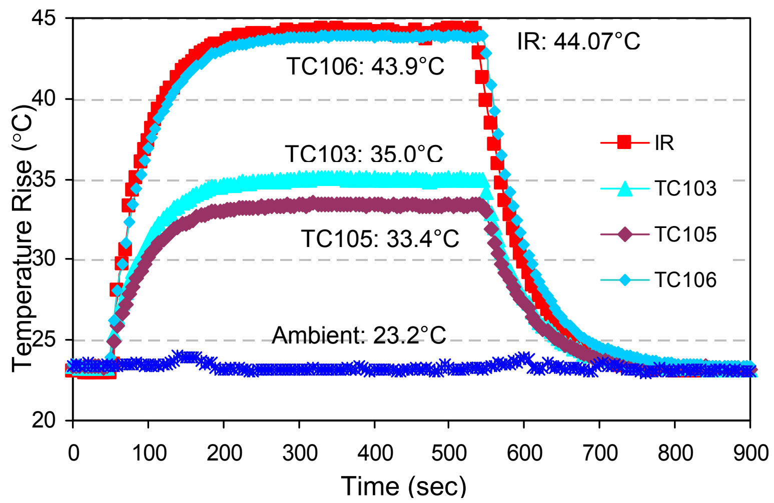

Figure 5.23 Measured Temperature for Experimental Study II

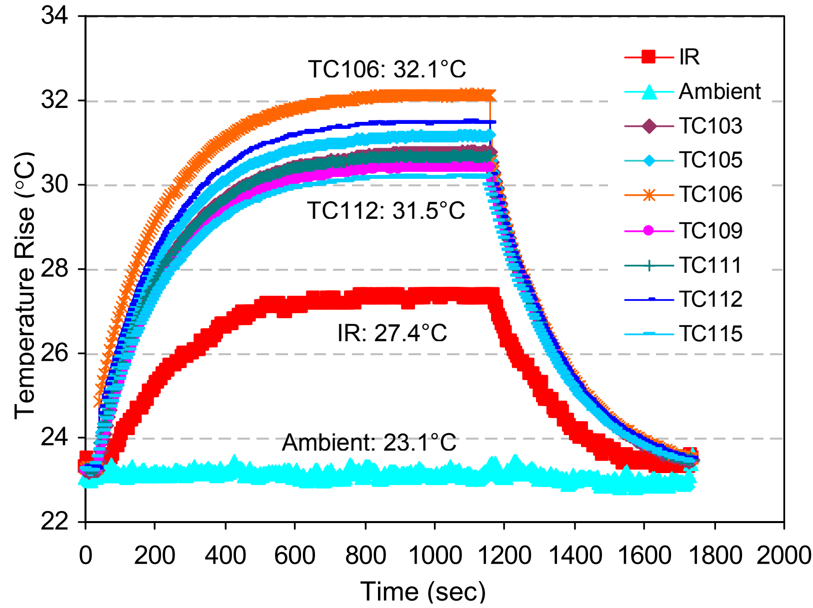

Figure 5.24 Measured Temperature for Experimental Study III

In all three cases, the junction temperature of the DC/DC IPEM could not be recorded since no thermocouple was embedded in the module. However, the junction temperature of each case was predicted using the measured data and the calculated thermal resistance of the respective layers within the module. The thermal resistance of the respective layer, R, was calculated using Eq. 5.2:

$$R = \frac{\iota}{k \cdot A_e}, \tag{5.2}$$

where ι is the thickness of the respective layer, k is the thermal conductivity of the layer, and A_e is the effective heat conduction area.

The structure of the DC/DC IPEM in a two-dimensional view is illustrated in Figure 5.25. To obtain the individual thermal resistance of each layer shown in the figure, the effective heat conduction area, A_e, of each layer was defined by the confined area of MOSFET 1 as shown in Figure 5.26. The effective area for other layers is 108.5 mm^2. The calculated thermal resistance for each layer is summarized in Table 5.5. Several assumptions were made while using Eq. 5.2 for obtaining the one-dimensional thermal resistance values:

1. heat conduction through the side of the heat source to the ceramic carrier is negligible
2. heat spreading on the metallization layer is small due to its very thin layer
3. heat spreading is also small at low thermal conductivity layers such as the DBC ceramic layer

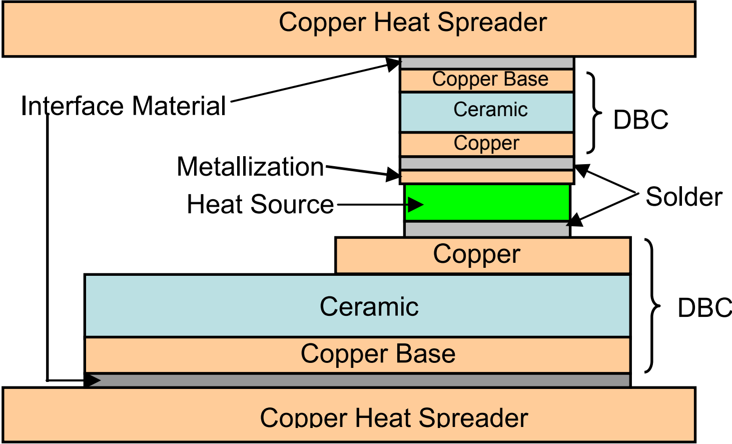

Figure 5.25 Schematic of 1-D DC/DC IPEM Structure

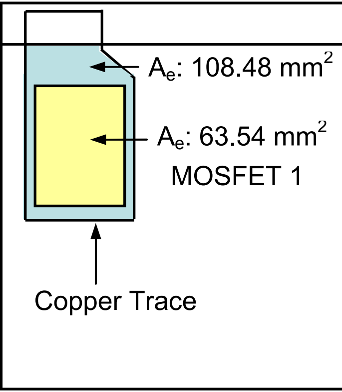

Figure 5.26 Effective Area for Thermal Resistance Calculation in Equation 5.2

Table 5.5 Calculated Thermal Resistance for the Layers Illustrated in Figure 5.25

Description	Thermal Resistance (°C/W)
Silicon Chip	0.057
Bottom Solder	0.157
Copper Trace	0.007
DBC Ceramic	0.225
DBC Copper Base	0.007
Bottom Interface Material	0.583
Bottom Heat Spreader	0.07
Metallization Via Holes	0
Top Solder	0.157
Top DBC Trace	0.012
Top DBC Ceramic	0.231
Top DBC Copper Base	0.012
Top Interface Material	0.996
Top Heat Spreader	0.12

With the known temperatures for two locations on the module as well as the power loss, the junction temperature can be calculated. Figure 5.27, 5.28, and 5.29 show the one-dimensional thermal resistance networks for the three investigated cases. In the first case, the junction temperature of the module was obtained using Eq. 5.3:

$$\frac{T_j - T_{IR}}{R_{metallization}} + \frac{T_j - T_{101}}{R_{BottomEq.}} = Q\,, \tag{5.3}$$

where T_j is the junction temperature, T_{IR} is the measured temperature from infrared image, T_{101} is the measured temperature from thermocouple TC101 shown in Figure 5.22, $R_{metallization}$ is the thermal resistance of the metallization, and $R_{BottomEq.}$ is the equivalent thermal resistance of the bottom solder and the DBC layers, and Q is the measured power dissipation. Since the measured maximum temperature from the infrared camera is assumed to be the junction temperature, the thermal resistance of the metallization was taken to be zero at the point where the interconnection on the metallization were in contact with the top surface of the heat source.

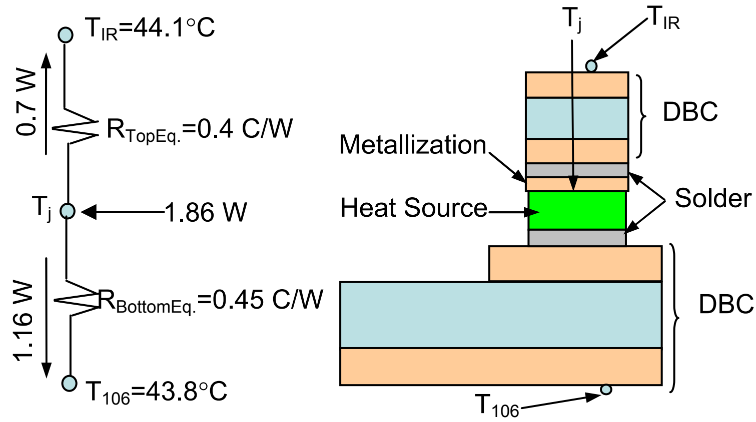

Figure 5.27 One-dimensional Thermal Resistance Network for Case I

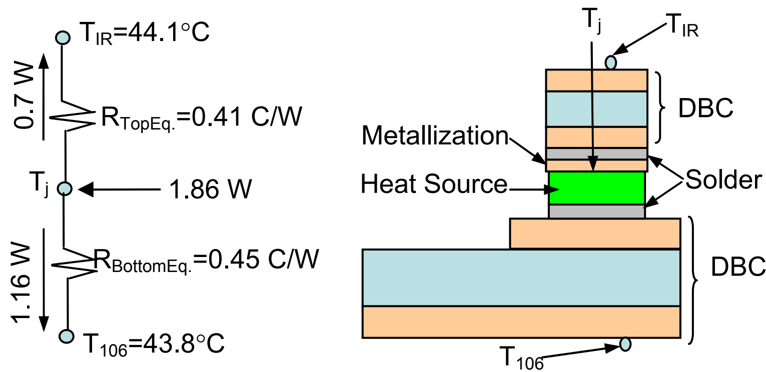

Figure 5.28 One-dimensional Thermal Resistance Network for Case II

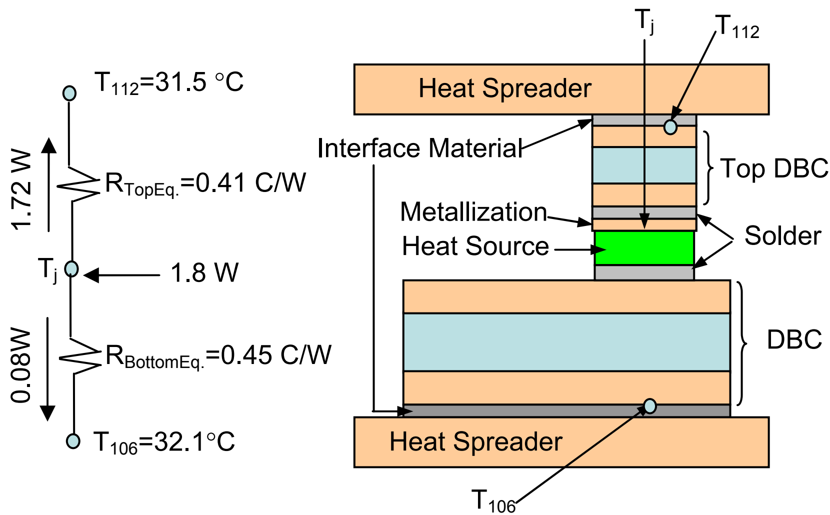

Figure 5.29 One-dimensional Thermal Resistance Network for Case III

Similarly, the junction temperature in Case II was estimated using Eq. 5.4:

$$\frac{T_j - T_{IR}}{R_{TopEq.}} + \frac{T_j - T_{106}}{R_{BottomEq.}} = Q, \quad (5.4)$$

where $R_{TopEq.}$ is the equivalent thermal resistance of the top solder and the top DBC layers, T_{106} is the measured temperature from thermocouple TC106 shown in Figure 5.23, and $R_{BottomEq.}$ is the equivalent thermal resistance of the bottom solder and the DBC layers.

Finally, the junction temperature in Case III was predicted using Eq. 5.5:

$$\frac{T_j - T_{112}}{R_{TopEq.}} + \frac{T_j - T_{106}}{R_{BottomEq.}} = Q, \quad (5.5)$$

where T_{112} is the measured temperature from thermocouple TC112 shown in Figure 5.24 and T_{106} is the measured temperature from thermocouple TC106 shown in Figure 5.24. Likewise, the R_{TopEq} and $R_{BottomEq.}$ in Eq. 5.5 are the same as the those defined in Eq. 5.4.

By using the described method, the junction temperatures for all three cases are found and summarized in Table 5.6. With the predicted junction temperature, the heat conducted to the top and the bottom surface of the module can be calculated for all three cases. In Case I, all of the heat was conducted through the backside of the heat source through the bottom solder layer to the DBC layers and to the ambient. It was observed that the metallization layer has a high spreading resistance and thus creating hotspot on the module as shown in Figure 5.30.

Table 5.6 Predicted Junction Temperature

Case Study	Junction Temperature
I	42.5 ± 2 °C
II	44.36 ± 2 °C
III	32.18 ± 0.5 °C

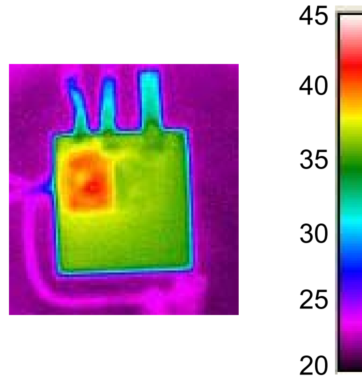

Figure 5.30 Infrared Image of DC/DC IPEM for Case I

The idea of adding additional an DBC substrate on the metallization layer was to provide an additional heat path from the heat source to the ambient. Although the spreading resistance on the metallization is high, the heat transfer was practically in one direction from the localized hotspots on the metallization to the top DBC. Consequently, the heat was then transferred to the ambient through convection. As shown in Figure 5.28, 38% of the generated heat was transferred through the top surface after adding the top DBC substrate on top of the metallization layer compared to zero heat transfer through the top surface in Case I.

Similarly, adding heat spreaders on both sides also enhanced the heat transfer from the heat source to the ambient from both top and bottom sides with a larger surface area for convection to overcome the extra thermal resistance added to the overall thermal resistance of the module. In Case III, almost 95% of the heat was extracted through the top surface due to its effectiveness in transferring heat from the lower thermal resistance heat path between the heat source and the top side of the module.

A common parameter, junction-to-ambient thermal resistance, was used to evaluate the thermal performance of the DC/DC IPEM under three different cases. The junction-to-ambient thermal resistance, R_{ja}, measures the electronic package's heat dissipation capability from the heat source's active surface (junction) to the ambient via all heat paths. The R_{ja} is determined by Eqn 5.6:

$$R_{ja} = \frac{T_j - T_a}{Q} \quad , \tag{5.6}$$

where T_j is the junction temperature or maximum temperature of the package, T_a is the ambient temperature, and Q is the power dissipation from the heat source.

Table 5.7 summarizes the predicted temperature rise, T_j-T_a, and the junction-to-ambient resistance, R_{ja}, for all three cases. Since the power dissipation and the ambient temperature for all three cases were different, a fair method of comparing their thermal performance is through the evaluation of their R_{ja}. It is shown in Table 5.7 that we can achieve an improvement of almost 20% by adding an additional top DBC substrate compared to Case I. Further improvement can be achieved in Case III where about 62% can be achieved over Case I by adding additional copper heat spreaders on both top and bottom sides of the module.

5.6.5 Micro-channel Cooling

The increasing heat generation in electronic components has motivated the research on the micro-channel cooling technology. Micro-channel cooling utilizes coolant such as water to carry the heat from the hotspots through small channels to effectively transfer large amount of heat from hotspots to the least heated place and eventually to the ambient.

Preliminary studies were performed to examine the possibility and advantages of implementing micro-channel cooling for the IPEMs. Two initial ideas described in section 4.6.4 were studied. In the first study, a copper cap with micro channels covered the top side of the module. Preliminary results in Figure 5.31 shows that the channels in the copper cap can reduce the maximum temperature of the module from 88.1°C to 62.4°C, a 25.7°C temperature drop. The temperature difference across the channel was as much as 1°C. Yet, the result is very dependable on the specified pressure drop across the channels.

Table 5.7 Predicted Temperature Rise and Junction-to-ambient Thermal Resistance

Case Study	T_j-T_a	R_{ja}
I	19.7	14.07
II	21.18	11.29
III	9.68	5.38

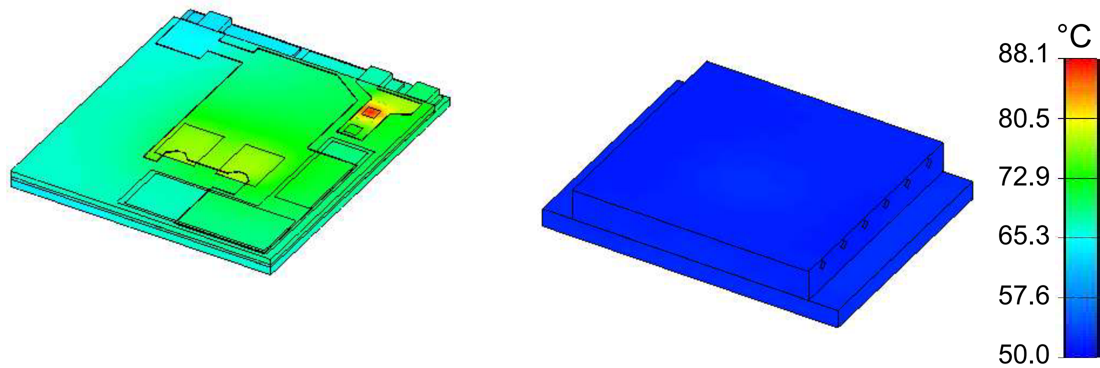

(a) Model Without Copper Cap (b) Model With Copper Cap

Figure 5.31 Temperature Distribution of IPEM Model With and Without Copper Cap

Further study was conducted to reduce the number of the channels in the copper cap. Instead, two channels were laid on top of the heat sources only in the copper cap as shown in Figure 4.14 to effectively transfer the heat from the hotspots to the water. Again, the result is very dependent on the inlet flow condition, which is the inlet water velocity in this case. Figure 5.32 shows the temperature distribution of the water in the channels. The temperature rise of the water was only as much as 2°C although the maximum temperature of the module can be reduced from 88.1°C (Figure 5.31(a)) to 61.8°C in this case.

To reduce the distance form the heat sources to the liquid channels, micro-channels were etched onto the copper of the top DBC. In this study, different inlet water velocities ranging from 5 m/s to 300 m/s were investigated to identify the advantages we can get from micro-channel cooling. Note in comparison, the speed of sound in water at 50°C is about 1541 m/s, so the values at the high end are practically unrealistic, but are included for comparative purposes only. Figure 5.33 compares the maximum temperature rise of the module with different inlet velocity to the model without micro-channel cooling. We can see further improvement of as much as 60% when increasing the inlet velocity from 5 m/s to about 80 m/s. However, further increase in the inlet velocity actually reduces the improvement of using the micro-channel cooling. The improvement can drop to less than 30% when increasing the inlet velocity to 300 m/s. The improvement in the reduction of temperature rise in CoolMOS 2 chip can drop to as little as 3%.

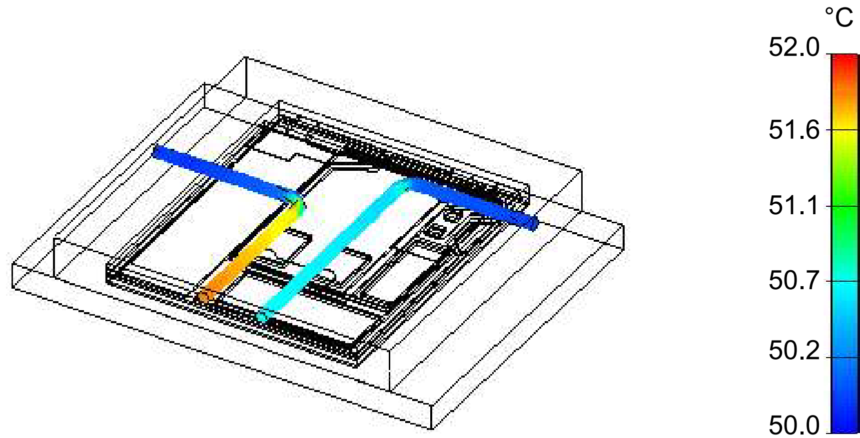

Figure 5.32 Temperature Distribution of the Water Within the Copper Cap

As shown in Figure 5.33, the improvement we can get by implementing micro-channel cooling does not always increase with the inlet flow velocity although one may expect so. One phenomenon was observed from the numerical simulation that additional amount of heat was actually transferred from the channels to the top DBC rather that the liquid in the channel carrying away the heat loss from the top DBC. This is because additional heat was created at high flow velocity in small channel due to the friction at the channel wall and friction within the fluid. Consequently, this increased the power loss of the module and reduced the improvement of implementing micro-channel cooling. For example, the improvement for CoolMOS 2 chip can be reduced to as little as 3% due to more frictional heat generation in the longer channel as well as the location of the CoolMOS 2 chip towards the end of the channel.

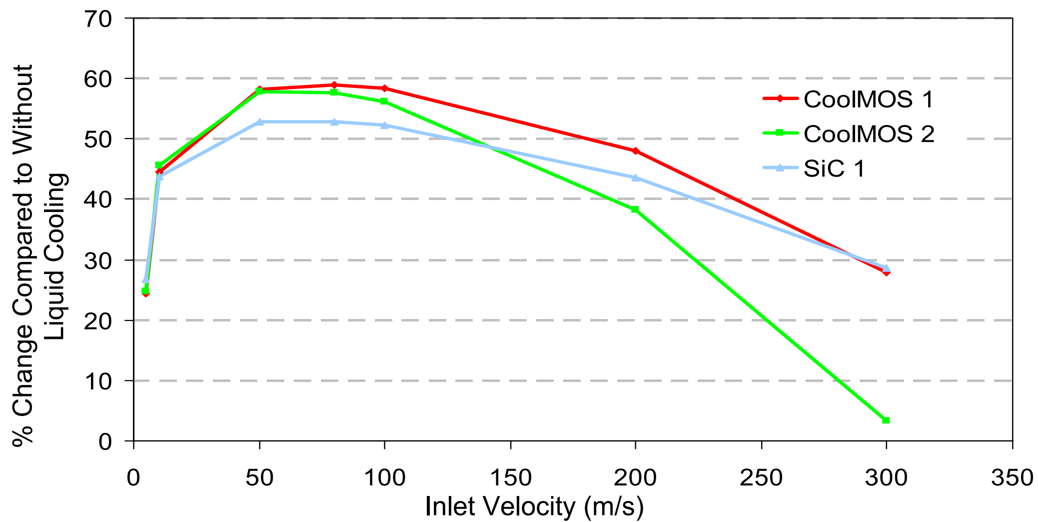

Figure 5.33 Effect of Inlet Flow Velocity on the Thermal Performance of the IPEM

Although this was a preliminary study on the possible implementation of micro-channel cooling for the IPEMs, one can expect a high heat transfer coefficient at the wall of the channel. As shown in Figure 5.34, the heat transfer coefficient at the channel wall is as high as $3x10^6$ W/m^2-K, which is much higher than forced convection. Therefore, we can achieve much better thermal performance by implementing micro-channel cooling than forced air convection.

5.7 Summary

The lack of knowledge in the thermal performance of power electronic modules packaged using new packaging techniques creates the need to have an in depth understanding on the thermal behavior of such modules. Similarly, the introduction of Embedded Power technology has created a lack of understanding of the thermal performance of Embedded Power modules such as IPEMs. For this reason, this research dedicates to provide thermal analysis and characterization of the IPEMs. Specifically, these studies aim to:

- understand the overall thermal performance of the IPEMs
- understand the mutual effect among the heating chips
- identify better ceramic materials for use to enhance the heat transfer within the IPEMs
- understand the metallization design parameters on the ability of transferring heat within the IPEMs
- understand the effect of the polyimide thickness on the heat transfer within the IPEMs
- evaluate and introduce integrated cooling strategies for improving the thermal performance of the IPEMs

It was found that the DBC ceramic dominates the ceramic carrier in transferring heat away from the power chips, the distance between the two MOSFET chips is not an important parameter in the thermal design, and the metallization contact area, type, and thickness have relatively small impact on the chip temperature (~4%). This research also

evaluated several integrated cooling strategies such as structural enhancement, double-sided cooling, and integrated micro-channel cooling. Improvement ranging from 30% to 60% can be observed with the implementation of these integrated cooling strategies.

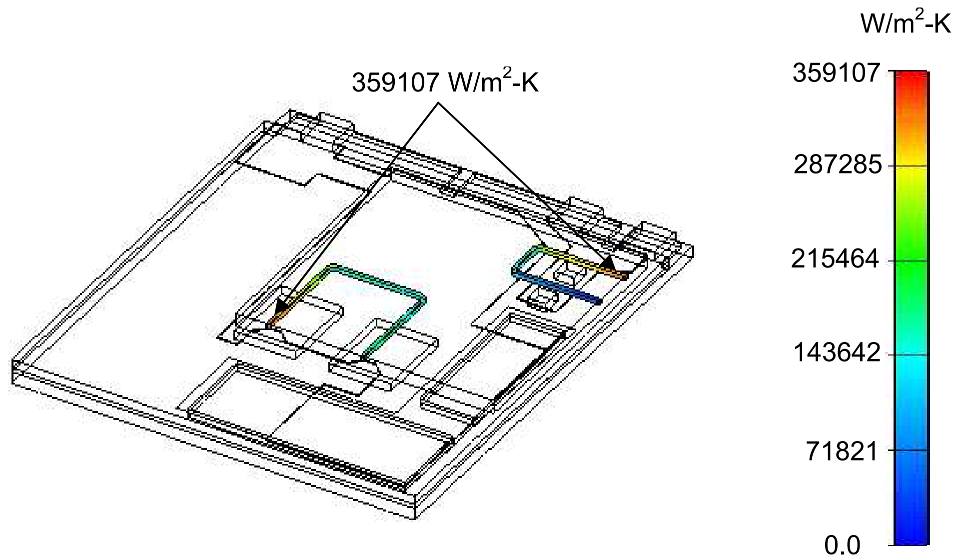

Figure 5.34 Heat Transfer Coefficient on the Channel Wall

Chapter 6

Thermal Design Guidelines for Embedded Power Modules

Engineers and other professionals always routinely work in the problem solving and design environment to invent new products as well as to improve current engineering designs. Engineering design is an open-ended process. To fulfill a particular need for the best result, all suitable solutions have to be considered. Although the designer's scientific knowledge plays an important role in the engineering design, it is generally accepted that experience also plays a crucial part in engineering design.

Design guidelines are often useful when redesigning an old product or designing a new product. The idea behind the design guidelines is that there exists a fundamental set of principles that determines good design practice. These design guidelines can be derived from the knowledge when a set of judgments based on the design rules can yield correct solutions to all problems. To initiate thermal design guidelines for the Embedded Power modules, this chapter presents some useful thermal design guidelines for the Embedded Power modules.

6.1 Design for Thermal Performance Concepts

6.1.1 General Engineering Design Practice

Engineering design is aimed at the creation of products that must function correctly within the constraints of defined need to ensure the required performance. Each designer has his or her own way of designing, and it reflects the way he or she views the design process. Ulrich et al. [73] showed a general design process in engineering design that included the design planning, concept development, system-level design, detail design, testing and refinement, as well as production ramp-up (Figure 6.1).

Any engineering problem starts with the need for certain engineering product and the problem statement. Modeling is a technique used by the designer to define a real situation for generating quantitative solutions. Relevant approximations in the modeling

are critical for obtaining the best solution to the engineering problem. Therefore, it is critical that the designer must have a clear understanding of the physical basis of the real situation. While engineering design is an open-ended process, very often more than one solution exists to the engineering problem. The best solution is generally found based on the designer's scientific knowledge and experience. The final stage of the design process involves the evaluation of the solutions to find the optimal solution.

Similarly, in the thermal design, the first task is to identify the objectives of the thermal design. The most common objective of the thermal design in electronics is to keep the junction temperature of the semiconductor devices at or below a given temperature such as 125°C. Three general ways of analyzing the design situation include

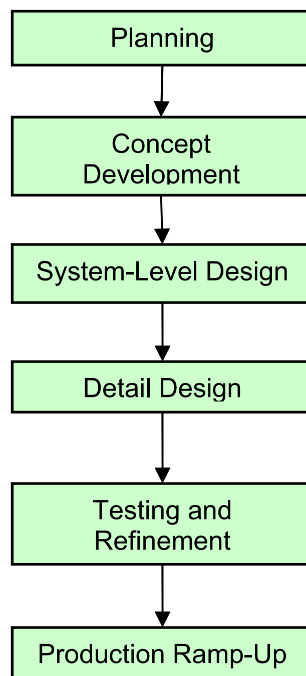

Figure 6.1 Block Diagram of the Engineering Design Process

analytical analysis, mathematical modeling, and experiments. Some common solutions to achieve this objective include justified selection of heat sinks, high thermal conductivity interface materials, or other cooling technologies such as heat pipes, liquid cooling, and cryogenic cooling. Optimization of the design generally concentrates on selectively choosing the best nominal values of design parameters that optimize performance reliability at lowest cost. Finally, the best design parameter quantity will be chosen as the output of the design for prototype preparation.

6.1.2 Thermal Design Practice in Power Electronics

In current power electronics systems, the thermal performance of the power electronics components affects the system performance and reliability. Overheating of power electronics components can result in device malfunction and consequently cause severe catastrophe in our daily lives. Regardless of the application, high temperatures make the electronic components unreliable and more likely to fail. Good thermal management not only can reduce the thermally-induced failures but also enhance the performance of the power electronics components. As Rybnikov et al. [74] and Viswanath et al. [75] stated, the performance of a processor depends on the temperature of the processor. The clock speed of the processor is higher at low temperature.

Thermal performance of power electronics components can be defined as the ability to operate within the maximum temperature limit as well as dissipate heat out from the component to the ambient. Having a good thermal design can avoid the components operating outside their critical temperature or overheating. An effective way of addressing the relevant thermal design is through a set of thermal design rules based on conventional practices.

A thermal design process in power electronics, either in module level or system level, can be illustrated in Figure 6.2. General input to the thermal design includes the heat loss of the electronic components, the electronic package information such as the structure of the package, the environment condition, as well as the electrical circuit and packaging constraints. Thermal modeling can be performed with analytical analysis or mathematical modeling. We can always use one-dimensional or two-dimensional heat

equations to evaluate the thermal performance of some electronic components. However, the thermal phenomena in most electronic components and systems are complex and three-dimensional. In addition, the thermal design in electronic systems not only involves heat transfer but also fluid flow. Therefore, numerical modeling is needed to analyze this complicated situation by solving the flow field and the heat transfer either simultaneously or iteratively.

If mathematical modeling is used as a tool for thermal analysis, experimental validation is always required to validate the accuracy of the mathematical model. The experimental validation involves conducting experiments that the numerical results can be compared to. With the validated thermal models, various studies can be conducted to study the influence of the design parameters on the thermal performance of the power electronic components and systems. By identifying the critical design parameters during the parametric studies, the critical design parameter can then be optimized to achieve the best result. Finally, the prototype can be built using the optimized design parameters for further performance evaluation.

However, with the increase functionality in the power electronics, thermal design has become more complex. The need for having a concurrent engineering design process in which electrical, packaging, and thermal designs are performed in parallel is essential in order to achieve a good product design. In this case, the flow chart shown in Figure 6.2 is no longer applicable, and a new flow chart should be made available to show the interaction among the multidisciplinary area designs.

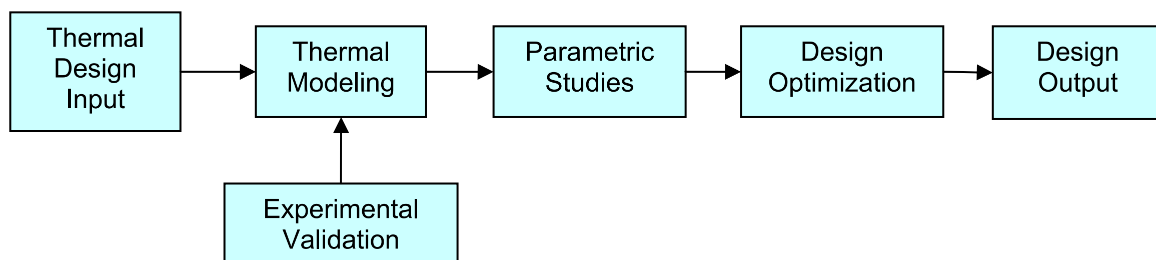

Figure 6.2 Generic Thermal Design Flow Process

Figure 6.3 shows the flow chart of interactive thermal design using concurrent engineering design process. This process is much complicated than the flow chart shown in Figure 6.2. In the concurrent engineering design process, the optimized parameters are checked with electrical performance limitations and package manufacturing constraints for optimal performance and manufacturability [76]. Good design is an iterative process as shown in Figure 6.3. It involves analyzing all the possible solutions before deciding on the final solution.

6.2 Types of Design Guidelines

A design guideline is defined by a standard or principle by which to make a judgment or determine a policy or course of action [77]. Design guidelines can be in the form of theoretic, empirics, or practices that relate the thermal behavior of the power electronics package to the thermal design requirements. By understanding the thermal behavior of the component, the thermal designer can choose relevant materials, geometries, cooling strategies to optimize the thermal performance of the component.

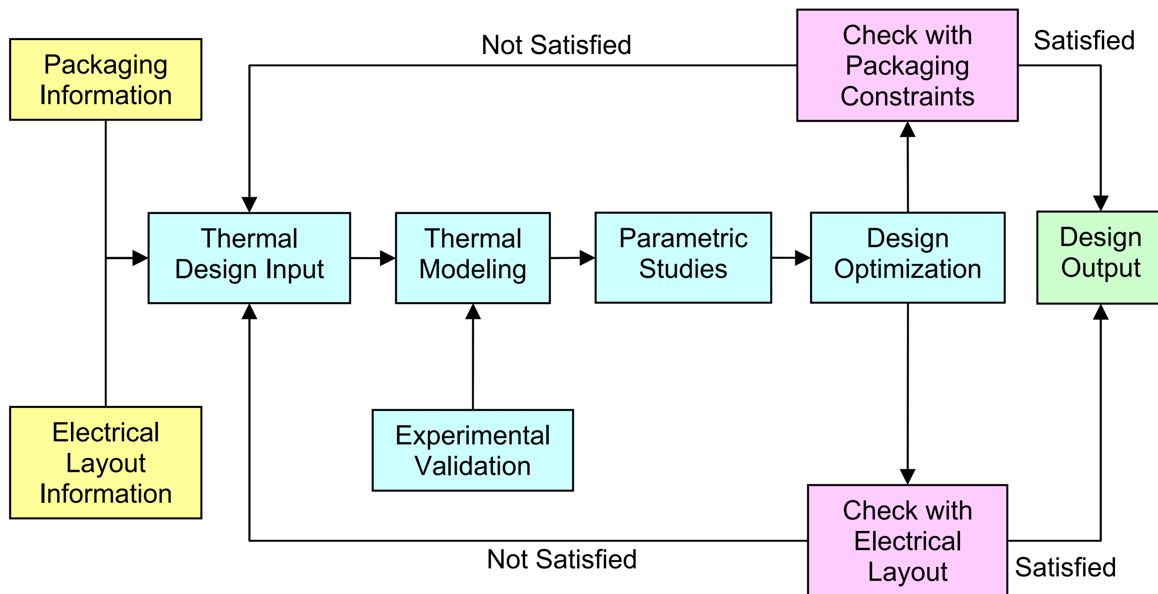

Figure 6.3 Concurrent Engineering Design Flow Process for Embedded Power Modules

The role of the design guidelines is to provide some insight to the design parameters during the design process. Although the designer may be faced with the available choices for the design, the main point in using the design guidelines is to recognize the available information as well as the known constraints. Common thermal design goals in the power electronic components typically relate to the thermal performance, reliability, cost, as well as weight and size reduction. Package design constraints can constitute information on the package manufacturing, assembly, electrical performance, and environment limitations.

General guidelines are broader theoretical considerations which are not confined necessarily to a single engineering mechanism. Generally, design guidelines are formal statements of what have been known or the embedded knowledge implanted in routine work. According to Dix et al. [78], conceptual guidelines are applicable during early stage of the design activities and detailed guidelines are applicable during later stage of the design activities. Conceptual design guidelines gather all the elements of the design as a whole. The conceptual design is the initial rough design concept. It is an early process where brainstorming ideas are put into preliminary analysis. On the other hand, detailed design expands the preliminary design to the extent that the design is sufficiently implemented. It involves the specification of how an individual component of a system will function.

Suh [79] presented the axiomatic approach to design in which basic principles govern decision making in design. The axiomatic approach is a design procedure. According to Suh [79], there are only two design axioms derived from the generalization of good design practice that govern good design:

Axiom 1 The Independence Axiom

Axiom 2 The Information Axiom

Axiom 1 states that the design parameters and the functional requirements are related such that the specific design parameters can be adjusted to satisfy its corresponding functional requirements without affecting other functional requirements. In addition, Axiom 2 states that the best design is a functionally uncoupled design that has the minimum information content.

Similarly, corollaries or may be called design rules for design are all derived from the two basic axioms. These corollaries can be expressed as the following:

Corollary 1 Decoupling of Coupled Design

Corollary 2 Minimization of Functional Requirements

Corollary 3 Integration of Physical Parts

Corollary 4 Use of Standardization

Corollary 5 Use of Symmetry

Corollary 6 Largest Tolerance

Corollary 7 Uncoupled Design with Less Information

While the different design guidelines mentioned are applicable to the thermal design of the Embedded Power modules, this research work used different design guideline concepts to achieve a set of thermal design guidelines for the Embedded Power modules.

6.3 Thermal Modeling Guidelines for Embedded Power Modules

While most of the thermal behavior in electronics is complex and three-dimensional, numerical modeling is often used to mathematically describe and obtain information on the thermal response of the electronics either in steady state or transient conditions. Similarly, to understand the thermal behavior of the irregular structure of the Embedded Power modules as well as its complexity in the heat flow within the modules is to use numerically modeling method. With commercially available numerical software such as Flotherm®, Icepack®, I-DEAS ESC, Sinda, and Ansys, one can easily use the software to model the heat flow within the module.

Although the lead time for learning these software packages differ, their capabilities do not vary significantly. Therefore, the designer can use whichever software that he or she is comfortable with. However, the designer should always perform experimental validation of the thermal models to ensure the accuracy of the software program in modeling the heat equations as well as the Navier-Stokes equations. There are three main heat transfer modes; namely, conduction, convection, and radiation. Eq. 6.1 shows the equation for conduction in steady state, mainly named Fourier's Law of conduction:

$$k \cdot (\frac{\partial^2 T}{\partial x^2} + \frac{\partial^2 T}{\partial y^2} + \frac{\partial^2 T}{\partial z^2}) = \rho \cdot C_p \cdot V \cdot \frac{\partial T}{\partial t}, \quad (6.1)$$

where k is the thermal conductivity, T is the temperature, x is the x-direction, y is the y-direction, z is the z-direction in Cartesian coordinate, ρ is the density, C_p is the constant pressure heat capacitance, V is the volume, and t is the time.

Equation for heat convection, Newton's second law of cooling, is shown in Eq. 6.2:

$$Q = h \cdot A \cdot (T - T_\infty), \quad (6.2)$$

where Q is the heat dissipation, h is the heat transfer coefficient, A is the convection area, T is the object temperature, an T_∞ is the ambient air temperature. In addition, the heat transfer through radiation mechanism in electronics cooling is governed by Stefan-Boltzmann law and can be described by Eq. 6.3:

$$Q = \varepsilon \cdot \sigma \cdot A \cdot (T^4 - T_s^{\ 4}), \quad (6.3)$$

where Q is the heat dissipation, ε is the emissivity, σ is the Stefan constant (5.67 x 10^{-8} $W/m^2\text{-}K^4$), A is the area, T is the object temperature, and T_s is the surrounding temperature.

In computational fluid dynamic analysis, Navier-Stokes equations are commonly used to calculate the fluid flow field. Navier-Stokes equations are the foundation of fluid mechanics and describe the fluids in motion. For example, the governing equations solved by I-DEAS ESC are the time-averaged Navier-Stokes equation for three-dimensional flows. These equations expresses the conservation of mass, conservation of energy, and conservation of momentum of the fluid flow at all situations.

Thermal simulations can be performed using different methods depending on the objectives of the study. In most system level thermal modeling for electronic systems, the understanding of the fluid flow within the electronic enclosure is desired to predict accurate temperature distribution within the electronic equipment. In this case, a CFD-based thermal simulation is preferred because it helps analyzing airflow and direction. Ultimately, the local heat transfer coefficient values can be obtained from the CFD simulation for predicting the temperature of critical components within electronic

equipment. If the heat transfer coefficient values are known, a CFD-based thermal simulation is not necessary required. Thus, the simulation is simplified to the conduction problem only. This reduces the finite element model size as well as the computational time.

This technique can also be applied to module-level thermal analysis with known equivalent heat transfer coefficients on the surfaces of the module. With the potential smaller finite element size without CFD analysis, the thermal modeling at module level can be more detailed. This allows for representing the package in sufficient geometric detail to capture all relevant thermal paths accurately. In addition, the flexibility in model changes such as parametric analyses, sensitivity analysis, component placing studies, and component sizing analyses in the preliminary design allows for shorter computational time and sensible results.

The accuracy of the input parameters in the model is critical for obtaining accurate results. A sensitivity analysis is important to study how sensitive the outcomes are to the changes in the inputs. The sensitivity of a given parameter refers to how sensitive a given output variable is to changes in that input parameter. It is important to understand these sensitivities to determine their effects on the design studies conducted using the numerical simulations.

In identifying sensitive input parameters for the thermal modeling of IPEMs, critical input parameters and output variables were identified and are summarized in Table 6.1. The critical input parameters include the interface material thicknesses and the thermal conductivities of the interface materials. The input parameters are represented by the equivalent thermal resistance of each interface layer within the model. The critical output variables are the chip temperatures.

The sensitivity coefficient for an output variable *j* to an input parameter *i* was defined as a dimensionless term, X_{ij}^{+}:

$$X_{ij}^{+} = \frac{\delta T_j^{+}}{\delta \beta_i^{+}} = \frac{\Delta T_j^{+}}{\Delta \beta_{Si}^{+}}. \tag{6.4}$$

where $\Delta\beta_{Si}^{+}$ us the dimensionless parameter of the difference of the perturbed parameter defined in Eq. 6.5:

$$\Delta\beta_{Si}^{+} = \left|\frac{\delta\beta_{Si}}{\beta_{Ni}}\right| = \left|\frac{\beta_{Si} - \beta_{Ni}}{\beta_{Ni}}\right|, \tag{6.5}$$

where β_{Ni} is the nominal parameter value and β_{Si} is the perturbed value. Thus, for a 5% variation in the nominal parameter value,

$$\left|\frac{\beta_{Si} - \beta_{Ni}}{\beta_{Ni}}\right| = \left|\frac{(\beta_{Ni} + 0.05\beta_{Ni}) - \beta_{Ni}}{\beta_{Ni}}\right| = \left|\frac{0.05 \cdot \beta_{Ni}}{\beta_{Ni}}\right| = 0.05\,. \tag{6.6}$$

That is, $\Delta\beta_{Si}^{+}$ represents a 5% variation in the nominal parameter value, β_{Ni}. The non-dimensional temperature, ΔT^{+}, is defined by:

$$\Delta T^{+} = \left|\frac{T_N(\beta_{Ni}) - T_S(\beta_{Si})}{T_N(\beta_{Ni}) - T_\infty}\right|, \tag{6.7}$$

where T_∞ is the ambient temperature, and $T_N(\beta_{Ni})$ and $T_S(\beta_{Si})$ are the respective predicted temperature for each parameter using β_{Ni} and β_{Si}. Note that $T_N(\beta_{Ni})$ is also referred to as the nominal temperature.

Figure 6.4 shows the result of the sensitivity of the input parameters on the output variables. The most sensitive input parameter in the model is the thermal conductivity of the solder material, especially to the temperature of the SiC diode followed by the copper material. In addition, the temperature of the SiC diode 1 is relatively sensitive to the thickness of the solder layer between the SiC diode 1 and the DBC trace compared to other input parameters. Overall, the result shows that the input parameters such as the thickness and the thermal conductivity of the interface materials are insensitive (X_i^{+}<<1), thus, indicating that these input parameters do not have significant effect on the results presented in Chapter 5.

Despite the advances in numerical modeling, any mathematical model is a simplified model of the reality. Therefore, validation of the numerical model becomes crucial in determining the exactness of mathematical model. Experimentation is the most common way of conducting validation on the numerical model. In validating the thermal model, the simulation results are compared to the experimental data. The validated

thermal model can better predict the temperature distribution of the component. Thus, it can then be used for various thermal design purposes without building the actual prototype.

In summary, the guidelines for the thermal modeling of Embedded Power modules can be listed as the following:

- Know the goals of the thermal modeling (e.g. thermal analysis, model validation, thermal design optimization)
- Understand the geometry and the structure of the Embedded Power modules including the interfaces
- Collect information on the thermal properties of the materials used in the Embedded Power modules
- Understand the heat transfer phenomena (conduction, convection, radiation) within the electronic package and from the package to the environment
- Understand the heat flow path within the package
- Know the boundary conditions (e.g. power loss, interfacial conditions, environmental condition)

6.4 Thermal Testing Procedure and Guidelines

Thermal testing is widely used for several purposes such as thermal characterization of electronic components and equipment, validation of numerical models, as well as thermal study on the electronic components and systems. Thermal testing usually involves temperature measurements using temperature sensors and thermography infrared thermometer. Commonly used temperature sensors for experimentation include thermocouple wires, thermistor, and resistive temperature devices (RTD). Other method includes diode temperature sensing technique. In addition, Azar et al. [80] presented liquid crystal imaging for temperature measurement of electronic devices.

Table 6.1 Description and Nominal Values of Parameters Used in Sensitivity Analysis

Sensitivity Parameter, β_i	Description of the Represented Thermal Resistance	Nominal Value, β_{Ni}
Solder 1 (t)	Thickness of the Solder Between CoolMOS 1 and DBC Copper Trace	0.53 mm
Solder 2 (t)	Thickness of the Solder Between CoolMOS 2 and DBC Copper Trace	0.53 mm
Solder 3 (t)	Thickness of the Solder Between SiC 1 and DBC Copper Trace	0..39 mm
Epoxy 1 (t)	Thickness of the Epoxy Between CoolMOS 1 and Ceramic Carrier	0.51 mm
Epoxy 2 (t)	Thickness of the Epoxy Between CoolMOS 2 and Ceramic Carrier	0.51 mm
Epoxy 3 (t)	Thickness of the Epoxy Between SiC 1 and Ceramic Carrier	0.51 mm
Polyimide_Top (t)	Thickness of the Top Polyimde	0.127 mm
Polyimide_Bottom (t)	Thickness of the Bottom Polyimde	0.127 mm
Copper (k)	Thermal Conductivity of Copper	395 W/m-K
Alumina (k)	Thermal Conductivity of Alumina	26 W/m-K
Aluminum Nitride (k)	Thermal Conductivity of Aluminum Nitride	180 W/m-K
Silicon (k)	Thermal Conductivity of Silicon	117 W/m-K
Silicon Carbide (k)	Thermal Conductivity of Silicon Carbide	490 W/m-K
Gel (k)	Thermal Conductivity of Gel	0.2 W/m-K
Solder (k)	Thermal Conductivity of Solder	51 W/m-K
Polyimide (k)	Thermal Conductivity of Polyimide	0.3 W/m-K
Epoxy (k)	Thermal Conductivity of Epoxy	1.4 W/m-K

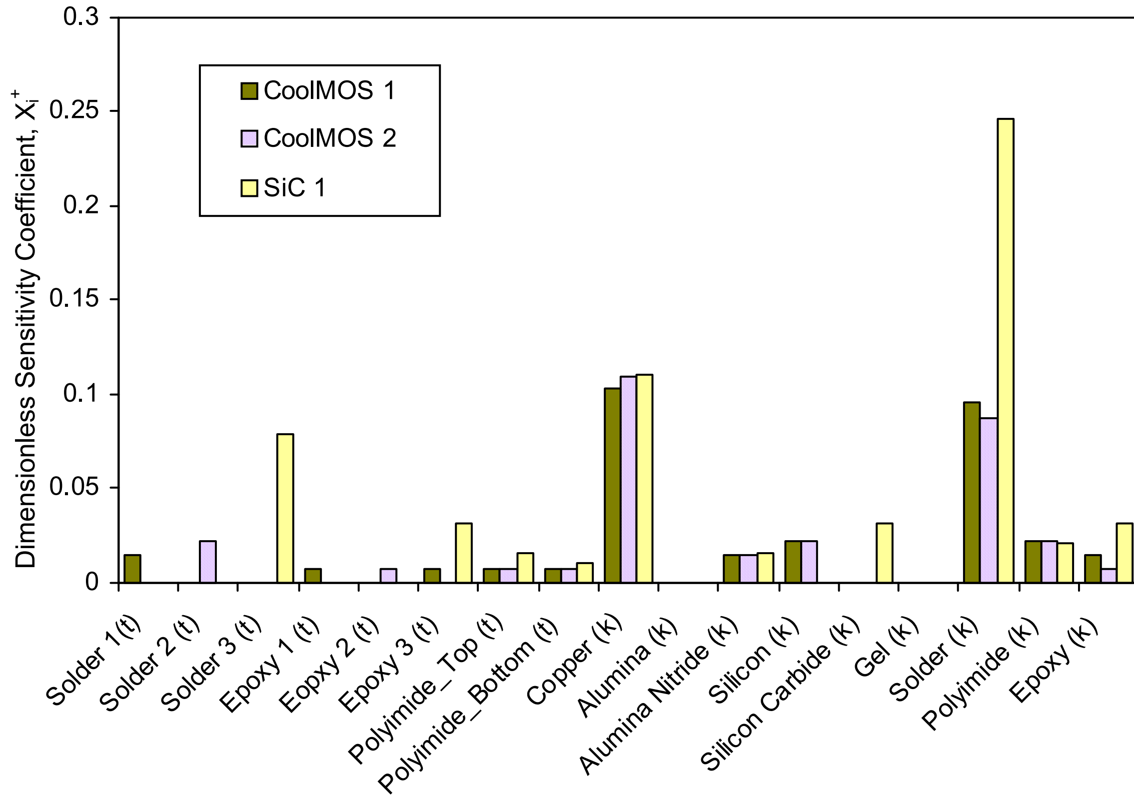

Figure 6.4 Dimensionless Sensitivity Coefficient for Each Input Parameter in the Numerical Model

In addition to temperature measurement, thermal testing sometimes also involves airflow measurement especially in electronic equipment where the flow field has a great impact on the thermal performance of the electronic equipment. Cooling of electronic systems by natural or forced convection requires knowledge of the fluid flow. Therefore, it is important to understand the need for velocity measurement and the right practices and sensors suitable for electronic enclosures. Methods to measure airflow include using hotwire anemometer, laser doppler velocimetry (LDV), pitot tube anemometer, and thermal anemometer. Other measurement techniques are particle tracing, pressure probe, and particle image velocimetry (PIV) [81].

Finally, understanding the thermal measurement errors is as important as conducting the right experiment. Knowing the measurement errors can reduce the misunderstanding on the accuracy of the measurement. Details on some common thermal measurement errors can be found in [82].

In summary, the guidelines for the thermal testing of Embedded Power modules can be summarized as the following:

- Understand the objectives of the thermal testing
- Know the environment you test the module (flow velocity, fan speed, size of the enclosure, ambient temperature)
- Use the right type of sensors for your measurement
- Employ optimum sensor placement strategies (best place to place the sensors for minimum noise, methods of attaching sensors)

6.5 Thermal Design Guidelines for Embedded Power Modules

The purpose of the design guidelines is to provide more suggestive and general rules in determining and predicting the thermal performance of the Embedded Power modules. Although the guidelines documented here are more towards abstract (principle) guidelines, some detailed guidelines will also be discussed.

The thermal design of the Embedded Power modules was based on simplicity, efficiency, and reliability where these three functional restraints were defined in "solution neutral" environment. Trade-offs in different ceramic materials, chip-to-chip distances, copper trace areas, dielectric material thicknesses, metallization thicknesses, metallization materials, and metallization interconnect patterns were considered with respect to the electrical performance limitations and the package manufacturing limitations.

In summary, the guidelines for the thermal design of Embedded Power modules can be summarized as the following.

I. Ceramic Material Selection

In Embedded Power modules, there are two layers where ceramic substrates are used for electrical insulation. These layers are also aimed to function as good thermal path for conducting the heat from the power chips to the outer surface of the package. One of these layers is the DBC ceramic layer while the other one is the ceramic carrier layer. The heat conduction through these layers is proportional to the thermal

conductivity of the layer but inversely proportional to the thickness of the ceramic layer as expressed in Eq. 6.8:

$$Q_{cer} = k_{cer} A_{cer} \frac{\Delta T}{t} = \frac{\Delta T}{R_{cer}}, \tag{6.8}$$

where Q_{cer} is the heat transfer through the ceramic layer, k_{cer} is the thermal conductivity of the ceramic, A is the area of the ceramic, ΔT is the temperature difference between the two conducting surface of the ceramic, t is the thickness of the ceramic layer, and R_{cer} is the thermal resistance of the ceramic layer. Therefore, in selecting the ceramic material from the thermal perspective, the higher thermal conductivity of the ceramic material with the smallest thickness can yield good heat transfer through the ceramic layers.

It was also found in this research that the ceramic carrier has less impact on the overall temperature of the module since most of the heat is transported through the solder layer to the DBC. Therefore, having low thermal resistance on the DBC layer can help improve the thermal performance of the module. While DBC substrate is commonly used in power electronic packaging, new materials with a lower thermal resistance than the DBC substrate can be good candidates for its replacement.

II. Chip Placement

Each power chip is soldered to the DBC copper trace in the Embedded Power modules. The distance between the chips does not have significant influence on the chips temperatures. This is because the major heat path from the chip is through the solder layer and to the individual DBC copper trace layer. From there, the heat is conducted through the DBC ceramic layer and the DBC bottom copper layer. Therefore, the mutual effect of the two chips on different copper trace is small.

If more than one chip is sharing the same DBC copper trace, the mutual effect between the chips is still insignificant due to the thin layer of the copper trace and the minimal heat spreading within the copper trace layer. As a result, the distance between the chips will be determined by the packaging constraint. Overall, the distance between the chips is not a major factor influencing the thermal performance of the module since the heat flow from the power chips is mostly confined by the thinness of the DBC layers

that restrict lateral heat spreading. Therefore, the heat flow from the power chips to the DBC layers through the solder layers is considered to be one dimensional.

III. Design of Metallization Interconnect

The metallization provides electrical interconnections to the multiple chips within the module. The direct contact between the metallization and the power chip is the interconnect vias. The pattern and size of the vias are limited by the design of the aluminum bond pad on the power chips. From the thermal perspective, the larger the contact area for the interconnect vias on the power chip, the better the heat conduction is. Therefore, fully utilize the bond pad pattern on the power chips is desired.

On the other hand, the thickness of the metallization and the material used for the metallization do not have an influential impact from the thermal perspective. However, it is always wise to decide these design parameters based on the trade-offs among electrical performance and the reliability viewpoint. Figure 6.5 summarizes the impact of the metallization design parameters on the thermal performance of the module.

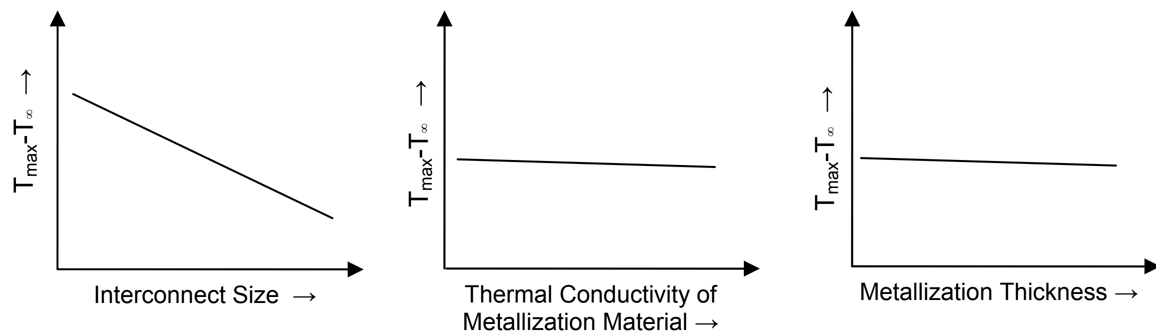

(a) Interconnection Size (b) Metallization Material (c) Metallization Thickness

Figure 6.5 Impact of Metallization Design Parameters on Temperature Rise of the Module

IV. Thermal Management for Embedded Power Modules

The studies in this research have shown that the most effective way of reducing the maximum temperature of the module is to have effective heat dissipation strategies from the package to the environment. While most of the heat is transported through the soldered side of the power chips, heat extraction through the top side of the power chips is also desired. Metallization is the structure that has direct contact with the power chips from the top. However, the very thin layer of metallization does not help in spreading heat over the layer but results in hotspots.

To further extract the heat from these hotspots, localized cooling is desired. This can be achieved through both active and passive cooling strategies. Mechanically assisted cooling systems are said to provide active cooling since they require energy. Active cooling includes refrigeration and thermo-electric cooling. Passive cooling strategies are widely used in electronic cooling. Typical passive cooling techniques apply high thermal conductivity adhesives, silicone gel, and epoxy to replace low thermal conductivity interface materials. Other cooling strategies include liquid cooling, spray cooling, and heat pipes.

Reducing the package thermal resistance, R_{j-c}, shall be one of the goals of the thermal design for the Embedded Power modules. Though it has shown that the most influential parameter in reducing the maximum temperature of the module is the external thermal resistance, R_{c-a}, any design effort in reducing the R_{j-c} is valuable. A further effort should extend to enhance the thermal design of the module such that the heat from the package can be carried away to the ambient easily. Consequently, this requires a low R_{c-a} and thus desires effective mechanisms to transfer the heat from the package to the ambient. Several different strategies such as double-sided cooling can be employed to achieve low R_{c-a} as shown in the previous chapter.

6.6 Summary

In summary, there is no one unique design path to follow in the thermal design of Embedded Power modules. The designer should consider multiple design options before deciding the final design that best prescribed the objective of the design. The thermal

design steps are iterative with the input from and output to the electrical designer and the packaging engineer. Common design parameters for the Embedded Power modules are materials, interfaces, and geometric configurations. The role of the thermal designer is to select the most compatible design parameters with trade-offs among the design goals and constraints. Finally, as a thermal designer, you have to think logically, avoid technical conceit, and avoid disguised assumptions.

Chapter 7

Conclusions

Growing dependence on power electrics has caused an urge in the need for high reliability power electronics to convert raw forms of electric power to different forms for individual applications. The demands on performance, cost, and reliability have drastically influenced the packaging and interconnection technologies in this field. New packaging and interconnection technologies are desired to handle multiple chips with high power density packaged in a smaller volume. With ever-rising heat fluxes in continuously miniaturized power electronics, the understanding of heat transfer phenomena in power electronics is becoming crucial to the design, providing proper thermal management for high reliability.

The trend toward higher power density requires a greater attention to heat transfer. The primary goal in thermal design is to limit the junction temperature of the power electronics modules. With the lack of knowledge of the impact of the new packaging technology on the thermal performance of the module, a good understanding of the thermal behavior of the module can help in both identifying potential thermal failure and designing appropriate thermal management strategies for the module. Simulation tools and experimentation are commonly used to perform the thermal analysis. Advanced thermal management such as forced air cooling, liquid cooling, and heat pipes are extensively used to improve the thermal performance of electronic components and equipment. Consequently, substantially higher thermal conductivity materials will also aid in adequately dissipating heat loads from high heat flux power chips.

In this research, we performed a thorough thermal analysis and achieved an in depth understanding of the thermal behavior of Embedded Power modules. We also accomplished several goals discussed in Chapter 1. The summary and contributions of this research are discussed in the following.

7.1 Contributions

I. Understanding of the thermal behavior and heat transfer in Embedded Power modules

a. *The studies have shown that the hotspots in the module are the power chips, as one might expect*. Heat flow from the power chips through the bottom side and the top side are considered virtually one dimensional. The heat from the power chip is barely conducted laterally to the ceramic carrier due to the low thermal conductivity of the interfacial material—epoxy.

b. *This research has found that the position of the chips within the module and the size of the power chips can result in different junction-to-ambient thermal resistance, R_{j-a}, for the chips.* The chip temperature rise maintained a linear relationship with the power loss although the chips were packaged using Embedded Power technology. The results were also useful to determine the allowable power loss for the module under variable ambient temperature with an air velocity of 2.2 m/s.

c. *The methodology for obtaining the thermal resistance matrix to describe the thermal resistance of a multi-chip module was demonstrated.* The prediction errors using the resistance matrix were examined against numerical results. This study has shown that the resistance matrix can predict the temperature of the individual chip in a multi-chip module within an acceptable error margin of 5% to 10% in the heat dissipation range of 10 W to 30 W.

d. *Overall, the studies in this research have demonstrated the use of two different methods (numerical and experimental) in obtaining information on the thermal behavior of the Embedded Power module.* The studies discussed in previous chapters have also shown how and where these two different methods can be used to acquire necessary information on the thermal performance or the thermal behavior of the module.

II. Understanding of the effect of the material properties and geometrical sizing of specific structure on the thermal performance and the stress distribution of planar multi-layer structures

a. *The DBC ceramic dominates the ceramic carrier in transferring the heat away from the power chips.* While a ceramic substrate is commonly used in the packaging of the Embedded Power modules, a high thermal conductivity value ceramic substrate can substantially help in improving the heat transfer within the module. Common ceramic materials are alumina and aluminum nitride. The thermal conductivity of aluminum nitride is about six times higher than alumina although aluminum nitride is much more expensive than alumina. The study has shown that replacing the alumina ceramic carrier with aluminum nitride or ALOX™ substrate can reduce the maximum temperature rise of the module by 3%. Further improvement of 9% can be achieved by replacing the alumina DBC substrate with aluminum nitride.

b. *The temperature rise of the module can be reduced as much as 5% with an optimized polyimide thickness*. Investigation on the thickness of the polyimide layer was performed to further understand the task of polyimide layer in effectively transporting the heat within the heat path in the module.

c. *The distance between the two MOSFET chips is not an important parameter in the thermal design.* Studies on the effect of the chip-to-chip distance and copper trace area on the thermal performance of the DC/DC IPEM using simplified models were presented. The placement of the MOSFET should be considered from other factors such as the length of the electrical interconnects as well as the overall layout constraints. In addition, the size of the copper trace area should also be determined based on the best electrical performance as well as the overall layout constraints.

d. *The metallization contact area, type, and thickness have relatively small influence on the chip temperature compared to von Mises stress*. The study on the design parameters of the metallization layer provides some insight on the effect of different interconnect patterns, metallization thicknesses, and metallization materials on the thermal and thermomechanical performances of the Embedded Power modules using

metallization bonding as the interconnect method. Key findings from this preliminary study include:

- Temperature rise of the module is directly related to the total contact surface area of the interconnect pattern. On the other hand, the von Mises stress depends on the interconnect pattern rather than the total contact surface area. The study had shown that using 6 holes and 9 holes interconnect patterns yielded the same maximum von Mises stress since the interconnect patterns for both cases were round. Instead, replacing the round pattern with large continuous surface such as rectangular pattern would reduce the stress on the silicon die. However, the improvement obtained in the stress reduction in the metallization was greater than the increase in the stress on the silicon die (6.4% vs. 3.5%).
- Increasing the metallization thickness slightly improved the thermal performance of the module. On the other hand, considerable increase in stress was observed by increasing the metallization thickness more than 16x of the baseline thickness on the metallization.
- The matching of CTE dominates the effect of the thermal conductivity of the material in selecting a better material for the metallization. Of all the materials investigated in this study, molybdenum is the most suitable material when considering the trade-offs between the thermal and thermomechanical performance.
- The von Mises stress distributions and the maximum average von Mises stress on both the silicon and the metallization do not vary significantly (within 5%) in comparing four different sets of restraints defined in the stress model.

III. Development of detailed numerical modeling techniques for planar multi-layer structures

a. *A modeling methodology was developed for integrated power electronics modules*. An approach to assess the needed accuracy level in thermal analysis of integrated power electronics modules is presented to aid in efficient and timely heat transfer analysis. The methodology could also be applied to any complex electronic package

in general. The module conduction is modeled in great detail accounting for the different materials and geometric complexities.

b. *Numerical models of the IPEMs were developed using a commercial finite element program, I-DEAS.* Thermal simulations were performed using computational fluid dynamics code in I-DEAS, ESC, to identify hotspots as well as to predict steady-state temperature distributions within the modules. The detailed modeling of the heat transfer phenomena in the IPEMs is very challenging due to the complexness of the geometry, the unknown interface conditions within the module a priori, and the unverified material properties. This research also demonstrated a methodology for validating numerical model with experimental data. The exact experiment environment was modeled and the results show that the numerical model can predict the temperature of the IPEMs with about 5% difference of experimental data.

c. *Different ways of defining constraints on the stress models were explored.* This study particularly investigated four different constraint sets to understand the sensitivity of the simulation results on different constraints. The results showed that both the von Mises stress and stress distribution are not influenced by different constraints studied here.

IV. Introduction of new integrated cooling strategies for planar multi-layer structures

a. *The study shows that structural enhancement can reduce the maximum temperature of the module by as much as 24%.* Studies in this research have shown that simple modifications on the geometry or the material can significantly improve the thermal performance of the IPEMs. Finding ways to create direct heat paths from the heat sources proves to be an effective method to improve the thermal performance of the module.

b. *Improvement ranging from 30% to 60% can be observed with the implementation of double-sided cooling and further improvement can be achieved through micro-channel cooling.* By soldering additional DBC on the top side of the module enables the employment of double-sided cooling for the module. This opens up various

cooling strategies that can be used for different applications such as single and two phase forced air and liquid cooling. To reduce the internal thermal resistance of the module, several combinations of the ceramic materials were studied. The use of DBC and Thermal Clad™ were also compared but the use of DBC proved to be better than Thermal Clad™. Similarly, preliminary study on integrating micro-channel cooling into the structure of the module also shows great improvement on the thermal performance of the module. While a specific structure was used as the case study in this study, the discussed methods of improving the thermal performance of module are applicable to general Embedded Power packages.

V. Development of thermal design rules for planar multi-layer structures

The purpose of developing thermal design rules is to suggest some guiding principles that are behind most thermal designs in Embedded Power modules and help future design and development of the Embedded Power modules. Very often in the process of the new design of similar product, designers have to learn by making mistakes. Possibly they will have to repeat the same type of mistakes as the previous designers before they realize what went wrong. Therefore, this research seeks to provide some guidelines to avoid such mistakes as well as replication of similar analyses in the future.

a. *A few guidelines were developed to perform thermal analysis of Embedded Power modules using commercial software*. Thermal analysis using commercial numerical modeling tool has become popular approach for analyzing the heat transfer in electronics. Simulation is a power tool for the analysis of new product designs. Thus, simulations are widely used for predicting the performance of a system, identifying potential thermal problems, verifying a design, and evaluating possible solutions to the problems. To achieve successful simulation studies, the user needs to understand the capability of the software as well as the shortcoming of the software.

b. *A thermal testing procedure and guideline for Embedded Power modules was outlined*. Experiments are often conducted to evaluate, compare, and provide insight into the design. In addition, experimentation can also validate numerical models. Validation is an essential phase in the numerical model development process for any simulation to avoid major and serious modeling errors. Consequently, any mistake in

performing the experiments or taking the measurements will lead to inaccurate information and design.

c. *A <u>thermal design guideline for the Embedded Power modules</u> was outlined*. These guidelines include ceramic material selection, chip placement, design of the metallization interconnect, and thermal management for the Embedded Power modules.

7.2 Recommendations

Detailed Models. In general, all power losses in switch mode power electronics consist of switching loss and conduction loss. These losses are calculated based on the switching waveforms of the voltage and current for switching loss and resistances of resistive elements in the circuit for conduction loss. The current thermal models used in this dissertation are for steady-state conditions. These models assume that the power loss from the power chip was constant as an average loss over time and uniformly distributed on the top surface of the power chips. Although it was demonstrated that these assumptions is feasible and can be greatly validated by experimental results, future thermal models should include the capability of using the waveform of the power loss over time as the boundary conditions and perform transient analysis in detail. In addition, a detailed distribution of the power loss on the power chips is desired for further identifying the hotspots on the chips.

New Materials. The selection of the packaging materials is important in achieving improved performance electrically and thermally as well as reliability. Although the current materials used in the Embedded Power modules are commercially available, the selection of the packaging materials should continue to search for emerging packaging materials that may provide promising improved performance. In particular, high thermal conductivity solder, power chips materials, insulation materials such as polyimide, and ceramic substrates are always appreciated in achieving better thermal performance for the module.

New Cooling Technologies. The studies in this dissertation show that the external heat extraction from the module to the ambient is more significant than the passive thermal

management strategies (such as the rearrangement of the chips) within the module. Although this research has demonstrated the possible implementation of integrated cooling strategies and its advantages, future investigations should include implementing these strategies into power electronics systems testbeds. In addition, future work should also focus on developing new cooling strategies (such as liquid cooling, two-phase cooling, spray cooling) that can be integrated structurally into he Embedded Power modules.

Design Rules. This dissertation outlines some guidelines for the thermal design of the Embedded Power modules. While these guidelines are applicable to the future thermal design of any multi-chip modules, specific design rules are also desired for the future design of the module. Since the best design for the Embedded Power modules is done by a team that is expert in multidisciplinary area, both mechanical and electrical engineering, future effort should focus on developing specific rules to provide back-of envelope calculations with known error margin.

Bibliography

[1]. *Intel Pentium 4 Processor in the 478-Pin Package Thermal Design Guidelines* (Santa Clara: Intel Corporation, 2002) http://developer.intel.com/design/pentium4/guides/24988903.pdf

[2]. Intel Corporation, "Expanding Moore's Law—Raising the Bar," http://www.intel.com/labs/eml/.

[3]. R. Mahajan, R. Nair, V. Wakharkar, J. Swan, J. Tang, and G. Vandentop, "Emerging Direction for Packaging Technologies," *Intel Technology Journal*, Volume 6, Issue 2, May 2002, pp. 62-75.

[4]. *Heat Density Trends in Data Processing, Computer Systems and Telecommunication Equipment* (Santa Fe: The Uptime Institute, 2001) http://www.upsite.com/TUIpages/whitepapers/tuiheat1.0.html.

[5]. B. A. Myers, "Cooling Issues for Automotive Electronics," ElectronicsCooling, August 2003, pp. 24-27.

[6]. Data Points, "Electronic Motor Drive Market Projected to Top $19 Billion by 2005," *Power Electronics Technology Magazine*, September, 2001, pp. 10.

[7]. S. Mulgaonker, B. Chambers, and M. Mahalingam, "An Assessment of the Thermal Performance of the PBGA Family," *IEEE Transactions on Components, Packaging, and Manufacturing Technology*-Part A, Vol. 18, No. 4, December 1995, pp. 739-748.

[8]. M. Mita, T. Kumakura, S. Inoue, and Y. Hiraki, "Advanced TAB/BGA Multi-Chip Staked Module for High Density LSI Packages," *Proceedings of Multi-Chip Module Conference*, 1994, pp. 68-76.

[9]. T. D. Yuan, "Thermal Performance Characteristics Comparison Between Flip-chip and Wirebond Ceramic Multichip Modules," *Proceeding of Multi-Chip Module Conference*, 1996, pp.44-48.

[10]. Y. G. Kim, "Folded Staked Package Development," *Proceedings of 52nd Electronic Components and Technology Conference*, 2002, pp. 1341-1346.

[11]. J. W. Balde, *Foldable Flex and Thinned Silicon Multichip Packaging Technology*, 1st Edition (Massacuhusetts: Kluwer Academic Publishers, 2003), pp. 1-14.

[12]. J. U. Meyer, M. Schuettler, O. Scholz, W. Haberer, and T. Stieglitz, "Flexible, Microarray Interconnection Technique Applied to Biomedical Microdevices," *Foldable Flex and Thinned Silicon Multichip Packaging Technology*, 1st Edition (Massacuhusetts: Kluwer Academic Publishers, 2003), Chapter 6, pp. 154-158.

[13]. X. Fan and S. Haque, "Emerging MOSFET Packaging Technologies and Their Thermal Evaluation," *Proceedings of 8th Inter-society Conference on Thermal Phenomena in Electronic Systems (I-THERM)*, 2002, pp. 1102-1108.

[14]. B. Ozmat, "Interconnect Technologies and the Thermal Performance of MCM," IEEE Transaction on Components, Hybrids, and Manufacturing Technology, Vol. 15, No. 5, October 1992, pp. 860-869.

[15]. K. Sienski, R. Eden, and D. Schaefer, "3-D Electronic Interconnect Packaging," *Proceedings of Aerospace Applications Conference*, Vol. 1, 1996, pp. 363-373.

[16]. B. Ozmat, V. A. K. Temple, and J. K. Azotea, "An Advanced Packaging Technology for High Performance Power Devices," *Proceedings of the 32nd Intersociety Energy Conversion Engineering Conference*, Vol. 1, 1997, pp. 687-693.

[17]. R. Fisher, R. Fillion, J. Burgess, and W. Hennessy, "High Frequency, Low Cost, Power Packaging Using Thin Film Power Overlay Technology," Proceedings of 10th Applied Power Electronics Conference & Exposition (APEC), Vol. 1, 1995, pp. 12-17.

[18]. T. Stockmeier and W. Tursky, "Present and Future of Power Electronics Modules," *Proceedings of Center for Power Electronics Systems (CPES) Seminar*, 2000, pp. 3-9.

[19]. Fuji Semiconductor, Inc., "Power Module IPM," http://www.fujielectric.co.jp/eng/denshi/scd/prod_pm.html (Saddle Brook, NJ: Fuji Semiconductor, Inc.)

[20]. Eupec Inc., "Econopack+ — A New IGBT Module for Optimized Inverter Solutions," http://www.eupec.com/p/e/pdf/ed_pcim_2000_bostonf.pdf (Nurembug, Germany: Eupec, Inc.)

[21]. Toshiba America Electronic Components, Inc., "Six-In-One Package Offers Low-Cost IGBT Solution for Industrial Drive Market," http://www.toshiba.com/taec/press/to-717.htm (Irvine, CA: TAEC, 1997)

[22]. A. B. Lostetter, F. Barlow, and A. Elshabini, "An Overview to Integrated Power Module Design for High Power Electronics Packaging," *Journal of Microelectronics Reliability*, Vol. 40, Issue 3, March 2000, pp. 365-379.

[23]. Z. Liang and F. C. Lee, "Embedded Power Technology for IPEMs Packaging Applications," *Proceedings of 16th Applied Power Electronics Conference and Exposition (APEC)*, Vol. 2, 2001, pp. 1057-1061.

[24]. Z. Liang and J. D. van Wyk, "Planar Metallization Interconnected 3D Multi-chip Module," *Proceedings of 53rd Electronic Components and Technology Conference (ECTC)*, 2003, pp. 1090-1094.

[25]. Z. X. Liang, J. D. van Wyk, F. C. Lee, D. Boroyevich, E. P. Scott, J. Chen, and Y. Pang, "Integrated Packaging of a 1 kW Switching Module Using a Novel Planar Interconnect Technology," *IEEE Transactions on Power Electronics*, Vol. 19, Issue 1, 2004, pp. 242-250.

[26]. G. L. Ginsberg and D. P. Schnorr, *Multichip Modules & Related Technologies*, 1st Edition (New York: McGraw-Hill, Inc., 1994), pp. 1-229.

[27]. A. Bergles, "Evolution of Cooling Technology for Electrical, Electronic, and Microelectronic Equipment," IEEE Transactions on Components and Packaging Technologies, Vol. 26, No. 1, March 2003, pp. 6-15.

[28]. D. Price, "A Review of Selected Thermal Management Solutions for Military Electronic Systems," *IEEE Transactions on Components and Packaging Technologies*, Vol. 26, No. 1, March 2003, pp. 26-39.

[29]. K Azar, "Advanced Cooling Concepts and Their Challenges," Presentation at Therminic 2002.

[30]. C. D. Patel, "Backside Cooling Solution for High Power Flip Chip Multi-chip Modules," *Proceedings of Electronic Components and Technology Conference (ECTC)*, 1994, pp. 442-449.

[31]. T. Y. Lee, "An Investigation of Thermal Enhancement on Flip Chip Plastic BGA Packages Using CFD Tool," *IEEE Transactions on Components and Packaging Technologies*, Vol. 23, No. 3, September 2000, pp. 481-489.

[32]. L. Liang, J. D. Wilson, N. Brathwaite, L. E. Mosley, and D. Love, "High-Performance VLSI Through Package-Level Interconnects," *Proceedings of 39th Electronic Components Conference*, 1989, pp. 518-523.

[33]. M. S. Pittler, D. M. Powers, and D. L. Schnabel, "System Development and Technology Aspects of the IBM 3081 Processor Complex," *IBM Journal of Research and Development*, Vol. 26, No. 1, January 1982, pp. 2-11.

[34]. R. C. Chu, U. P. Hwang, and R. E. Simons, "Conduction Cooling for an LSI Package: A One-Dimensional Approach," *IBM Journal of Research and Development*, Vol. 26, No. 1, January 1982, pp. 45-54.

[35]. A. J. Blodgett and D. R. Barbour, "Thermal Conduction Module: A High-Performance Multilayer Ceramic Package," *IBM Journal of Research and Development*, Vol. 26, No. 1, January 1982, pp. 30-36.

[36]. S. Oktay and H. C. Kammerer, "A Conduction-Cooled Module for High-Performance LSI Devices," *IBM Journal of Research and Development*, Vol. 26, No. 1, January 1982, pp. 55-66.

[37]. I. Mudawar, "Assessment of High-Heat-Flux Thermal Management Schemes," *IEEE Transactions on Components and Packaging Technologies*, Vol. 24, No. 2, June 2001, pp. 122-141.

[38]. T. Y. Lee, V. Hause, and M. Mahalingam, "Liquid Encapsulated MCM Package —Thermal Demonstration," *Proceedings of 5th Inter-society Conference on Thermal and Thermomechanical Phenomena in Electronic Systems (ITHERM)*, 1996, pp. 258-265.

[39]. X. Y. Chen, K. C. Toh, T. N. Wong, J. C. Chai, D. Pinjala, O. K. Navas, Ganesh, H. Zhang, and V. Kripesh, "Direct Liquid Cooling of a Stacked MCM," *Proceedings of 9th Inter-society Conference on Thermal and Thermomechanical Phenomena in Electronic Systems (ITHERM),* 2004, pp. 199-206.

[40]. M. C. Shaw, J. R. Waldrop, S. Chandrasekaram, B. Kagalwala, and X. Jing, "Enhanced Thermal Management by Direct Water Spray of High-Voltage, High Power Devices," Proceedings of 8th *Inter-society Conference on Thermal and Thermomechanical Phenomena in Electronic Systems (ITHERM)*, 2002, pp. 1007-1014.

[41]. W. R. Stubstad, "The Application of Thermoelectric Spot Cooling to Electronic Equipment," *IRE Transaction on Product Engineering and Production*, Vol. 5, Issue 4, December 1961, pp. 22-29.

[42]. J. P. Fleurial, A. Borshchevsky, M. A. Ryan, W. Phillips, E. Kolawa, T. Kacisch, and R. Ewell, "Thermoelectric Microcoolers for Thermal Management Applications," *Proceedings of the XVI International Conference on Thermoelectrics*, 1997, pp. 641-645.

[43]. R. E. Simons and R. C. Chu, "Application of Thermoelectric Cooling to Electronic Equipment: A Review and Analysis," *Proceedings of 16th IEEE Semiconductor Thermal Measurement and Management Symposium*, 2000, pp. 1-9.

[44]. G. L. Solbrekken, K. Yazawa, and A. Bar-Cohen, "Thermal Management of Portable Electronic Equipment Using Thermoelectric Energy Conversion," *Proceedings of 9th Inter-society Conference on Thermal and Thermomechanical Phenomena in Electronic Systems (ITHERM)*, Vol. 1 pp. 276-283.

[45]. C. Zweben, "Advanced Composites and Other Advanced Materials for Electronic Packaging Thermal Management," *Proceedings of International Symposium on Advanced Packaging Materials: Processes, Properties and Interfaces*, 2001, pp. 360-365.

[46]. S. Jha, "CUVAR—A New Controlled Expansion, High Conductivity Material for Electronic Thermal Management," *Proceedings of 45th Electronic Components and Technology Conference (ECTC)*, 1995, pp. 542-547.

[47]. H. L. Davidson, N. J. Colella, J. A. Kerns, and D. Makowiecki, "Copper-Diamond Composite Substrates fro Electronic Components," *Proceedings of 45th Electronic Components and Technology Conference (ECTC)*, 1995, pp. 538-541.

[48]. G. Ellison, *Thermal Computations for Electronic Equipment*, (New York: Van Nostrand Reinhold Company, 1984).

[49]. J. C. Eid, "Thermal Modeling with PC Spreadsheets," *Proceedings of 4th Semiconductor Thermal and Temperature Measurement Symposium (SEMI-THERM)*, 1988, pp. 40-49.

[50]. T. W. C. Mak and L. G. Feinstein, "A Simplified Modeling Technique for Finite Element Thermal Analysis of a Plastic SOIC Package," *IEEE Transaction on Components and Packaging Technologies*, Vol. 22, Issue 1, March 1999, pp. 6-10.

[51]. B. A. Zahn, "Evaluating Thermal Characterization Accuracy Using CFD Codes—A Package Level Benchmark Study of IcePak™ and Flotherm®," *Proceedings of 6th Inter-society Conference on Thermal and Thermomechanical Phenomena in Electronic Systems (I-THERM)*, 1998, pp. 322-329.

[52]. Y. Joshi, M. Baelmans, D. Copeland, C. J. M. Lasance, J. Parry, and J. Rantala, "Challenges in Thermal Modeling of Electronics at the System Level: Summary of Panel Held at the Therminic 2000," *Microelectronics Journal*, Vol. 32, Issues 10-11, October-November 2001, pp/ 797-800.

[53]. V. Eveloy, P. Rodgers, and M. S. J. Hashmi, "Numerical Prediction of Electronic Component Operational Temperature: A Perspective," *IEEE Transaction on Components and Packaging Technologies*, Vol. 27, No. 2, June 2004, pp. 268-282.

[54]. K. Azar, "Electronic Cooling and the Need for Experimentation," *Thermal Measurements in Electronic Cooling* (New York: CRC Press, 1997), pp. 1-43.

[55]. G. B. Kromann, "Thermal Management for Ceramic Multichip Modules: Experimental Program," *Proceedings of Multi-Chip Module Conference (MCMC)*, 1992, pp. 75-58.

[56]. P. Rodgers, V. Eveloy, J. Lohan, C. M. Fager, P. Tiilikka, and J. Rantala, "Experimental Validation of Numerical Heat Transfer Predictions for Single and Multi-component Printed Circuit Boards in Natural Convection Environments," *Proceedings of 15th Semiconductor Thermal Measurement and Management Symposium (SEMI-THERM)*, 1999, pp. 54-64.

[57]. J. Lohan, P. Rodgers, C. M. Fager, R. Lehtiniermi, V. Eveloy, P. Tiilikka, and J. Rantala, "Validation and Application of Different Experimental Techniques to Measure Electronic Component Operating Junction Temperature," *IEEE*

Transactions on Components and Packaging Technology, Vol. 22, No. 2, June 1999, pp. 252-258.

[58]. T. Gautier, "Construction and Validation of Thermal Models of Packages," *Proceedings of 7th Semiconductor Thermal Measurement and Management Symposium (SEMI-THERM)*, 1991, pp. 74-79.

[59]. JEDEC Standard, http://www.jedec.org.

[60]. R. Moffat, "Uncertainty Analysis," *Thermal Measurements in Electronic Cooling* (New York: CRC Press, 1997), pp. 46-80.

[61]. B. S. Lall, B. M. Guenin, and R. J. Molnar, "Methodology for Thermal Evaluation of Multichip Modules," *Proceedings of 11th Semiconductor Thermal Measurement and Management Symposium (SEMI-THERM)*, 1995, pp. 72-79.

[62]. J. W. Sofia, "Fundamentals of Thermal Resistance Measurement," 1995, http://www.analysistech.com/PDF_Files/fundamen.pdf.

[63]. L. Liang and A. Hamzehdoost, "Guidelines for Thermal Management of Multichip Modules," *Proceedings of 42nd Electronics Components and Technology Conference*, 1992, pp. 787-791.

[64]. B. S. Lall, A. Ortega, and H.Kabir, "Thermal Design Rules for Electronic Components on Conducting Boards in Passively Cooled Enclosures," *Proceedings of 4h Inter-society Conference on Thermal and Thermomechanical Phenomena in Electronic Systems (I-THERM)*, 1994, pp. 50-61.

[65]. T. Watanabe, M. Takayanagi, R. Iijima, K. Ishimaru, H. Ishiuchi, and Y. Tsunashima, "Design Guideline of HfSiON Gate Dielectrics for 65 nm CMOS Generation," *Symposium on VLSI Technology*, 2003, pp. 19-20.

[66]. C. Mead and L. Conway, *Introduction to VLSI Systems*, (Massachusetts: Addison-Wesley, 1980), pp. 47-51.

[67]. J. Valainis, S. Kaptanoglu, E. Liu, and R. Suaya, "Two-dimensional IC Layout Compaction Based on Topological Design Rule Checking," *IEEE Transactions on Computer-Aided Design of Integrated Circuits and Systems*, Vol. 9, Issue 3, March 1990, pp. 260-275.

[68]. N. Hedenstierna and K. O. Jeppson, "A Parallel Hierarchy Design Rule Checker," *Proceedings of 3rd European Conference on Design Automation*, 1992, pp. 142-146.

[69]. G. Suzuki and Y. Okamura, "A Practical Online Design Rule Checking System," *Proceedings of 27th ACM/IEEE Design Automation Conference*, 1990, pp. 246-252.

[70]. *I-DEAS Electronic System Cooling User's Guide* (Plano: UGS PLM Solutions Inc., 2004).

[71]. N. Zhu, J. D. van Wyk, and Z. Liang, "Thermal-mechanical Stress Analysis in Embedded Power Modules," *Proceedings of 35th IEEE Power Electronics Specialists Conference (PESC)*, Vol. 6, pp. 4503-4508.

[72]. F. P. Incropera and D. P. DeWitt, *Fundamentals of Heat and Mass Transfer*, 4th Edition (New York: Johns Wiley & Sons, Inc., 1996), pp. 8.

[73]. K. T. Ulrich and S. D. Eppinger, *Product Design and Development*, 2nd Edition (New York: Irwin McGraw-Hill, 2000), pp. 9.

[74]. V. Rybnikov and D. Mayorov, "Intel Pentium 4 1.6A GHz Overlocking, Thermal Monitor," Digit-Life.com, http://www.digit-life.com/article2/pentium416ghzoc/.

[75]. R. Viswanath, V. Wakharkar, A. Watwe, and V. Lebonheur, "Thermal Performance Challenges from Silicon to Systems," Intel Technology Journal, Q3, 2000, http://www.intel.com/technology/itj/q32000/articles/art_4.htm.

[76]. G. Kromann, V. Pimont, and S. Addison, "CFD and EDA Tools The Interoperability of Flotherm® and Board Station® / AutoTherm®: Concurrent Design of a Motorola PowerPC™ RISC Microprocessor-based Microcomputer," Freescale Semiconductor, Inc., http://www.freescale.com/files/archives/doc/white-paper/603604THERMAL.pdf.

[77]. M. Agnes, *Webster's New World College Dictionary*, 4th Edition (Cleveland: IDG Books Worldwide, Inc., 2000), pp. 631.

[78]. A. Dix, J. Finlay, G. Abowd, and R. Beale, *Human-Computer Interaction*, 2nd Edition (London: Prentice Hall, 1998).

[79]. N. P. Suh, *The Principles of Design* (New York: Oxford University Press, 1990), pp. 46-54.

[80]. K. Azar, J. R. Benson, and V. P. Manno, "Liquid Crystal Imaging for Temperature Measurement of Electronic Devices," *Proceedings of 7th Semiconductor Thermal Measurement and Management Symposium (SEMI-THERM)*, 1991, pp. 23-33.

[81]. K. Azar, "Measuring Fluid Velocity in Electronic Enclosures," *Electronics Cooling Magazine*, January 1998, http://www.electronics-cooling.com/Resources/EC_Articles/JAN98/article1.htm.

[82]. N. R. Keltner, "Heat Transfer Measurements in Electronics Cooling Applications," Electronics Cooling Magazine, September 1998, http://www.coolingzone.com/Content/Library/Papers/Sep%201998/Article%2003/Sep1998_03.html.

Appendix A

Thermal Couplings in ESC

A finite element model includes a mesh of nodes and elements. It is always the analyst's responsibility to make sure the mesh can model the heat transfer phenomena according to the physics of heat transfer. When the thickness of a layer is too thin to be meshed with solid mesh, this particular layer can be represented with an equivalent value in terms of thermal resistance, thermal conductance, or radiative coefficient. In I-DEAS ESC, these values are defined through thermal coupling. Thermal coupling provides conductance between unconnected elements with dissimilar meshes. It provides an additional heat path through which the heat may flow.

There are seven types of thermal coupling available for various applications in I-DEAS ESC. Based on the best information a user knows about the model, the use can select any of the thermal coupling type listed in Table A.1 to better describe the heat flow at the interfaces. Several considerations when using thermal couplings include the avoidance of false in-plane conductance and false heat concentrations.

Table A.1 Thermal Coupling Types

Thermal Coupling Type	Coupling Value	Typical Unit (SI)
Absolute	Conductance	W/°C
Conductive	Thermal Conductivity	W/m-°C
Constant Coefficient	Heat Transfer Coefficient	W/m^2-°C
Radiative	View-Factor	Unitless
Interface	Heat Transfer Coefficient	W/m^2-°C
Resistant	Resistance	°C/W
Edge	Heat Transfer Coefficient / Length	W/m^2-°C

A.1. Thermal Couplings for DC/DC IPEM

In the modeling of the DC/DC IPEM, the interfaces within the module were represented with equivalent thermal resistance values based on the thickness of the layer, the thermal property of the layer, and the conducting area of the layer. Five thermal couplings were defined in the DC/DC IPEM model at the interfaces illustrated in Figure A1.1. At the interface between the gate driver and the ceramic frame, the resistance of Epoxy A, R_{epoxyA}, is calculated using Eqn. A.1,

$$\begin{aligned} R_{epoxyA} &= \frac{L_{epoxyA}}{k_{epoxy} \cdot A_{gate}} \\ &= \frac{0.000127\text{m}}{1.43 \text{W}/_{\text{m}-\text{K}} \cdot 0.021\text{m} \cdot 0.09\text{m}}, \\ &= 0.496\,{}^{\circ}\text{C}/_{\text{K}} \end{aligned} \qquad (A.1)$$

where L_{epoxyA} is the thickness of the epoxy, k_{epoxy} is the thermal conductivity of the epoxy, and Agate is the bottom area of the gate driver.

Interface at Epoxy B illustrated in Figure A1.1 is the interface between the silicon and the ceramic carrier. This interface was modeled as the resistance of Epoxy B, R_{epoxyB}, and expressed in Eqn. A.2,

$$\begin{aligned} R_{epoxyB} &= \frac{L_{epoxyB}}{k_{epoxy} \cdot A_{MOSFET-ceramic}} \\ &= \frac{0.000508\text{m}}{1.43 \text{W}/_{\text{m}-\text{K}} \cdot 1.53\times10^{-5}\text{m} \cdot 1.24\times10^{-5}\text{m}}, \\ &= 12.845\,{}^{\circ}\text{C}/_{\text{K}} \end{aligned} \qquad (A.2)$$

where $A_{MOSFET\text{-}ceramic}$ is the contact area between the MOSFET chip and the ceramic carrier.

Finally, the solder layer between the MOSFET chip and the copper trace area was modeled as the equivalent thermal resistance of the solder layer, $R_{solderA}$. $R_{solderA}$ is calculated using Eqn. A.3,

$$
\begin{aligned}
R_{solderA} &= \frac{L_{solderA}}{k_{solder} \cdot A_{MOSFET}} \\
&= \frac{0.000127\text{m}}{51\,{}^{W}\!/_{m-K} \cdot 0.0072\text{m} \cdot 0.0088\text{m}}, \\
&= 0.0392\,{}^{\circ C}\!/_{K}
\end{aligned}
\tag{A.3}
$$

where $L_{solderA}$ is the thickness of the solder layer, k_{solder} is the thermal conductivity value of the solder, and A_{MOSFET} is the bottom area of the MOSFET chip.

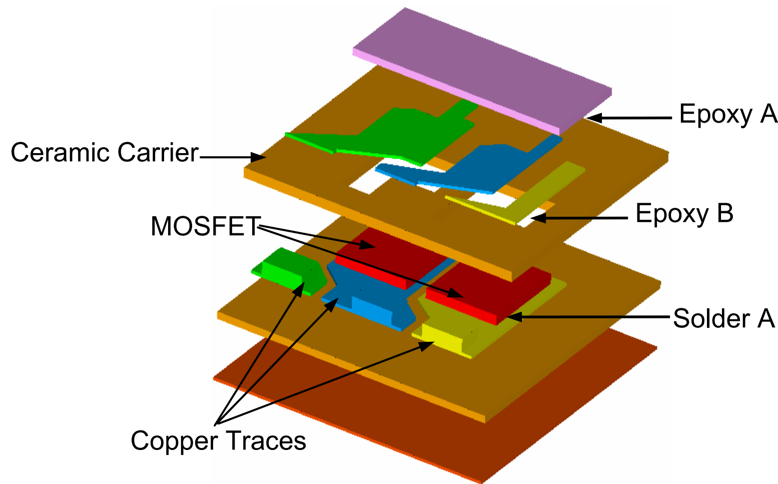

Figure A1.1 Locations of the Simplified Interface Conditions in DC/DC IPEM Model

A.2. Thermal Couplings for PFC IPEM

In the modeling of the PFC IPEM, the interfaces within the module were also represented with equivalent thermal resistance values. However, the modeling of the PFC IPEM is more complicated and thus it has more interface layers. The interfaces in PFC IPEM are shown in Figure A2.1. Six thermal couplings were defined in the PFC IPEM model at the interfaces. At the interface between the CoolMOS chip and the ceramic frame, the resistance of Epoxy C, R_{epoxyC}, is calculated using Eqn. A.4,

$$\begin{aligned} R_{epoxyC} &= \frac{L_{epoxyC}}{k_{epoxy} \cdot A_{CoolMOS-ceramic}} \\ &= \frac{0.000254\text{m}}{1.43\,{}^{\text{W}}\!/_{\text{m}-\text{K}} \cdot 0.00001788\text{m}}, \\ &= 9.8652\,{}^{\circ\text{C}}\!/_{\text{K}} \end{aligned} \tag{A.4}$$

where L_{epoxyC} is the thickness of Epoxy C and $A_{CoolMOS-ceramic}$ is the contact area between the CoolMOS chip and the ceramic carrier.

Similarly, the interface between the SiC diode and the ceramic frame is modeled with the resistance of Epoxy D, R_{epoxyD}, is calculated using Eqn. A.5,

$$\begin{aligned} R_{epoxyD} &= \frac{L_{epoxyD}}{k_{epoxy} \cdot A_{SiC-ceramic}} \\ &= \frac{0.000254\text{m}}{1.43\,{}^{\text{W}}\!/_{\text{m}-\text{K}} \cdot 5.08 \times 10^{-6}\,\text{m}}, \\ &= 35.2\,{}^{\circ\text{C}}\!/_{\text{K}} \end{aligned} \tag{A.5}$$

where L_{epoxyD} is the thickness of Epoxy D and $A_{SiC-ceramic}$ is the contact area between the SiC diode and the ceramic carrier.

In addition, the solder layers beneath the CoolMOS chips and the SiC diodes are represented by Solder B and Solder C respectively. The equivalent thermal resistances for Solder B and Solder C are expressed in Eqn. A.6 Eqn. A.7 correspondingly,

$$R_{solderB} = \frac{L_{solderB}}{k_{solder} \cdot A_{CoolMOS}} = \frac{0.000127m}{51 \, W/_{m-K} \cdot 0.00583m \times 0.00452m} = 0.095 \, {}^{\circ}C/_{K}, \tag{A.6}$$

$$R_{solderC} = \frac{L_{solderC}}{k_{solder} \cdot A_{SiC}} = \frac{0.000127m}{51 \, W/_{m-K} \cdot 0.0014m \times 0.0014m} = 1.186 \, {}^{\circ}C/_{K}, \tag{A.7}$$

where $L_{solderB}$ is the thickness of Solder B, $A_{CoolMOS}$ is the bottom surface area of the CoolMOS chip, $L_{solderC}$ is the thickness of Solder C, and A_{SiC} is the bottom surface area of the SiC diode.

Finally, the capability of the heat transfer through the two polyimide layers within the PFC IPEM model were also represented by equivalent thermal resistance values. Polyimide A is the layer between the ceramic carrier and the power stage metallization layers. The equivalent thermal resistance, R_{polyA}, is obtained using Eqn. A.8,

$$R_{polyA} = \frac{L_{polyA}}{k_{polyimide} \cdot A_{metallization}} = \frac{0.000127m}{0.3 \, W/_{m-K} \cdot 0.0004415m} = 0.96 \, {}^{\circ}C/_{K}, \tag{A.8}$$

where L_{polyA} is the thickness of Polyimide A, $k_{polyimide}$ is the thermal conductivity of the polyimide, and $A_{metallization}$ is the metallization area that has contact with the polyimide.

Similarly, the polyimide layer between the ceramic carrier and the copper traces is represented by the equivalent thermal resistance of Polyimide B, R_{polyB}. R_{polyB} is calculated using Eqn. A.9,

$$
\begin{aligned}
R_{polyB} &= \frac{L_{polyB}}{k_{polyimide} \cdot A_{trace}} \\
&= \frac{0.000127\text{m}}{0.3 \,{}^{W}\!/\!_{m-K} \cdot 6.41 \times 10^{-4}\,\text{m}}, \\
&= 0.66 \,{}^{\circ C}\!/\!_{K}
\end{aligned}
\qquad (A.9)
$$

where L_{polyB} is the thickness of Polyimide B and A_{trace} is the trace area that has contact with the polyimide.

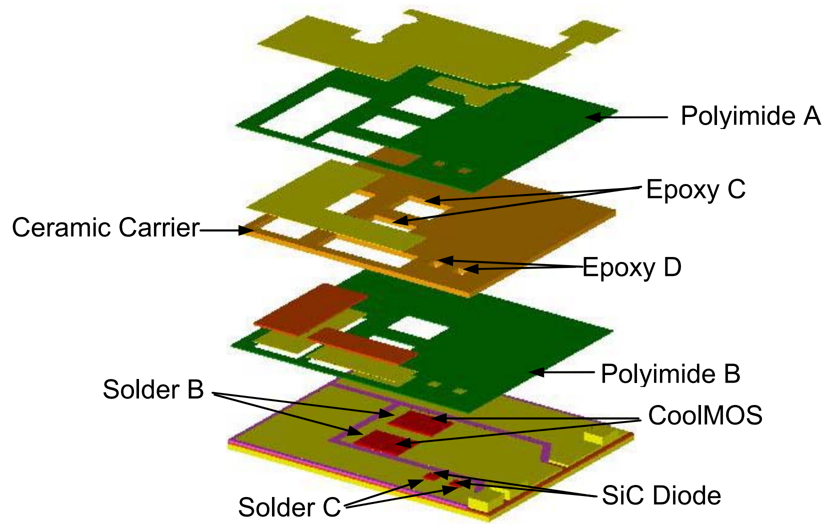

Figure A2.1 Locations of the Simplified Interface Conditions in PFC IPEM Model

Appendix B

Publications

Papers in Refereed Journals

1. Y. F. Pang, E. P. Scott, and K. A Thole, “Thermal Design and Optimization Methodology for Integrated Power Electronics Modules,” *ASME Journal of Electronic Packagin*g, to be published June, 2005.
2. Z. X. Liang, J. D. van Wyk, F. C. Lee, D. Boroyevich, E. P. Scott, J. Chen, and Y. F. Pang, “ Integrated Packaging of a 1kW Switching Module Using a Novel Planar Integration Technology," *IEEE Transactions on Power Electronics*, Vol. 19, No. 1, January 2004, pp. 242-250.

Papers Submitted to Journals and Under Review

1. Y. F. Pang and E. P. Scott, “Thermal Characterization of Multi-chip Modules—Integrated Power Electronics Modules,” submitted to the *IEEE Transactions on Components and Packaging Technologies*, September 2004.
2. Y. F. Pang, E. P. Scott, J. D. van Wyk, and Z. Liang, “Assessment of Some Integrated Cooling Mechanisms for an Active IPEM,” submitted to the *ASME Journal of Electronic Packaging*, August 2004.
3. M. Hernández-Mora, J. E. González, M. Vélez-Reyes, J. M. Ortiz-Rodríguez, Y. F. Pang, and E. P. Scott, “Dynamic Reduced Electrothermal Model for Integrated Power Electronics Modules (IPEM),” submitted to the *ASME Journal of Electronic Packaging*, July 2004.
4. Y. Wu, J. Chen, Y. F. Pang, J. H. Bøhn, D. Boroyevich, and E. P. Scott, “Software Integration for Multidisciplinary Power Electronics Design,” submitted to the *IEEE Transactions on Power Electronics*, May 2004.

Papers in Refereed Conference Proceedings

1. Y. F. Pang, E. P. Scott, J. D. van Wyk, and Z. X. Liang, “Assessment of Some Integrated Cooling Mechanisms for an Active IPEM,” *ASME International Mechanical Engineering Congress & Exposition (IMECE)*, 2004, paper # 59342.
2. Y. F. Pang, N. Zhu, E. P. Scott, and J. D. van Wyk, “Assessment of Thermo-mechanics for an Integrated Power Electronics Switching Stage,” submitted to *39th Industry Application Conference* (IAS), 2004.
3. Y. F. Pang and E. P. Scott, “Thermal Evaluation of DC/DC and PFC Integrated Power Electronics Modules,” Proceedings of the 9th *Inter-society Conference on Thermal Phenomena in Electronic Systems (ITHERM)*, 2004, pp. 700-705.

4. Y. F. Pang and E. P. Scott, "Thermal Characterization and Optimization of Active System IPEM," *ASME International Mechanical Engineering Congress & Exposition (IMECE)*, 2003, paper # 41415.
5. D. L. Minter, Y. F. Pang, and E. P. Scott, "The Effects of Various Cooling Scenarios on a System of Integrated Circuits," *ASME International Mechanical Engineering Congress & Exposition (IMECE)*, 2003, paper # 41667.
6. M. Hernández-Mora, J. E. González,_M. Vélez-Reyes, J. M. Ortiz-Rodríguez, Y. F. Pang, and E. P. Scott, "Dynamic Reduced Electrothermal Model for Integrated Power Electronics Modules (IPEM): Part I- Thermal Analysis," *ASME International Mechanical Engineering Congress & Exposition (IMECE)*, 2003, paper # 42446.
7. Z. X. Liang, F. C. Lee , J. D. van Wyk, D. Boroyevich, E. P. Scott, J. Chen, B. Lu, and Y. F. Pang, " Integrated Packaging of a 1kW Switching Module Using Planar Interconnect on Embedded Power Chips Technology," *18th Applied Power Electronics Conference & Exposition (APEC)*, 2003, Vol. 1, pp. 42-47.
8. Y. F. Pang, Z. Chen, E. P. Scott, and K. A. Thole, "Electrical and Thermal Layout Design and Optimization Considerations for DPS Active IPEM," *ASME International Mechanical Engineering Congress & Exposition (IMECE)*, 2002, paper # 33778.
9. M. Bikdash, Y. F. Pang, and E. P. Scott, "Generation of Equivalent Circuit Models from Simulation Data of a Thermal System," *ASME International Mechanical Engineering Congress & Exposition (IMECE)*, 2002, paper # 33782.
10. Z. Chen, Y. F. Pang, D. Boroyevich, E. P. Scott, and K. A. Thole, **"**Electrical and thermal layout design considerations for integrated power electronics modules," *37th Industry Application Conference* (IAS), 2002, Vol. 1, pp. 242-246.

Papers Submitted to Refereed Conference

1. Y. F. Pang, E. P. Scott, Z. X. Liang, J. D. van Wyk, "Experimental Evaluation of Double-sided Cooling for Integrated Power Electronics Modules," submitted to ASME InterPack.2005, San Francisco, July 17-22.

Papers in Non-refereed Conference Proceedings

1. Y. F. Pang and E. P. Scott, "Thermal Evaluation of DC/DC and PFC Integrated Power Electronics Modules," *2004 CPES Power Electronics Seminar Proceedings*, 2004, pp. 485-491.
2. Y. F. Pang, E. P. Scott, J. D. van Wyk, and Z. X. Liang, "Assessment of Some Integrated Cooling Mechanisms for an Active IPEM," *2004 CPES Power Electronics Seminar Proceedings*, 2004, pp. 520-524.
3. M. Hernández-Mora, J. E. González,_M. Vélez-Reyes, J. M. Ortiz-Rodríguez, Y. F. Pang, and E. P. Scott, "Dynamic Reduced Electrothermal Model for Integrated Power Electronics Modules (IPEM): Part I- Thermal Analysis," *2004 CPES Power Electronics Seminar Proceedings*, 2004, pp. 512-519.
4. J. M. Ortiz-Rodríguez, A. R. Hefner, M. Vélez-Reyes, M. Hernández-Mora, J. E. González, J. Chen, Y. F. Pang, and D. Boroyevich, "Lumped-Parameter Thermal

Modeling of an IPEM Using Thermal Component Models," *2004 CPES Power Electronics Seminar Proceedings*, 2004, pp. 103-108.

5. M. Bikdash, H. Rayadurgam, Y. F. Pang, and E. P. Scott, "Algorithm to Determine the Topology of a Thermal Equivalent Circuit from Simulation Data," *2003 CPES Power Electronics Seminar Proceedings*, 2003, pp. 32-38.
6. W. Dong, B. Lu, B. Yang, Z. Lu, F. C. Lee, Y. F. Pang, and E. P. Scott, "Integrated High Frequency DPS Front-end Converter," *2003 CPES Power Electronics Seminar Proceedings*, 2003, pp. 131-136.
7. D. L. Minter, Y. F. Pang, and E. P. Scott, "The Effects of Various Cooling Scenarios on a System of Integrated Circuits," *2003 CPES Power Electronics Seminar Proceedings*, 2003, pp. 615-621.
8. Y. F. Pang and E. P. Scott, "Thermal Characterization and Optimization of Active System IPEM," *2003 CPES Power Electronics Seminar Proceedings*, 2003, pp. 622-627.
9. Y. Wu, J. Chen, Y. F. Pang, J. H. Bøhn, D. Boroyevich, and E. P. Scott, "Automation of Multidisciplinary IPEM Modeling, Design, and Analysis," *2003 CPES Power Electronics Seminar Proceedings*, 2003, pp. 635-638.
10. P. Barbosa, F. C. Lee, J. D. van Wyk, D. Boroyevich, E. P. Scott, K. Thole, H. Ordendaal, Z. Liang, Y. F. Pang, E. Sewall, J. Chen, R. Chen, and B. Yang, "An Overview of the IPEM-Based Modular Implementation for Distributed Power Systems," *2002 CPES Power Electronics Seminar Proceedings*, 2002, pp. 70-76.
11. Y. F. Pang, Z. Chen, E. P. Scott, K. A. Thole, and D. Boroyevich, "Electrical and Thermal Layout Design and Optimization Considerations for DPS Active IPEM," *2002 CPES Power Electronics Seminar Proceedings*, 2002, pp. 77-82.

Papers Submitted to Non-refereed Conference

1. Y. F. Pang, E. P. Scott, Z. X. Liang, and J. D. van Wyk, "Experimental Study on the Double-sided Cooling for Integrated Power Electronics Modules," submitted to 2005 CPES Annual Conference, Blacksburg, April 17-20, 2005.
2. Y. F. Pang and E. P. Scott, "Thermal Design Rules for Embedded Power Multi-chip Modules," submitted to 2005 CPES Annual Conference, Blacksburg, April 17-20, 2005.
3. M. Mital, Y. F. Pang, E. P. Scott, and Z. X. Liang, "Thermal Evaluation of Integrated Power Electronics Modules for Power Conversion Systems," submitted to 2005 CPES Annual Conference, Blacksburg, April 17-20, 2005.
4. N. M. Martinez, J. O. Class, M. Mital, Y. F. Pang, N. Dukhan, and E. P. Scott, "Direct Comparison between a Heat Sink and a Foam Block Cooling of a Integrated Power Electronics Modules," submitted to 2005 CPES Annual Conference, Blacksburg, April 17-20, 2005.

Appendix C

Data Sheet for Papst-Motoren Axial Fan

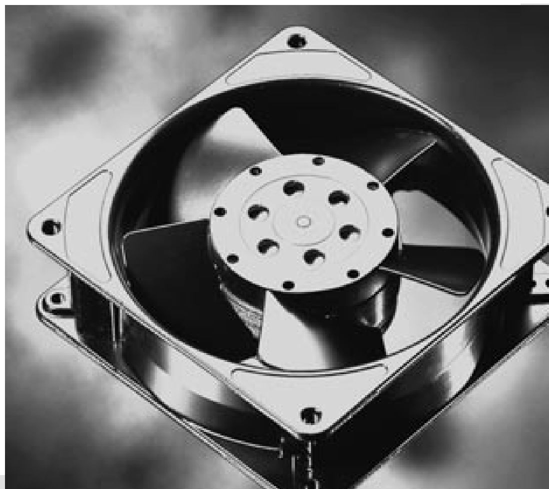

PAPST

- AC fans with external rotor shaded-pole motor. Impedance protected against overloading.
- Metal fan housing and impeller
- Air exhaust over struts. Rotational direction CW looking at rotor.
- Electrical connection via 2 flat pins 2.8 x 0.5 mm.
- Fan housing with ground lug and screw M 4x8 (TORX).
- Mass 540 g.

Series 4000 Z   119 x 119 x 38 mm

Air Flow	Air Flow	Nominal Voltage	Frequency	Noise		Sintec-Sleeve Bearings / Ball Bearings	Power Input	Nominal Speed	Temperature Range	Service Life L_{10} at 40 °C / at t_{max}	Curve	Type
m³/h	CFM	V	Hz	dB(A)	bels	□/■	Watt	min⁻¹	°C	Hours / Hours		
100	58.9	230	50	26	4.0	□	13	1700	-10...+65	50 000 / 27 500	1	4850 Z
115	67.7	230	50	30	4.3	□	13	1900	-10...+65	50 000 / 27 500	2	4580 Z
160	94.2	230	50	40	5.3	□	19	2650	-10...+50	37 500 / 30 000	3	4650 Z
160	94.2	230	50	40	5.3	■	19	2650	-40...+75	37 500 / 17 500	3	4656 Z
105	61.8	115	60	28	4.1	□	12	1800	-10...+70	52 500 / 25 000	4	4800 Z
120	70.6	115	60	32	4.4	□	12	2000	-10...+70	52 500 / 25 000	5	4530 Z
180	105.9	115	60	45	5.6	□	18	3100	-10...+60	40 000 / 25 000	6	4600 Z
180	105.9	115	60	45	5.6	■	18	3100	-40...+85	40 000 / 15 000	6	4606 Z

Available on request:
- Electrical connection via 2 single leads 310 mm long.

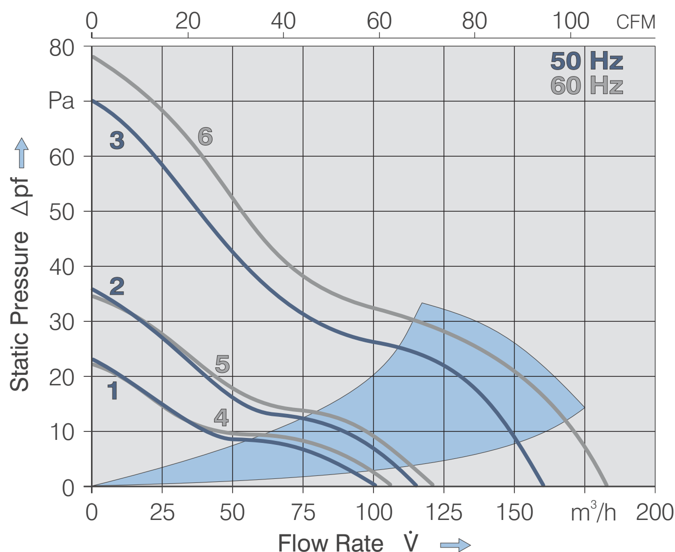

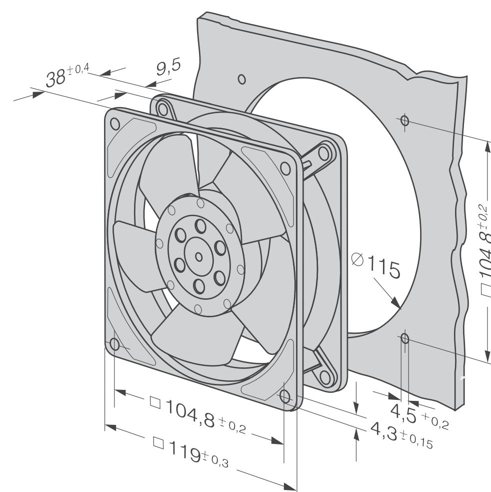

AC Axial Fans

Vita

Ying Feng Pang was born in Malaysia. In May 1998, she received her degree in Bachelor of Science in Mechanical Engineering at Michigan Technological University, Houghton, Michigan. She was a mechanical engineer in WeBlast Sdn Bhd, Kuala Lumpur, Malaysia from August 1998 to July 2000 prior to attending Virginia Tech for her graduate studies. She received her Master of Science in Mechanical Engineering in Fall 2002 from Virginia Tech, Blacksburg under supervision of Dr. Elaine Scott and Dr. Karen Thole. Her research topic focused on heat transfer in power electronics. She continued her graduate studies in pursuing her doctorate degree in mechanical engineering after receiving her master degree. In January 2005, she completed her graduate studies with a degree of Doctorate of Philosophy in Mechanical Engineering.